Est. 1984

ORIENTAL JOURNAL OF CHEMISTRY
An International Open Free Access, Peer Reviewed Research Journal

www.orientjchem.org

ISSN: 0970-020 X
CODEN: OJCHEG
2016, Vol. 32, No. (2):
Pg. 1003-1014

Impedance Spectroscopy Study of the AC Conductivity and Dielectric properties of 3, 5-Dimethylpyridine-Iodine Charge Transfer Complex

UTTAM MOHAN[1]*, PALLAVI GOGOI[2] and S.K. BARUAH[3]

[1]Department of Chemistry, D.H.S.K. College, Dibrugarh, Assam, India.
[2]Department of Chemistry, Tinsukia College, Tinsukia, Assam, India.
[3]Department of Chemistry, Dibrugarh University, Dibrugarh,Assam, India.
*Corresponding E-mail: uttamohan@rediffmail.com

http://dx.doi.org/10.13005/ojc/320226

(Received: March 12, 2016; Accepted: April 18, 2016)

ABSTRACT

Solid charge transfer complex of n-donor 3, 5-dimethylpyridine (3, 5-Lutidine) with σ acceptor iodine was prepared and characterised by using elemental analysis, UV-Vis, FTIR, ^{1}H NMR spectroscopy and powder XRD techniques. The electrical parameters of the prepared complex in the pellet form were studied at various temperatures and at wide frequency range by employing AC complex impedance spectroscopic technique. The Nyquist (cole-cole) plots have been successfully explained by employing (RC)(RC)(RC) equivalent circuit corresponding to grain , grain boundary and electrode contributions. The radii of the semicircular arc decrease with increase in temperature which suggests that the material exhibits negative temperature coefficient of resistance (NTCR) behaviour like semiconductors. Dielectric constant, ε' and dielectric loss, ε'' seems to decrease sharply with increase in frequency. The ac conductivity obeys the power law of frequency.

Keywords: Charge-Transfer complex, Impedance spectroscopy, Dielectric properties.

INTRODUCTION

Charge transfer (CT) or Donor-acceptor complexes are the most important and vastly studied organic species due to their unusual electrical, magnetic and optical properties[1]. In 1973, the CT complex TTF-TCNQ was reported as organic metal[2] and after that organic CT complexes have greatly attracted the attention of researchers for several decades, aimed mainly at the discovery of materials with good electrical conductivity or even room temperature superconductivity[3]. Recently attention has been turned to technologically relevant properties of CT complexes due to their potential in the development of electronic and optoelectronic devices[4].

Electrical conduction property of a donor-acceptor complex is mainly influenced by (a) electronic structure of the complex and (b)

molecular orientation (segregated stacking and mixed stacking) within the molecular assembly[5]. The electronic structure of a complex, $(D^{+\delta})(A^{-\delta})$ between the electron donor (D) and the electron acceptor (A), where δ is the degree of charge transfer from D to A, is primarily determined by the ionization potential (I_p) of D and electron affinity (E_a) of A. If $E_a > I_p$, then neutral electronic ground state of $\delta = 0$ is observed whereas the completely ionic state corresponds to $\delta = 1$ is obtained when $E_a < I_p$. Both neutral and completely ionic CT complexes are insulators due to small number of current carriers in $(D^0)(A^0)$ and large on-site coulomb repulsive energies in $(D^{+1})(A^{-1})$ complexes. Few CT complexes exhibited metallic electrical conduction[4] whose δ values ranges from 0.50 to 0.74. For example $(TTF^{+0.59})(TCNQ^{-0.59})$ is metallic conductor[2] with conductivity value 700 Scm^{-1}. It is reported[6] that mixed-valence CT complexes with segregated-stack structures generally exhibit metallic electrical conduction; otherwise alternating stack CT complexes are either semiconductor or insulator.

Similar to inorganic semiconductors, the conduction mechanism of organic CT complexes has been reported[7] in the light of band theory. To understand the transport mechanisms in a charge transfer complex their structural studies are of utmost importance. Several structural informations can be revealed from the dielectric properties study[8] of the CT materials which indeed, can be useful for the understanding of conduction mechanism in these materials. Besides, the origin as well as the nature of the various losses happening in these materials can be predictable from the study of frequency and temperature dependence of dielectric parameters, particularly in the range of frequency where the dielectric dispersion occurs.

Complex impedance spectroscopy (CIS) is a powerful technique to analyze the electrical properties of material having low conductivity. This technique involves the separation of grain, grain-boundary and grain-electrode effect, determination of relaxation frequency and measurement of real and imaginary part of impedance for a wide range of frequency[9]. Studies in many aspects including electrical conductivity of charge transfer complexes of pyridine analogue with halogens and interhalogens have been reported in literatures[10, 11]. However detailed study of frequency dependence AC conductivity and complex impedance spectroscopy of this important class of compounds are unexplored. The aim of the present study is to investigate the electrical properties of CT complex between 3, 5-dimethylpyridine with iodine using CIS.

ExPERIMENTAL

3, 5- dimethylpyridine (98+%) purchased from Aldrich Chemical Co., was used without further purification. Iodine from Ranbaxy fine chemical Ltd., was purified by resublimation. Hexane (Merck) was used after distillation as a solvent.

Synthesis and Characterization of Complexes

The solid CT complex of 3, 5- dimethylpyridine with Iodine was prepared by stirring equimolar quantities of the donor with acceptor in hexane, which on keeping for overnight resulted in precipitation of the complex as dark green solid. The separated solid was filtered and washed several times with minimum amount of hexane and dried under vacuum over anhydrous calcium chloride. The complex is characterised by routine technique like elemental analysis, powder XRD, ^{1}H NMR, UV-Vis and FTIR spectroscopy.

The elemental analysis of Carbon, Hydrogen and Nitrogen content were performed by using Perkin Elmer CHN 2400 Series II. The total halogen contents were estimated by simple gravimetric method with $AgNO_3$ solution. The electronic absorption spectra of the donor, acceptor and the resulting complex in a suitable solvent were recorded over a wavelength range of 200-900 nm using Shimadzu U-3900 spectrophotometer. The FT-IR spectra were recorded on a Shimadzu FT-IR spectrophotometer (IRPrestige-21) within the range of 4000-250 cm^{-1}. The ^{1}H-NMR spectra are recorded in $CDCl_3$ solvent. Powder XRD analysis was carried out at room temperature by using Co radiation ($\lambda = 1.7902$Å) in the range $2° \leq 2\theta \leq 70°$ at a scanning rate of 1°/min and step height of 0.05°.

Measurement of electrical properties

For measurement of electrical properties, the solid complex was pressed under 10 tons press by using a hydraulic press into disc type pellets of 13 mm diameter and the thickness were measured with a screw gauge. The thicknesses of the pellets

are in the range of 0.5mm to 1mm. Graphite pasting was applied on the opposite faces of the pellet and is sandwiched between two thin flat polished sheets of copper electrodes. AC conductance(G), impedance(Z), phase angle (θ), tangent loss (tan δ) and capacitance(Cp) were measured as a function of frequency, at different temperatures by using LCR HiTester (HIOKI 3522 frequency response analyzer) in the frequency range 10 Hz to 100 kHz. The impedance spectra were modelled as an 'equivalent circuit' by using MEIS 3.0 software[12] that uses LEVM fitting engine developed by James Ross Macdonald. LEVM is based on Complex Nonlinear Least Squares Method viz.; Levenberg-Marquardt Algorithm. The best fitted equivalent circuit has been determined by observing the coherence between the experimental and the simulated data in the complex impedance plots.

RESULTS AND DISCUSSION

Elemental analysis

Elemental analyses data (C, H, N and total halogen) of the complex were performed and the obtained results are as follows;

$C_7H_9N:I_2$, Mol. Wt. 360.81; Melting point = 96°C; Calc. : % C, 23.28; % H, 2.49; % N, 3.88; % Halogen, 70.35; Found: % C, 24.03; % H, 2.54; % N, 3.08, % Halogen, 71.12.

It has been observed that the experimental values agree quite well with the calculated values for 1: 1 complex.

UV-Vis spectroscopy

The electronic absorption spectra of the donor, acceptor and the resulting complex in hexane were recorded over a wavelength range of 200-900 nm. The additional absorption band at λ_{max} = 432nm indicates the formation of CT complex. (Figure 1)

FTIR Spectroscopy

Due to complex formation few selected IR frequencies of the donor are affected in both intensities and wave number values as shown in the FT-IR spectra of the solid CT complex and the donor in figure 2. This could be interpreted on the basis of expected electronic environment change upon complexation. The detailed vibrational assignments are reported in Table 1. These are in accordance with earlier works[13, 14].

It is observed that the spectra of 3, 5-dimethylpyridine-iodine complex shows all the principal features for free donor. Many modes of 3, 5- dimethylpyridine on complex formation have shifted to higher frequency in comparison to the free donor. Similar upward shifts were observed for metal coordinated pyridine[15] and metal coordinated pyridine analogues[16, 17, 18]. The upward shift may be due to coupling of the internal vibrations of the donor molecule with the N-I stretching vibration similar to metal-nitrogen bond as was in metal coordinated pyridine and its analogues. Thus, the vibrational spectra of the CT complex give the direct evidence

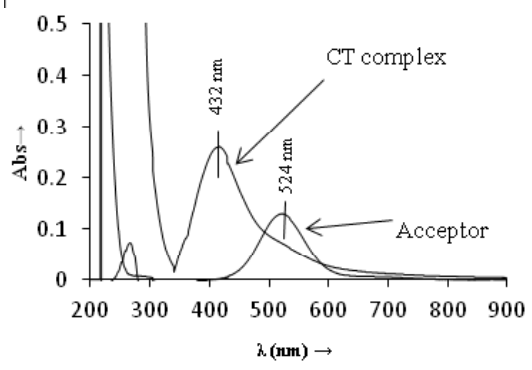

Fig. 1: UV-Vis spectra of 3,5-dimethylpyridine, Iodine and their CT complex

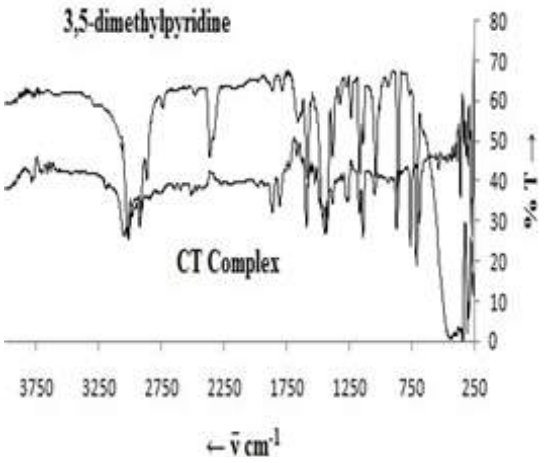

Fig. 2: FTIR spectra of 3,5-dimethylpyridine and its CT complex with iodine

that the 3, 5-dimethylpyridine molecules coordinated with the iodine through nitrogen atom.

1H-NMR Spectra

The ^{1}H-NMR ($CDCl_3$) spectrum of 3, 5-dimethylpyridine-iodine gave three distinct signals at δ=2.37 (s, 6H, -CH_3 protons), δ=7.61 (s, 1H, γ- ring proton), δ=8.30 (s, 2H, α-ring protons). The corresponding signals in the free donor (3, 5-dimethylpyridine) are at δ=2.31, 7.63 and 8.39 respectively. The signals due to protons of pyridine ring at α- & γ- positions were upfield which are due to the increase of the shielding of these protons as well as of the change of the magnetic environment on complex formation. The observed shifting of the chemical shifts values of the ring protons of pyridine is governed by two factors; (a) magnetic anisotropy of the N atom and (b) field associated with the nitrogen atomic dipole[19]. The displacement is more pronounced for the α- protons as these carbons are directly connected with the n-donor nitrogen atom. The signal of the methyl protons shifted to downfield on complexation which can be interpreted in terms of inductive effect[20].

Powder xRD Analysis

The powder XRD spectrum of CT Complex of 3,5- dimethylpyridine and iodine [Fig. 4] gave peaks at 2θ= 13.95°, 21.9°, 22.53°, 24.75°,25.10°, 26.65°, 27.30°, 29.60°, 33.10°, 33.60°and 34.10°corresponding to the new compound formed and indicating semi-crystalline structure of the complex[21]. The average grain size (D) of the sample was calculated from the most intense x-ray diffraction peak by using the classical Scherer[22] formula -

$$D = \frac{K\lambda}{\beta \cos\theta} \quad ...(1)$$

where λ is the x-ray wavelength (for Co radiation θ = 1.7902 Å), K is a constant (0.94 for Co grid), θ is the Bragg diffraction angle (half the scattering angle) and β is the full-width at half-maximum (FWHM) in radians of the main peak. The particle size of the material was found to be about 7.2 nm (2θ= 22.53°, β= 0.238 and d= 4.575). This value confirms that the particles of the complex are located within the nanoscale range.

Impedance Studies

Figure 5 shows the Nyquist plot for 3, 5- dimethylpyridine -Iodine complex over a wide frequency range and at several temperatures. The impedance spectrum of the complex under investigation is characterised by the appearance of a depressed semicircle whose radius decreases with the rise in temperature. In general we expect three

Table 1: FTIR Band Assignments of The Donor and The Complex

Donor (cm^{-1})	Complex	Assignment
3020 s	3049 s	C–H stretching
2980 s	3014 s	C–H stretching
2920 s	2960 vw	C–H (-CH_3) stretching
2866 m	2900 m	C–H (-CH_3) stretching
1860 vw	1865 w	First overtone of C–H vibration
1792 vw	1805 w	First overtone of C–H vibration
1585 s	1593 s	C=N stretching
1458 m	1466 vw	C=C stretching
1427 s	1442 s	C=C stretching
1381m	1384 m	Antisym. & Sym. -CH_3 deformation
1234 w	1267 w	Antisym. & Sym. -CH_3 deformation
1166 s	1170 m	The C–H in-plane bending vibrations
1141 m	1141 s	C–N stretching
1039 s	1047 m	C–C deformation
858 s	869 s	C-H torsion
713 s	759 s	C–H out of- plane bending vibrations

semicircular arcs corresponding to the grain (bulk), grain boundary and electrode contributions. It is also seen that the semicircles at all temperatures are somewhat depressed instead of having centres on the real axis. The reasons for such non-Debye type[23] behaviour may be due to the distribution of relaxation times within the bulk material[24] and distortion due to other relaxations[25]. The best fitted equivalent circuit for the material is composed of a series combination of three RC elements (fig 5a). The typical fitting results at various temperatures are illustrated in table 2. The standard deviations less than 0.05 confirm the validity of the proposed equivalent circuit. The high frequency RC element corresponds to the grain; the medium frequency corresponds to grain boundary and the low frequency corresponds to electrode contributions. Three distinct semicircular arcs are not observed as the values of bulk, electrode and grain boundary contributions are not far away. Hence the semicircular pattern in the Nyquist plot is due to the cascading effect of the three contributions.

The electrical conductivity (σ_i) is calculated by using the equation

$$\sigma_i = \frac{1}{R_i} \times \frac{t}{A} \quad ...(2)$$

where t is the thickness, A is the area of the pellet and R_i is the resistance obtain from

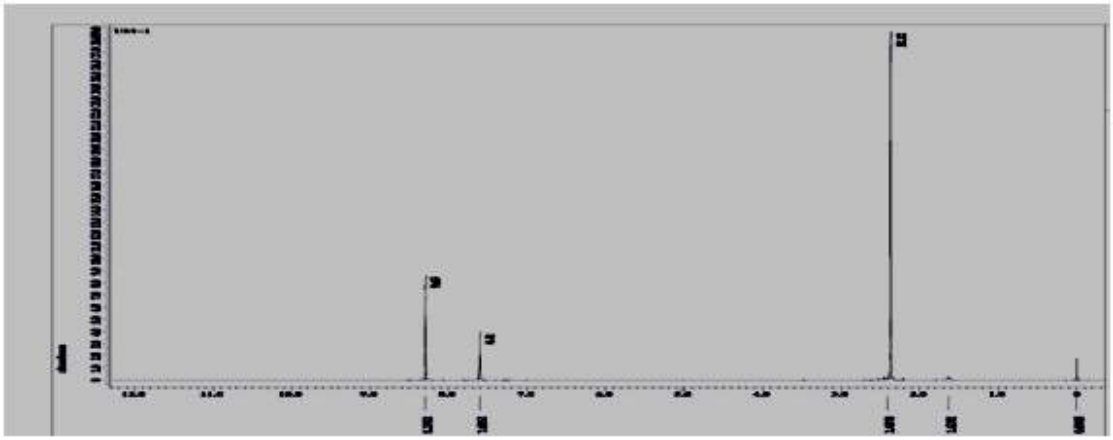

Fig. 3: ^{1}H NMR spectrum of 3,5-dimethylpyridine-iodine complex

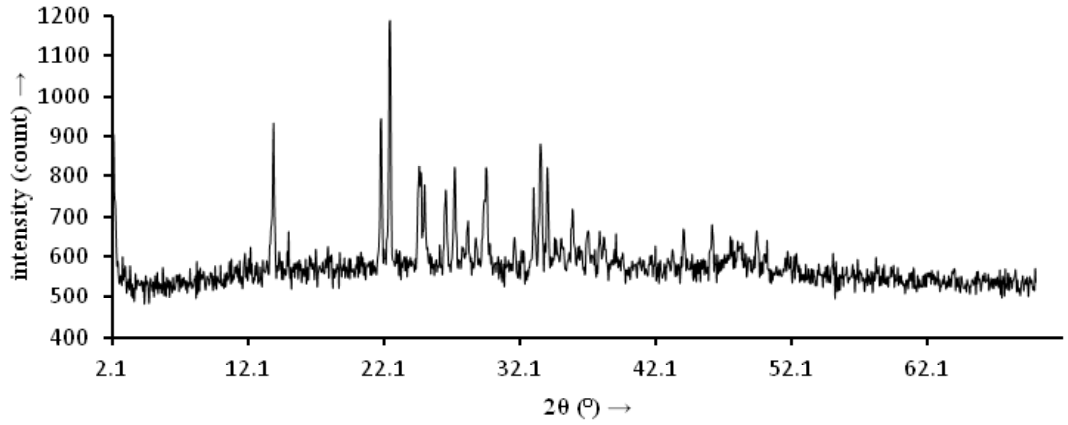

Fig. 4: x-ray diffraction pattern of 3,5-dimethylpyridine-Iodine complex

simulated data. It is seen that the total resistance, R_{total} obtained from the intercept of the semicircle on the low frequency side of the real axis (Z') follows the relation; $R_g + R_{gb} + R_{el} = R_{total}$,which once again confirms the validity of our proposed equivalent circuit. Figure 6 show that σ_i follows the well known Arrhenius relationship

$$\sigma_i = \sigma_0 \, e^{-\left(\frac{E_a}{K_B T}\right)} \quad ...(3)$$

The activation energy of conduction E_a is calculated from the slope of the logσ_i versus 1000/T curves and the values are $E_{a\,(g)}$ = 0.51eV, $E_{a\,(gb)}$ = 0.80eV, $E_{a\,(el)}$ = 0.98eV and $E_{a\,(total)}$ = 0.82eV.

Figure 7 shows the variation of real part of impedance (Z') with ac frequency at various temperatures. It is observed that Z' value decreases with the increase in frequency for different temperature and at higher frequencies the values of Z' merges for all the temperatures. The merging of Z' values in the higher frequency region may be an indication of the release of polarization effect[26]. In the lower frequency region, the Z' value decreases with the rise in temperature. Hence, the material exhibits negative temperature coefficient of resistance (NTCR) behaviour like semiconductors. The effect of increasing frequency and temperature is to reduce the barrier potential of the material which

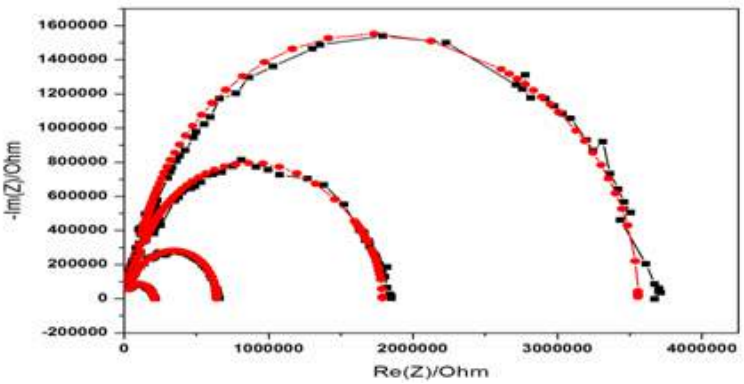

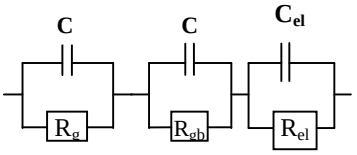

Fig. 5(a) '-(RC)-(RC)-(RC)-' Equivalent circuit

Fig. 5: Experimental (black) and Simulated (red) Nyquist plot for 3,5-dimethylpyridine-Iodine

Table 2: Simulated data of the electrical parameters for the proposed equivalent circuit

T (K)	R_g (Ω^{-1})	C_g (*F*)	R_{gb} (Ω^{-1})	C_{gb} (*F*)	R_{el} (Ω^{-1})	C_{el} (*F*)	Σ Ri
303	1.00×10^{5}	3.27×10^{-11}	2.43×10^{6}	2.62×10^{-11}	1.03×10^{6}	1.88×10^{-10}	3.56×10^{6}
313	8.37×10^{4}	3.14×10^{-11}	1.38×10^{6}	2.65×10^{-11}	3.23×10^{5}	3.79×10^{-10}	1.79×10^{6}
323	2.57×10^{4}	2.97×10^{-11}	4.65×10^{5}	4.43×10^{-11}	1.51×10^{5}	4.39×10^{-11}	6.41×10^{5}
333	2.09×10^{4}	1.88×10^{-11}	1.61×10^{5}	2.93×10^{-11}	2.99×10^{4}	1.07×10^{-09}	2.12×10^{5}

Table 3: Electrical parameters of 3, 5-dimethylpyridine-iodine complex

T (K)	Conductivity ($\Omega^{-1}cm^{-1}$)				Relaxation time, τ (s)		
	σ_g	σ_{gb}	σ_{el}	σ_{total}	τ (g)	τ (gb)	τ (el)
303	1.42×10^{-6}	5.84×10^{-8}	1.39×10^{-7}	3.40×10^{-8}	3.27×10^{-6}	6.38×10^{-5}	2.69×10^{-5}
313	1.70×10^{-6}	1.03×10^{-7}	4.40×10^{-7}	7.95×10^{-8}	2.63×10^{-6}	3.67×10^{-5}	8.57×10^{-6}
323	5.52×10^{-6}	3.06×10^{-7}	9.43×10^{-7}	2.22×10^{-7}	7.65×10^{-7}	2.06×10^{-5}	6.68×10^{-6}
333	6.80×10^{-6}	8.81×10^{-7}	4.76×10^{-6}	6.71×10^{-7}	3.94×10^{-7}	4.72×10^{-6}	8.74×10^{-7}

is consequently responsible for the enhancement of AC conductivity.

The variation of imaginary part of impedance (Z") with ac frequency at various temperatures is shown in figure 7(a). It is observed that with rise in frequency the Z" value increases first reach a maximum peak $Z"_{max}$ and decreases again. Although the peaking behaviour indicates the single relaxation process, the relatively narrow peak at 303K just indicates a narrow distribution of relaxation times in the system. The progressive broadening of this peak upon heating reveals that this distribution gradually becomes wider. It is also observed that the value of Z" decreases with temperature and the effect being more distinct at the peak position. With rise in temperature the peak i.e. value of $Z"_{max}$ shifted to the right. This observation indicates that many relaxation mechanisms are present in the CT material one of them is the temperature dependent electrical relaxation phenomenon indicated by the asymmetric peaks pattern[27].

The variation of (Z" /Z" max) with frequency at various temperatures is shown in figure 7(b). It is seen that there is a peak at each temperature with a somewhat asymmetric broadening and the broadening increases as temperature increases. The peak broadening suggests that there are various electrical processes with a distribution of relaxation times[28].

The relaxation time (τ) was calculated by using the relation[9]

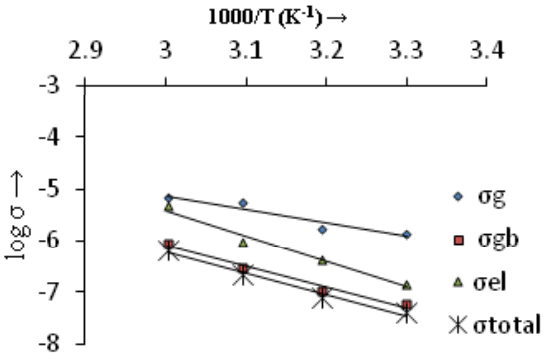

Fig. 6: Temperature dependance of conductivity of 3,5-dimethylpyridine-iodine complex

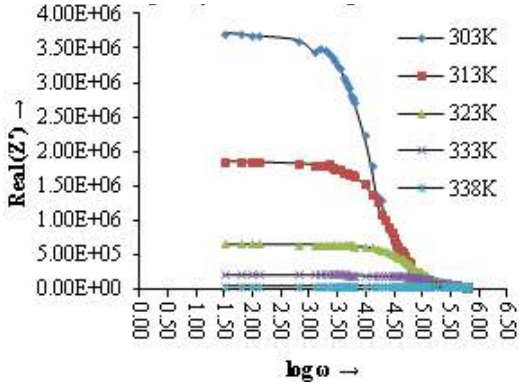

Fig. 7: Variation of real part of impedance with frequency at various temperatures

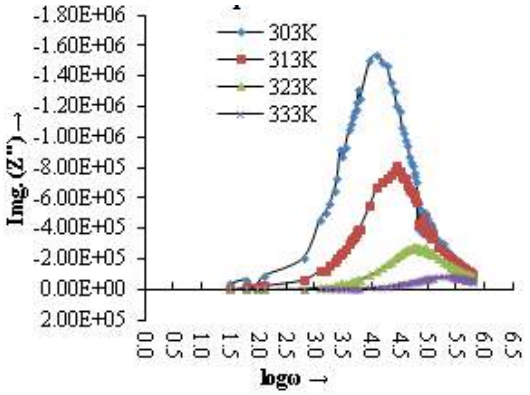

Fig. 7(a): Variation of imaginary part of impedance with frequency at various temperatures

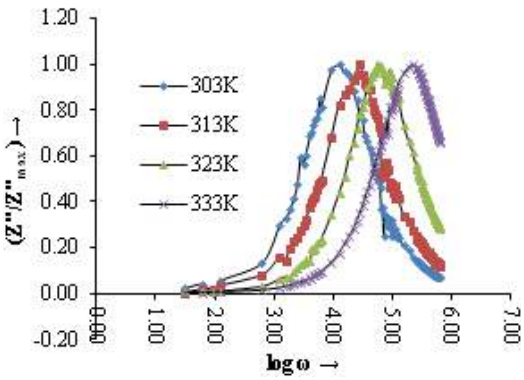

Fig. 7(b): Normalized imaginary part of impedance (Z"/Z"max) as a function of frequency at various temperatures

$$\tau = \frac{1}{\omega} = \frac{1}{2\pi f_{max}} = R_i C_i \quad ...(4)$$

From table 3, it is seen that with increasing temperature the value of relaxation time (τ) decreases, which indicates the semiconducting behaviour of the material. Further, like conductivity, relaxation times also follows the Arrhenius equation with activation energy $E_{a\,(\tau,g)}$ = 0.66eV, $E_{a\,(\tau,gb)}$ = 0.72eV, $E_{a\,(\tau,el)}$ = 0.94eV. (Fig. 8)

$$\tau_b = \tau_0\, e^{-\left(\frac{E_a}{K_B T}\right)} \quad ...(5)$$

Dielectric Properties

Figure 9 depicts the variation of real part of permittivity (i.e. dielectric constant, ε') with frequency at various temperatures. Figure 9(a) shows the variation of imaginary part of permittivity (i.e. dielectric loss, ε") with frequency at various temperatures. It is observed that both dielectric constant and dielectric loss decreases sharply with the increase in frequency in the low frequency region and remains almost constant at higher frequencies for all temperatures under investigation. No any anomalous behaviour or peaking behaviour is seen in the sample. The observed behaviour can be best explained in the light of space charge polarization and hopping model[29]. The decrease of the value of ε' with increase in frequency is a typical characteristic of the polar dielectrics[30]. All types of polarizations contribute in the low frequency region giving higher value of ε' but as the frequency is increased, contributions from the polarizations with large relaxation times cease resulting in the decrease in

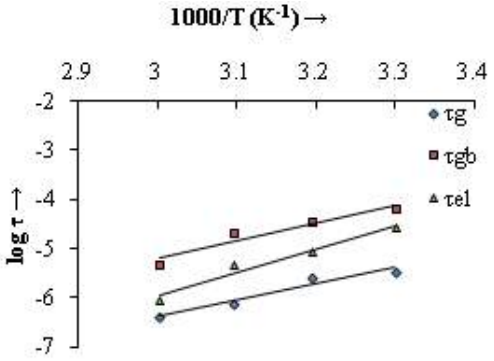

Fig. 8: Arrhenius plot for elaxation times

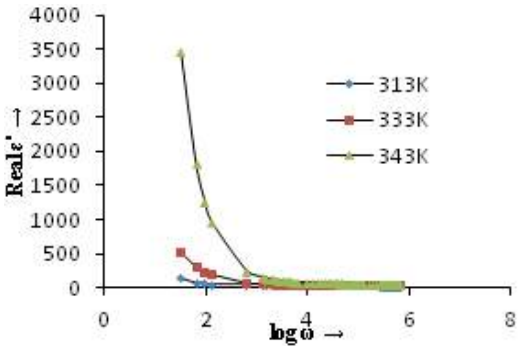

Fig. 9: Variation of Real part of dielectric constant with frequency at various temperaatures

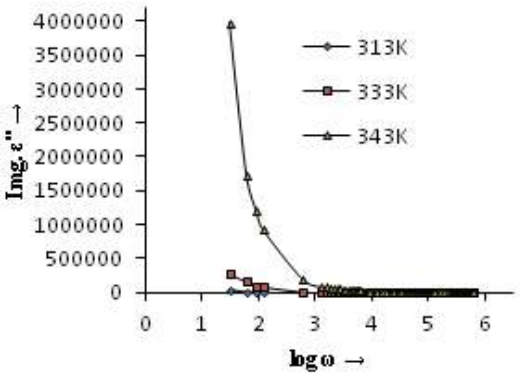

Fig. 9(a): Variation of imaginary part of dielectric constant with frequency at various temperatures

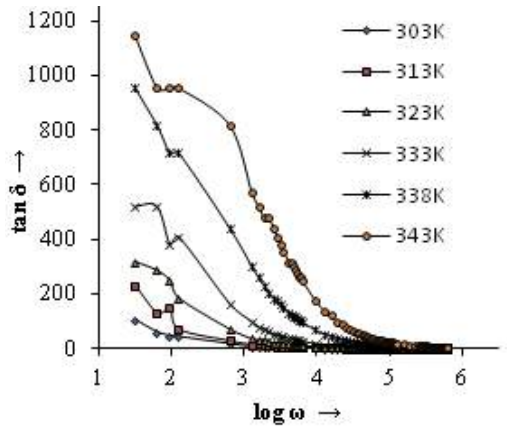

Fig. 10: Variation of tanδ with frequency at various temperatures

ε'. Both ε'and ε'' increases towards low frequencies reaching extremely high values that reflects the electrode-sample interface polarization effect which are further confirmed by the well-defined dc regime of the logσ variation with logω (fig.11). A many fold increase in the value of ε' has been observed for the sample at higher temperature. Therefore the dipolar and interfacial polarizations are present in the sample as these are strongly temperature dependent and occur prominently at low frequency region. The dispersion in the low frequency region can be attributed due to space-charge effect[41]. The high value of dielectric constant in the lower frequency region is due to the accumulation of charges at the electrode-sample interface giving a large bulk polarization of the material. As frequency increases the polarization decreases and attains a constant value. In high frequency region the dipoles cannot be able to follow changes of the field causing faster polarization leading to decrease even zero value of ε'.

The variation of tangent loss (tan δ) with frequency at different temperatures for the sample is shown in fig 10. At lower frequencies tan δ has a less prominent peak and after that the value of tan δ decreases rapidly with rise in temperature. Since the higher frequency region corresponds to low resistivity (due to grain) a small energy is required for the current carriers to flow and therefore low value of tan δ. It is further observed that the tan δ peak shifts to higher frequency value with the increase in temperature. The observation of tan δ peak at low frequency region where the conductivity is dominated by DC conduction indicates that the losses are mainly by conduction.

With the help of Wagner theory[29] the observed variation of dielectric loss (ε'' and tan δ) with frequency and temperature can be explained. The Wagner theory is based on the assumption that the dielectric material consists of conducting particles (grain) loosely distributed throughout a non-conducting, low-loss matrix. The applied external electric field causes interfacial polarization to the material. Beside temperature and frequency (of applied alternating electric field) the size, shape and orientation of the conducting particles has a decided effect on the dielectric loss. The loss factor is directly proportional to the volume percent of the conducting particles. If all the particles have the same conductivity, there will be a sharp loss maximum at a particular frequency. The presence of even very small quantities of a conducting material such as water can cause high dielectric losses. In general, increase in temperature tends to shorten the relaxation time, so the maximum (peak) dielectric loss becomes smaller and shifts to higher frequencies[32]. The effect of various shapes of conducting particles in non-conducting matrix upon the loss tangent in order of increasing loss tangent are flattened spheroids, spherical particles, elongated needle-like particles, and the concentric structure in which the conducting portion and the non-conducting portion in parallel[8].

Since, at lower frequencies, interfacial polarization and ionic conductance cause appreciable dielectric loss[33] the high dielectric loss value in the lower frequency region is due to the ionic conduction. Similar mixed ionic-electronic conduction in CT complexes has been reported earlier[5, 34, 35]. The higher loss at low frequencies is partly due to traces

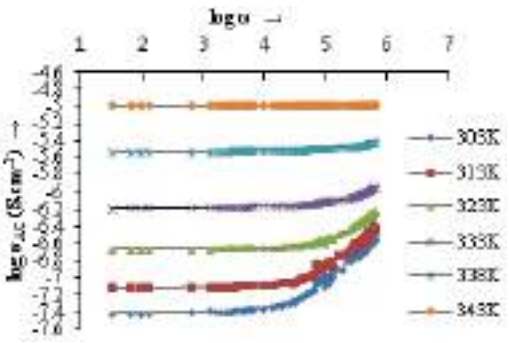

Fig. 11: Variation of AC conductivity with frequency at various temperatures

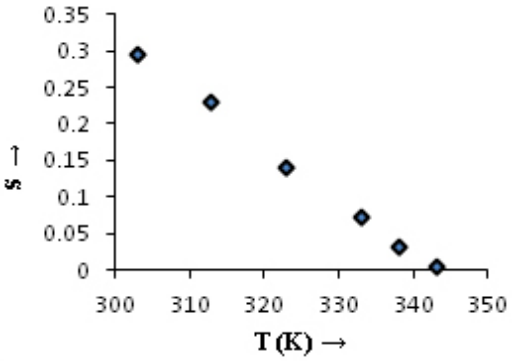

Fig. 11(a): Variation of frequency exponent with temperatures

of moisture in the CT material. Absorbed water may get ionized which results in higher dielectric losses from interfacial polarization and ionic conductance. Similar pattern of the tan δ vs frequency plot as those in fig.10 has been observed by Sillars[10] for concentric structure; hence the structure of our CT material might be that of the conducting particles extending entirely throughout the non-conducting matrix so that the two portions form a parallel circuit. An increase in temperature particularly increases the dielectric losses probably because of high ionic conductance (ionization of the CT complex and absorbed moisture providing the necessary ions). Another cause for the high value of dielectric loss may be due to defects. Imperfection of the material increases at higher temperature and consequently the value of tan δ increases[11].

AC Conductivity study

The variation of AC conductivity with frequency at different temperatures can be understood from the figure 11.

It is seen that AC conductivity increases with the increase in temperature for all frequencies which is attributed to thermal activation. At low frequencies conductivity is nearly frequency independent and in the higher frequency region, dispersion in conductivity has been observed. This pattern was attributed to non-relaxor behaviour of the material[36]. The dispersion is more prominent at lower temperature. These observations can be best explained by using the Jonscher's universal power law[37] -

$$\sigma_{ac}(\omega) = \sigma_{dc} + A\omega^{s} \quad ...(6)$$

where, $\sigma_{ac}(\omega)$ is the AC conductivity, σ_{dc} is the DC conductivity independent of frequency, ω is the angular frequency which equals to $\omega = 2\pi f$, A is a constant and S is the frequency exponent having values between 0 and 1. The frequency exponent S can be obtained from the slope of the plot between logσ versus logω and the intercept of the horizontal portion on the vertical axis equals to $\log\sigma_{dc}$. It is obvious that the value of S decreases with the rise of temperature as shown in figure 11(a). The AC conduction mechanism is considered to be due to barrier hopping[38, 39]. According to this model S can be expressed as-

$$S = 1 - \left(\frac{6K_B T}{w_H}\right) \quad ...(7)$$

where w_H is the barrier height or optical band gap which can be calculated by substituting the value of S, K_B and T. It is seen that the value of optical band gap (or binding energy of charge carriers) is 0.22 to 0.18 eV for the tested temperature range.

CONCLUSIONS

Elemental analysis reveals that 3,5-dimethylpyridine form solid 1:1 CT complex with iodine. Complex impedance analysis indicates the grains, grain boundaries and electrode are responsible in the conduction mechanism of the CT complex. Thus the electrical property of the material is described by three parallel R_gC_g, $R_{gb}C_{gb}$ and $R_{el}C_{el}$ elements connected in series. The conductivities of the CT complex pellet follow the Arrhenius law with activation energy 0.51eV, 0.80eV, 0.98eV and 0.82eV for grain, grain boundary, electrode and total conductivity respectively. The complex shows negative temperature coefficient of resistance (NTCR) behaviour and exhibit temperature dependence relaxation phenomenon. The relaxation is found to be of non-Debye type and the relaxation time (τ) decreases with increasing temperature and obey the Arrhenius law. Dielectric constant, ε' and dielectric loss, ε'' decreases sharply with increase in frequency and increases with rise in temperature. The high value of dielectric loss tangent may be the result of ionization of the complex. The frequency dependence AC conductivity follows the Jonscher's universal power law.

ACKNOwLEDGEMENTS

This work was supported by the U.G.C., NERO under FIP Grant. The authors are thankful to Sudarsan Gogoi, Tezpur University for simulating the impedance data.

REFERENCES

1. Ulanski, J. *Synth. Met*. **1990**, *39*, 13-24. DOI.10.1016/0379-6779 (90)90195-Q
2. John Ferraris, D.O.; Cowan, V.; Walatka, Jr.; Perlstein, J.H. *J. Am. Chem. Soc.* **1973**, *95*, 948-949. DOI: 10.1021/ja00784a066
3. Coleman, L.B.;Cohen, MJ.; Sandman, D.J.; Yamagishi F.G.; Garito A.F.; Heeger A.J. *Sol. State Commun.* **1973,** *12***,** 1125 – 1132.
4. Jurchescu, O.D.; Goetz, K.P.; Vermeulen, D.; Payne M.E.; Kloc C.; McNeil, L.E. *J. Mater. Chem. C*. **2014**, *2*, 3065-3076. DOI: 10.1039/c3tc32062f
5. Akamatu, H.; Inokuchi, H.; Matsunaga, Y. *Nature*, **1954**,*173*, 168-169. DOI:10.1038/173168a0
6. Saito, G.; Murata, T. *Phil. Trans. R. Soc. A.* **2008**, *366*, 139-150. DOI: 10.1098/rsta.2007.2146
7. Boumedjout, M.; Bendjeddou, A.; Abbaz,T.; Sihamtiaouianine; Kaboub, L.; Gouasmia, A.; Villemin, D.; *Oriental Journal of Chemistry*, **2015**, *31(4)*,1887-1895. DOI: 10.13005/ojc/310405
8. Sillars, R.W. *Electrical Engineers, Journal of the Institution of*. **1937**, *80(484)*, 378-394. DOI: 10.1049/jiee1.1937.0058
9. Barsoukov, E.; Macdonald, J.R.; editors. *Impedance Sprectroscopy: Theory, Experiment, and Applications,* **2005**, *2nd ed*. Wiley-Interscience, New York.
10. Foster, R. *Organic Charge transfer complexes*, **1969**, Academic Press, London.
11. Gur'yanova, E.N.; Gol'dshtein, I.P.; Romm, I.P.; *Donor-Acceptor Bond*, **1975**, Keter Publishing House, Jerusalem.
12. MEISP, March, 2002. Kumho Chemical Laboratories, Korea.
13. Vennila, P.; Govindaraju, M.; Venkatesh, G. *Elixir Vib. Spec*. **2013**, *65B*, 20204-20211.
14. Marcos, J.I.; Oter, J.C.; Tocon, I.L.; Arenas, J.F. *Journal of Molecular Structure*, **1999**, *476*, 139–150.
15. Topaqli, A.; Bayan, S.; *Spectroscopy letters*. **1996**, *29(2)*, 277-291. DOI:10.1080/00387019608001602
16. Kantarci, Z.; Bayrak, C.; Bayari, S.; *J.Mol. Struct*. **1997**, *407*, 155-163. DOI: 10.1016/S0022-2860(96)09739-6
17. Bayari, S.; Topaqli, A.; Aydinli, A. *The Spectroscopy Letts*. **1994**, *27(9)*, 1083-1096. DOI:10.1080/00387019408006967
18. Akyuz, S.; Pasaoglu, H.; Davies, J.E.D. *J. Mol. Struct*. **1994**, *317*, 215-221. DOI:10.1016/00222860(93)07851M
19. Gil, V.M.S.; Murrel, J.N. *Trans. Faraday Soc*. **1964**, *60*, 248-255. DOI: 10.1039/TF9646000248
20. Baruah, S.K.; Baruah, P.K. *Asian J. Chem.* **2004**, *16(2)*, 688-694.
21. Rzokee, A.A.; Ahmad, A. *Journal of molecular Structure*, **2014**, *1076*, 453–460. DOI:10.1016/j.molstruc.2014.08.002
22. Alexaner, L.; Klug, H.P. *Journal of Applied Physics*, **1950**, *21*, 137-142. DOI: 10.1063/1.1699612
23. Suman, C.K.; Prasad, K.; Choudhary, R.N.P. *Indian Journal of Engineering & Materials Sciences*, **2008**, *15*, 157-162.
24. Barde, R.V.; Nemade, R.K.; Waghuley, S.A. *Journal of Asian Ceramic Societies*, **2015**, *3*, 116-122. DOI:10.1016/j.jascer.2014.11.006
25. Hafidi, E.; El Omari, M.; El.Omari, M.; Bentayeb, A. Bennazha, J. El Maadi, A. Chehbouni M. *Arabian Journal of Chemistry*, **2013**, *6*, 253–263. DOI: 10.1016/j.arabjc.2011.01.028
26. Plocharski, J.; Wieczoreck, W. *Solid State Ionics*, **1988**, *28-30*, 979-982. DOI:10.1016/0167-2738(88)90315-3
27. Suman, C.K.; Prasad, K.; Choudhary, R.N.P.; *Adv. Appl. Ceram*. **2005**, *104*, 294-299. DOI:10.1179/174367605X62580
28. Suman, C.K.; Prasad, K.; Choudhary, R.N.P. *J. Mater. Sci*. **2006**, *41*, 369-375. DOI: 10.1007/s10853-005-2620-5
29. Jianjun, L.; Duan, CG.;Yin, WG.; Mei, W.N.; Smith R.W.; Hardy, John R. *Physical Review B.* **2004**, *70*, 144106(1-7). DOI: 10.1103/PhysRevB.70.144106
30. Singh, N.K.;Kumar, P.; Kumar, A.; Sharma, S. *Journal of Engineering and Technology Research,* **2012***, 4(6),* 104-113. DOI: 10.5897/JETR12.002
31. Shirsath, S.E.; Jadhav, S.S.; Toksha, B.G.; Patange S.M.; Jadhav, K.M. Scr. *Mater.* **2011***, 64,* 773-776. DOI:10.1016/j.scriptamat.2010.12.043

32. Stoops, W.N. *J. Am. Chem. Soc.* **1934***, 56(7)*, 1480–1483. DOI: 10.1021/ja01322a011
33. Hazen, T.; Wangsgard, P.; *J. Electrochem. Soc.* **1946***, 90(1)*, 361-375. DOI: 10.1149/1.3071752
34. Nishizaki, S.; Kusakawa, H.; *Bull. Chem. Soc. Jpn.* **1963***, 36*, 1681-1683.
35. Singh, R.A.; Singh, V,K.; 1997. *Bull. Mater. Sci.* **1997***, 20(3),* 305-315.
36. Naceur, H.; Megriche, A.; El Maaoui, M.; *Oriental Journal of Chemistry*, **2013**, *29(3),* 937-944. DOI: 10.13005/ojc/290311
37. Jonscher, A.K. *Nature,* **1977***, 267*, 673-679. DOI:10.1038/267673a0
38. Elliott, S.R. *Philos.Mag.* **1977***, 36,* 1291-1304. DOI:10.1080/14786437708238517
39. Ali, A.A.; Shaaban, M.H.; *Solid State Sci.* **2010***, 12*, 2148-2154. DOI:10.1016/j. solidstatesciences.2010.09.016

Ionics
DOI 10.1007/s11581-016-1794-y

ORIGINAL PAPER

Mixed ionic and electronic conductivity study of charge transfer complexes of some substituted pyridines with iodine monochloride (ICl) by AC impedance spectroscopy

Uttam Mohan[1,2] · **Pallavi Gogoi**[3] · **S. K. Baruah**[2]

Received: 26 April 2016 / Revised: 26 July 2016 / Accepted: 2 August 2016

Abstract Mixed ionic and electronic conductivity of three solid charge transfer (CT) complexes of pyridine, 4-methylpyridine (γ-picoline) and 3,5-dimethylpyridine (3,5-lutidine) with ICl (iodine monochloride) are reported. Electrical parameters of the prepared complexes in the pellet form are evaluated at various temperatures and at wide frequency range by employing AC complex impedance spectroscopic technique. Suitable equivalent circuits for the Nyquist plots, which provide the most realistic model of the electrical properties of the CT complexes, have been suggested. Both transport number measurements and impedance spectra reveal that the conduction in γ-picoline-ICl complex is mainly due to ions, in 3,5-dimethylpyridine-ICl complex, it is due to both ions and electrons and in pyridine-ICl complex, it is predominantly due to electrons. The a.c. conductivity measurements of the CT complexes have been carried out in the frequency range of 10–10^5 Hz within the temperature range of 303–353 K. The variation of a.c. conductivity with frequency follows the Jonscher's universal power law. The temperature dependence of electrical conductivity suggests the semiconducting behaviour of the materials.

Keywords CT complex · Mixed conduction · Impedance spectra · Transport number

Introduction

The intermolecular interaction between electron donor D and electron acceptor A leads to the formation of a new molecular assembly, DA, called charge transfer (CT) complex, first introduced by Mulliken [1, 2]. Organic CT complexes and salts have extensively been investigated in various areas of chemistry and material sciences both from the theoretical and experimental aspects as they exhibit diverse kind of interesting physical properties and functionalities related to optical, magnetic, electrical (super) conductivity and dielectric properties [3, 4]. Since the discovery of the first metallic type CT complex TTF-TCNQ in 1973 [5], attention to organic CT complexes has been focussed for several decades, aimed mainly at the discovery of materials with good electrical conductivity or even room temperature superconductivity [6]. Later on, attention has been turned to technologically relevant properties of CT complexes due to their potential in the improvement of electronic and optoelectronic devices [7].

The solid organic CT complexes are one of the most important subclasses of organic semiconductors [8, 9] which often exhibit similar conduction mechanism to inorganic semiconductors where hole and electron conduction layers are typical carriers separated by a band gap. CT complexes exhibiting mixed ionic-electronic conduction have also been reported [10–13].

Although, the electrical conductivity of charge transfer complexes of pyridine analogue with halogens and interhalogens has been reported in literatures [14–16]; however, the detailed studies of frequency dependence a.c. conductivity and complex impedance spectroscopy of these complexes

Electronic supplementary material The online version of this article (doi:10.1007/s11581-016-1794-y) contains supplementary material, which is available to authorized users.

✉ Uttam Mohan
uttamohan@rediffmail.com

[1] D. H.S.K. College, Dibrugarh, Assam, India

[2] Department of Chemistry, Dibrugarh University, Dibrugarh, Assam, India

[3] Department of Chemistry, Tinsukia College, Tinsukia, Assam, India

Post-checked on 16 August 2016

are lacking. In this paper, the electrical properties of the CT complexes obtained by the interactions of three n-donors namely pyridine, 4-methylpyridine and 3,5-dimethylpyridine with iodine monochloride (ICl) as σ-acceptor are reported.

Despite the fact that the electrical conduction property of a donor-acceptor complex depends upon many factors, to manifest high conductivity, the mixed valence (or partial CT state) electronic structure and specific molecular packing architecture (segregated stacking and mixed stacking) within the molecular assembly are the most essential criteria [17]. The degree of charge transfer, δ from donor (D) to acceptor (A), in the complex ($D^{+\delta}A^{-\delta}$) is primarily governed by the ionization potential (I_p) of D and electron affinity (E_a) of A. A neutral CT complex with $\delta = 0$ is obtained if $E_a > I_p$, whereas the completely ionic state corresponds to $\delta = 1, 2.....$ when $E_a < I_p$. Both neutral and completely ionic CT complexes are insulators with few exceptions [18, 19]. It is reported [7, 20] that mixed valence CT complexes within the window $0.50 < \delta < 0.74$ with segregated stacks of the D and A components generally exhibit metallic electrical conduction; otherwise, alternating stack CT complexes are either semiconductors or insulators.

For the study of microstructural and electrical properties of many electronic materials, the AC impedance spectroscopy has long been used as a non-destructive experimental technique [21]. In this technique, a sinusoidal perturbation is applied on the test system and the AC response is analysed. The ratio of the voltage response to the current perturbation is the impedance which is calculated as a function of the frequency of the perturbation. The interpretations of the impedance spectra ($-Z''_{im}$ vs Z'_{real}) are aided by analogy to physically plausible equivalent circuits involving simple components such as capacitors and resistors connected in many modes. From this analysis, a meaningful insight into the material behaviour can be obtained. The analysed values of the electrical parameters (conductivity, dielectric constant, loss, capacitance, etc.) give explicit results when compared with those measured at arbitrarily selected fixed frequencies. This powerful technique is useful for the measurement of real and imaginary part of impedances for a wide range of frequency, determination of relaxation frequency and separation of grain, grain boundary and grain-electrode effects [22, 23].

Experimental

Materials

Pyridine (from Ranbaxy Lab. Ltd.), 4-methylpyridine (from Sigma Aldrich), 3,5-dimethylpyridine (from Sigma Aldrich) and ICl (from Ranbaxy fine chemical Ltd.) were used without further purification. Hexane (Merck) was used after distillation as a solvent.

Synthesis and characterization of complexes

The solid CT complexes of the pyridine analogue with ICl were prepared by stirring equimolar quantities of the donor with ICl in hexane, which resulted in precipitation of the complex as light yellow solid. The separated solids were filtered and washed several times with minimum amount of hexane and these are dried under vacuum over anhydrous calcium chloride. The resultant complexes were characterised by routine techniques like elemental analysis, UV-Vis, FTIR, ^{1}H-NMR spectroscopy and powder XRD.

The elemental analysis of the carbon, hydrogen and nitrogen content was performed by using Perkin Elmer CHN 2400 Series II analyzer. The total halogen contents were estimated by a simple gravimetric method with $AgNO_3$ solution.

The electronic absorption spectra of the donors, acceptor and the resulting complexes in hexane were recorded over a wavelength range of 200–900 nm using Shimadzu U-3900 spectrophotometer. The diffuse reflectance spectra of the solids were recorded with a JASCO V-750 UV Visible spectrophotometer in the region 200–900 nm.

The FT-IR spectra were recorded on a Shimadzu FT-IR spectrophotometer (IRPrestige-21) within the range of 4000–250 cm^{-1}.

The ^{1}H-NMR spectra were recorded in $CDCl_3$ solvent. Powder XRD analysis was carried out at room temperature by using Cu radiation (λ = 1.5405 Å) in the range $2° \leq 2\theta \leq 70°$ at a scanning rate of 1°/min and step height of 0.05°.

Electrical properties

The solid complexes were pelletized into discs of 13 mm diameter by using a hydraulic press (Spectralab) at a pressure of 9 Kbar. The thicknesses (0.5 to 1.5 mm) were measured with a screw gauge. Uniform graphite layer was applied on the opposite faces of the pellets and was sandwiched between two thin sheets of copper electrodes with even surface. Before recording the data, each sample was sintered at 50 °C for 30 min to ascertain the interface contact between the electrodes and the sample. The electrical properties were measured by complex impedance method using LCR HiTester (HIOKI 3522) frequency response analyser in the frequency range from 10 Hz to 100 kHz. AC conductance (G), impedance (Z) and phase angle (θ) were measured as a function of frequency at different temperatures. The sample cell was kept for 30 min at each measuring temperature in order to reach its thermal equilibrium. The impedance spectra were modelled as an 'equivalent circuit' by using complex non-linear least squares fitting of both real and imaginary part of impedance. LEVM 3.0 software [24] has been used for fitting purpose. The best fitted equivalent circuit has been determined by observing the coherence between the experimental and the simulated data

in the complex impedance plots. D.C. conductance of the pellets was measured at various temperatures by using Keithley 2400 source meter. Electrical conductivity was calculated using the pellet dimensions and the measured resistance.

Determination of ionic transport number

The total ionic transport numbers, t_{ion}, were evaluated by the standard Wagner polarization technique [25]. The cell 'SS| CT complex |SS' was polarized by a step potential of about 1 V and the resulting current was monitored as a function of time [26, 27], where SS stands for stainless steel. The SS acted as blocking electrodes for the above cell. The t_{ion} values were evaluated from the polarization current curve by using the following equation:

$$t_{ion} = \frac{(i_i - i_f)}{i_i} \quad (1)$$

where i_i and i_f are the initial and final steady state currents, respectively.

Results and discussion

Elemental analysis

Elemental analyses data (C, H, N and total halogen) of the complexes were given in Table 1. It is observed that the experimental values agree quite well with the calculated values for 1:1 complexes. The same stoichiometries in the solution state are confirmed by the linearity of the Benesi-Hildebrand plots (S1).

UV-Vis spectroscopy

In the electronic absorption spectra (S2) of the resulting complexes (in hexane), an additional absorption band at λ_{max} = 333.4, 316.8 and 322.4 nm for pyridine-ICl, 4-methylpyridine-ICl and 3,5-dimethylpyridine-ICl complexes, respectively, indicates the formation of CT complexes.

In the diffuse reflectance spectra of the solid complexes (Fig. 1), the bands at 256, 322 and 371 nm for pyridine-ICl, at 239, 262, 301 and 361 nm for 3,5-dimethylpyridine-ICl and at 253, 312 and 427 nm for 4-methylpyridine-ICl complexes

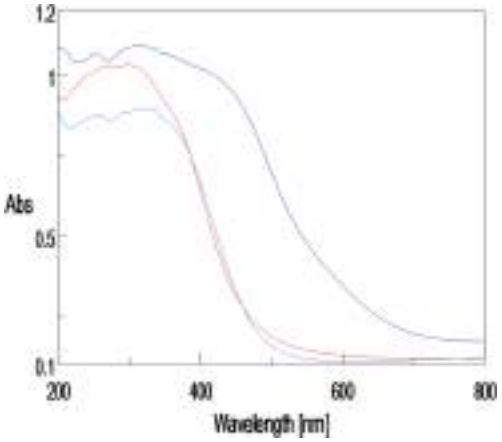

Fig. 1 Diffuse reflectance spectra of pyridine-ICl (*blue*), 3,5-dimethylpyridine-ICl (*red*) and 4-methylpyridine-ICl (*purple*) complexes

indicate the presence of ICl_2^- ion in the solid state [28]. The formation of ICl_2^- ion is attributed to the solid state transformation of the CT complexes (e.g. 4-methylpyridine-ICl) as follows:

$$2\,\gamma\text{–Pic–ICl} \rightarrow (\gamma\text{–Pic}_2\text{–I})^+ + ICl_2^-$$

The optical band gaps of the CT complexes were estimated from the optical absorption edge of the spectrum by using the Tauc relation [29]

$$A h\nu = \left(h\nu - E_g\right)^n \quad (2)$$

where A is the absorbance, E_g is the optical band gap corresponding to a particular absorption of photon of energy hν and n is ½ for allowed direct, 3/2 for forbidden direct, 2 for allowed indirect and 3 for forbidden indirect transitions in the material. It is observed that $(Ah\nu)^{1/2}$ versus hν plots are linear (Fig. 2) and the intercept on the energy axis on extrapolating; the linear portion of the curves to A = 0 gives the indirect band gap. The values of E_g are given in Table 2.

FTIR spectroscopy

Few selected IR frequencies of the donor on complex formation are affected in both intensities and wave number values (S3a–c). This could be interpreted on the basis of expected electronic environment change upon

Table 1 Elemental analysis data of the CT complexes

Complex	C, %		H, %		N, %		Halogens, %	
	Cal.	Found	Cal.	Found	Cal.	Found	Cal.	Found
Py-ICl	24.86	24.36	2.07	2.12	5.80	5.62	67.26	67.05
4-MePy-ICl	28.19	28.25	2.74	3.04	5.48	5.30	63.58	63.84
3,5-DiMePy-ICl	31.18	30.60	3.34	3.37	5.19	5.24	60.28	60.33

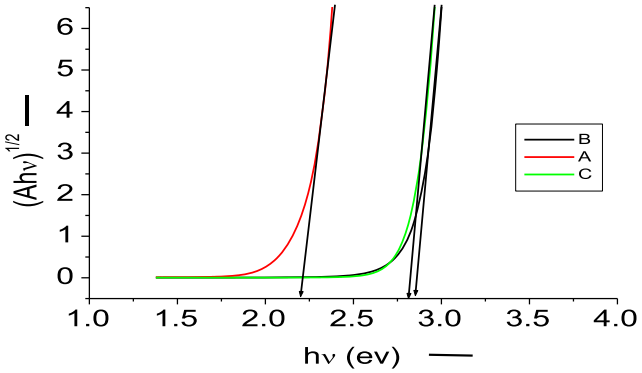

Fig. 2 $(Ah\nu)^{1/2}$ vs hν (photon energy) plot of **A** 4-methylpyridine-ICl (*red*), **B** 3,5-dimethylpyridine-ICl (*black*) and **C** pyridine-ICl (*green*) complexes

Table 2 Physical properties, optical band gap and ionic transport no. of the CT complexes

Complex	Colour	m.p. (K)	E_g (ev)	t_{ion}
Py-ICl	Light yellow	132	2.85	0.11
4-MePy-ICl	Yellow	113	2.21	0.95
3,5-DiMePy-ICl	Light yellow	170	2.78	0.58

complexation. The detailed vibrational assignments were reported in Table 3. These assignments were in accordance with earlier works [30, 31].

It is observed that the spectra of the CT complexes show all the principal features for free donors. Many modes on complex formation have been shifted to higher frequency in comparison to the free donor. Similar upward shifts were observed for metal coordinated pyridine [32] and metal coordinated pyridine analogues [33, 34]. It has been reported [35] that iodine monochloride (ICl) has an allowed fundamental absorption at 382 cm^{-1} in the gas phase and the I-Cl stretching frequency decreases on complex formation with strong donor like pyridine. The bands at 290 cm^{-1} for pyridine-ICl, 265 cm^{-1} for 4-methylpyridine-ICl and 273 cm^{-1} for 3,5-dimethylpyridine-ICl complexes have been assigned to I-Cl stretching in the complexes [36].

^{1}H-NMR spectra

The ^{1}H-NMR spectra of CT complexes (S4a-c) showed the δ values for ring and methyl group protons in the donor molecules are shifted towards lower field (Table 4). The smallest change was observed for α protons on comparing the chemical shifts of β, γ and methyl protons; it could be explained by the paramagnetic effect observed previously [37] in free donors. The observed down-field shift for all protons is attributed to the decrease of electron density on each ring carbon as a consequence of partial positive charge at the nitrogen atom on complex formation.

Table 3 FTIR frequencies (cm^{-1}) of the donors and their CT complexes

Pyridine	Py-ICl	4-MePy	4-MePy-ICl	3,5-DiMePy	3,5-DiMePy –ICl	Assignment
3074s	3093s	3066w	3139w	3020s	3049s	C–H stretching
3026s	3063s	2960w	3080m	2980s	3014s	C–H stretching
–	–	2922m	2968vw	2866m	2900m	C–H ($-CH_3$) stretching
1923w	1845w	–	1928m	1860vw	1865w	overtone of C–H vibration
–	–	–	1836w	1792vw	1805w	overtone of C–H vibration
1580s	1599s	1589s	1610vs	1585s	1593s	C=N stretching
1481m	1525s	1458s	–	1458m	1466vw	C=C stretching
1439s	1477m	–	1421s	1427s	1442s	C=C stretching
–	1323w	1375w	1373w	1381m	1384m	Antisym. and Sym. CH_3 deformation
1215s	1244m	–	–	1234w	1267w	
1145s	1192m	1226vw	1249m	1166s	1170m	The C–H in-plane bending vibrations
1066m	1157m	1157w	1201s	1141m	1141s	C–N stretching
1029m	1060s	1059w	1060s	1039s	1047m	C–C deformation
991m	1014w	1031w	1020s	858s	869s	C–H torsion
700m	742m	777s	810vs	713s	759s	γ (C–H)
690w	684w	–	707w	–	692m	δ ring
605m	634w	–	545s	–	536vw	
405m	424vw	–	486s	–	–	γ ring
–	374s	–	358w	–	362s	X-sensitive
–	290s	–	265s	–	273s	ν_{I-Cl}

v- very, s- strong, m- medium, w- weak

Table 4 ^{1}H Chemical shifts (δ ppm) of the CT complexes and the parent donors

Compound	Hα	Δα	Hβ	Δβ	Hγ	Δγ	–CH_3 β	–CH_3γ	Δ–CH_3
Pyridine	8.50	–	7.04	–	7.46	–	–	–	–
Pyridine-ICl	8.67	0.17	7.47	0.43	8.02	0.56	–	–	–
4-methylpyridine	8.50	–	7.16	–	–	–	–	2.41	–
4-methylpyridine-ICl	8.51	0.01	7.28	0.12	–	–	–	2.48	0.07
3,5-dimethylpyridine	8.25	–	–	–	7.27	–	2.23	–	–
3,5-dimethylpyridine-ICl	8.29	0.04	–	–	7.60	0.33	2.40	–	0.17

Powder XRD analysis

The room temperature X-ray diffraction pattern of pyridine-ICl complex (S5a) showed a good agreement with the single crystal data [38]. The good agreement between the observed (d_{obs}) and calculated (d_{cal}) inter-planar spacing (Table 5) confirmed that the prepared complex has a monoclinic structure, as reported earlier, with unit cell lattice parameters $a = 4.274$ Å, $b = 12.319$ Å, $c = 14.094$ Å, $\beta = 94.99°$ and unit cell volume 739.3 Å^3.

For the lack of crystal structure data about 4-methylpyridine-ICl and 3,5-dimethylpyridine-ICl complexes, Powder-X software has been applied in order to index the diffraction pattern. It is found that the diffraction pattern of both the complexes are best fitted to a monoclinic unit cell with the estimated lattice parameters $a = 8.335$ Å, $b = 12.830$ Å, $c = 18.313$ Å, $\beta = 90.03°$ and $V = 1958.3$ Å^3 for 4-methylpyridine-ICl and for 3,5-dimethylpyridine-ICl complex are $a = 6.636$ Å, $b = 18.935$ Å, $c = 8.789$ Å, $\beta = 97.06°$ and $V = 1095.99$ Å^3. The inter-planar spacing (d_{hkl}) values were calculated by using Eq. (3) for monoclinic system and a quite good agreement between the observed (d_{obs}) and calculated (d_{cal}) values (Table 5) confirmed the estimated unit cell parameters.

$$\frac{1}{d_{hkl}^2} = \frac{h^2}{a^2 \mathrm{Sin}^2\beta} + \frac{k^2}{b^2} + \frac{l^2}{c^2 \mathrm{Sin}^2\beta} - \frac{2hl\mathrm{Cos}\beta}{ac\mathrm{Sin}^2\beta} \quad (3)$$

The average grain size (D) of the samples was calculated from the most intense x-ray diffraction peak by using the classical Scherer [39] formula

Table 5 Comparison of d_{obs} and d_{cal} (Å) values of some reflections for the CT crystals at room temperature

Pyridine-ICl			4-methylpyridine-ICl			3,5-dimethylpyridine-ICl		
h k l	d_{obs} (Å)	d_{cal} (Å)	*h k l*	d_{obs} (Å)	d_{cal} (Å)	*h k l*	d_{obs} (Å)	d_{cal} (Å)
0 0 2	7.049	7.073	0 1 1	10.766	10.508	1 1 1	7.788	7.872
0 1 2	6.087	6.126	0 0 4	4.588	4.578	0 3 1	6.385	6.235
0 2 1	5.605	5.675	0 1 4	4.350	4.312	0 1 3	4.523	4.552
0 2 2	4.607	4.660	1 0 4	4.032	4.013	1 0 3	4.095	4.030
0 1 3	4.361	4.407	1 2 3	3.920	3.907	0 3 3	3.877	3.875
0 3 0	4.022	4.130	1 3 2	3.510	3.514	1 4 2	3.800	3.799
0 3 1	3.949	3.965	2 1 3	3.323	3.325	0 5 2	3.587	3.588
0 2 3	3.775	3.752	2 0 4	3.079	3.082	0 0 4	3.510	3.498
0 3 2	3.697	3.567	3 1 2	2.580	2.604	3 5 0	3.088	3.086
0 0 4	3.531	3.537	1 4 4	2.509	2.506	4 4 0	2.866	2.868
0 3 3	3.084	3.107	2 1 6	2.416	2.418	0 5 4	2.685	2.682
0 4 0	3.047	3.098	1 4 5	2.315	2.318	2 5 4	2.307	2.308
0 2 4	3.000	3.071	–	–	–	4 3 3	2.277	2.278
0 4 1	2.955	3.026	–	–	–	4 4 3	2.167	2.188
0 4 2	2.859	2.837	–	–	–	3 5 4	2.094	2.094
0 3 4	2.753	2.686	–	–	–	–	–	–
0 4 3	2.661	2.589	–	–	–	–	–	–
1 0 0	2.547	2.483	–	–	–	–	–	–
1 1 1	2.320	2.366	–	–	–	–	–	–
1 3 1	2.072	2.082	–	–	–	–	–	–
1 3 2	1.977	1.997	–	–	–	–	–	–

$$D = \frac{K\lambda}{\beta \operatorname{Cos}\theta} \quad (4)$$

where λ is the x-ray wavelength (for Cu-Kα radiation λ = 1.5405 Å), K is a constant (0.90 for Cu grid), θ is the Bragg diffraction angle (half the scattering angle) and β is the full width at half maximum (FWHM) in radians of the main peak. The average particle size for pyridine-ICl, 4-methylpyridine-ICl and 3,5-dimethylpyridine-ICl complexes was found to be 55, 45 and 61 nm, respectively.

Impedance studies

The Nyquist diagrams (−Z vs Z′) are shown in Fig. 3a–c for pyridine-ICl at 303, 313, 318, 323, 333, 343 and 353 K; for 4-methylpyridine-ICl at 303, 313, 318, 323, 328, 333 and 338 K and for 3,5-dimethylpyridine-ICl at 303, 318, 323, 333, 338 and 343 K. The spectra 3a and 3c relative to pyridine-ICl and 3,5-dimethylpyridine-ICl consist of a single semicircle whose radii decrease with the rise in temperature. The spectra 3b related to 4-methylpyridine-ICl are characterised by the appearance of depressed semicircles at higher frequencies with an inclined spike on the low frequency side. The inclined spike on the low frequency side of the semicircles in the spectrum of 4-methylpyridine-ICl is a characteristic of polarization phenomena at the electrode-material interface. Hence, conduction in 4-methylpyridine-ICl is ascribed mainly due to ions. The absence of inclined spike in the impedance spectrum of pyridine-ICl and tiny spike like portion in the low frequency side of the impedance spectrum of 3,5-dimethylpyridine-ICl attribute to either electronic or mixed ionic-electronic conduction [40].

Equivalent circuit fitting

The electrical behaviour of a system can be interpreted in terms of an equivalent circuit containing real electrical elements in various combinations. It should be worth mentioning that a particular electrical circuit can be customized in a variety of combinations of simple electrical elements but at a halt results the same overall a.c. response. Though, there is no unique equivalent circuit for a particular system; however, an equivalent circuit can be selected on the basis of the following criteria:

(i) Keeping in mind as to what kind of impedances is probable to be present in the system in question and how they connected.
(ii) Whether the response of the proposed circuit is consistent to the experimental data.
(iii) Whether the simulated values of the circuit elements (R, C, etc.) are realistic and their variation with temperature is logical.

In general, an equivalent circuit used to describe the impedances of polycrystalline solid materials consists of three parallel RC elements connected in series corresponds to grain interior, grain boundary and electrode [41]. A single parallel RC element gives one semicircular arc passing through the origin in the Nyquist −Z vs Z′ plot and the low frequency intercept on the real Z′ axis corresponds to the resistance R of the element. We expect three semicircular arcs corresponds to the grain (bulk), grain boundary and electrode contributions. In practice, all the semicircles may not be noticed. They may overlap, depress or distort due to the presence of (i) distribution in relaxation times and (ii) very small differences of the time constants of various relaxation processes, if any. The non-ideal nature of the experimental impedance spectrum enforced to fit the experimental data to evaluate the contributions of various circuit elements which otherwise cannot be worked out from the experimental spectrum. In this paper, LEVM 3.0 software [24] has been used for fitting purpose.

Pyridine-ICl complex Although the impedance spectrum (Fig. 3a) seems like a single semicircle at the first sight, the experimental data did not fit well to an equivalent circuit containing a single parallel RC element. The best fit is achieved by using an equivalent circuit comprising of three RC elements connected in series (Fig. 4a). Hence, in this complex grain, grain boundary and electrode contributions are responsible for total hindrance in the material. The values of all parameters of the equivalent circuit, after fitting at different temperatures, are given in Table 6. The validity of the proposed equivalent circuit is confirmed by the excellent coherence between the experimental and the simulated data in the complex impedance plots. The temperature variation of the R_i parameters (in terms of σ_i) obeys the Arrhenius law (Fig. 5).

4-methylpyridine-ICl complex The existence of low frequency straight line indicates the presence of double layer capacitance of electrode-material interface [42] and the semicircular portion corresponds to the parallel combination of resistance and capacitance. But the angle of inclination of the straight line and depressed semicircle indicate the presence of distributed microscopic properties of the material, which is called constant phase element (cpe). Hence, cpe has been introduced in place of ideal capacitive circuit element. The experimental complex impedance spectrum can be best fitted to the equivalent circuit given in Fig. 4b. The depressed semicircle corresponds to the parallel combination of bulk resistance and a constant phase element (cpe) in series with another cpe corresponds to the inclined spike due to interfacial polarization. The inclined spike (as observed in case of a real solid electrolyte) in the complex impedance plot indicates that 4-methylpyridine-ICl complex is mainly ionic. However, for an ideal solid electrolyte, one would expect a vertical straight line (instead of inclined one) on the low frequency side followed by a perfect semicircle (instead of depressed one) in the complex impedance plot.

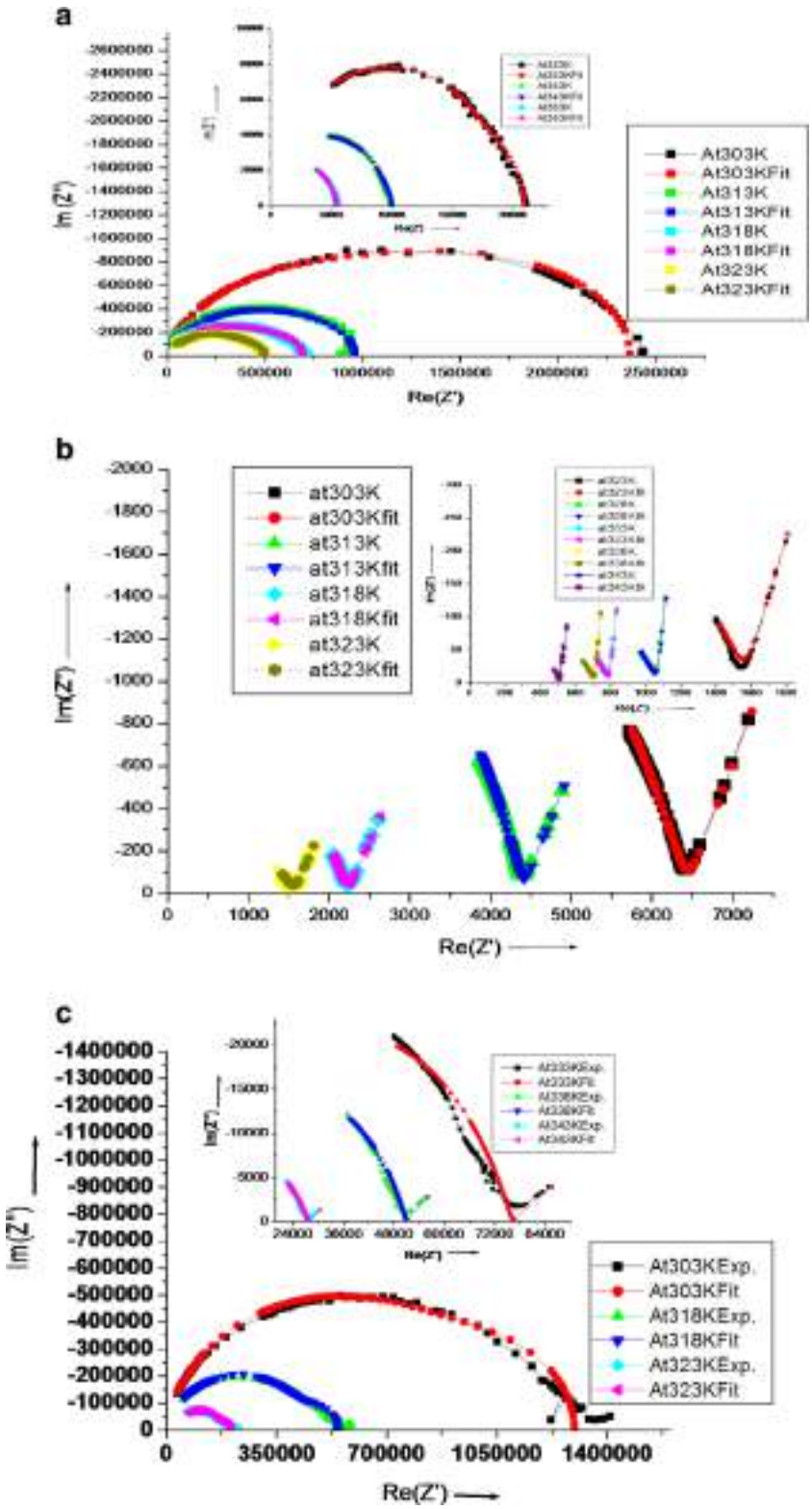

Fig. 3 Nyquist plots of **a** pyridine-ICl, **b** 4-methylpyridine-ICl and **c** 3, 5-dimethylpyridine-ICl complex

3,5-dimethylpyridine-ICl complex The impedance spectra at lower temperatures of this complex have been best fitted to an equivalent circuit comprising of three RC elements connected in series corresponding to grain, grain boundary and electrode interface. However, at 333 K and above, a spike at lower frequency region of the impedance spectra become prominent indicating different conduction mechanism at higher temperatures. Hence, similar equivalent circuit as that

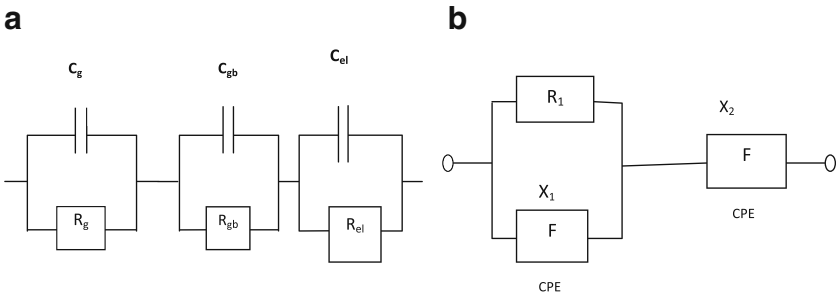

Fig. 4 Equivalent circuit **a** –(RgCg)–(RgbCgb)–(RelCel)– and **b** –(Rcpe)–(cpe)–

of 4-methylpyridine-ICl complex (i.e. 4b) is appropriate for the spectra at 333, 338 and 343 K. At higher temperatures, ionization of the complex transforms the material from mixed conductor to predominantly ionic conductor.

The total conductivity (σ_T) of the sample has been calculated using the total resistance and the dimensions of the pellet with the following equation:

$$\sigma_T = \frac{1}{R_T} \times \frac{t}{A} \quad (5)$$

where t is the thickness, A is the area of the pellet and R_T is the total resistance estimated from the experimental spectrum at low frequency intercept of the semicircle with the real axis. Similarly, the bulk conductivity (σ_g) has been calculated using bulk resistance (R_g) value obtained from fit data. It is also seen that the value of ΣR_i from fit data (Table 6) equals to the value of R_{Total} estimated from experimental spectrum (Table 7) which once again confirms the validity of the proposed equivalent circuits.

AC conductivity study

The frequency dependence of a.c. conductivity i.e. logσ vs logω plots for 4-methylpyridine-ICl complex is characterised by three distinct regimes (i) low frequency polarisation region (ii) the medium frequency plateau region and (iii) high frequency dispersion region (Fig. 6). But for pyridine-ICl and 3,5-dimethylpyridine-ICl complex, only the later two regions

Table 6 Fitted equivalent circuit parameters for the CT complexes

T (K)	R1(Ω^{-1})	C1(F)	R2(Ω^{-1})	C2(F)	R3(Ω^{-1})	C3(F)	$\Sigma R_i(\Omega^{-1})$
Pyridine-ICl							
303	1.12×10^5	4.53×10^{-11}	9.63×10^5	2.60×10^{-11}	1.31×10^6	8.80×10^{-11}	2.38×10^6
313	9.51×10^4	3.67×10^{-11}	5.70×10^5	2.99×10^{-11}	2.79×10^5	1.90×10^{-10}	9.44×10^5
318	8.45×10^4	2.50×10^{-11}	3.85×10^5	2.50×10^{-11}	2.24×10^5	2.09×10^{-10}	6.94×10^5
323	8.31×10^4	2.28×10^{-11}	2.91×10^5	2.75×10^{-11}	1.23×10^5	3.24×10^{-10}	4.97×10^5
333	7.91×10^4	1.86×10^{-11}	1.00×10^5	5.05×10^{-11}	2.96×10^4	1.13×10^{-9}	2.09×10^5
343	5.90×10^4	1.67×10^{-11}	3.40×10^4	1.04×10^{-10}	6.37×10^3	3.79×10^{-9}	9.94×10^4
353	4.32×10^4	1.69×10^{-11}	1.04×10^4	3.10×10^{-10}	1.43×10^3	1.61×10^{-8}	5.50×10^4
3,5-dimethylpyridine-ICl							
303	7.72×10^4	3.65×10^{-11}	8.26×10^5	1.51×10^{-11}	4.14×10^5	1.72×10^{-10}	1.32×10^6
318	5.55×10^4	2.46×10^{-11}	3.72×10^5	1.61×10^{-11}	1.25×10^5	5.42×10^{-10}	5.53×10^5
323	3.47×10^4	6.92×10^{-12}	1.36×10^5	2.00×10^{-11}	3.82×10^4	1.16×10^{-9}	2.09×10^5
	CPE 1		R1(Ω^{-1})	CPE 2			
	Ca 1	Phi 1		Ca 2	Phi 2		
333	1.57×10^{-9}	6.43×10^{-1}	7.63×10^4	4.33×10^{-11}	4.25		7.63×10^4
338	1.60×10^{-9}	6.46×10^{-1}	5.09×10^4	6.04×10^{-11}	4.31		5.09×10^4
343	4.54×10^{-9}	5.78×10^{-1}	2.77×10^4	1.27×10^{-10}	4.28		2.77×10^4
4-methylpyridine-ICl							
303	6.71×10^{-9}	6.23×10^{-1}	6.42×10^3	1.43×10^{-4}	5.17×10^{-1}		6.42×10^3
313	5.38×10^{-9}	6.81×10^{-1}	4.38×10^3	2.50×10^{-4}	4.85×10^{-1}		4.38×10^3
323	4.99×10^{-7}	3.79×10^{-1}	1.57×10^3	5.93×10^{-4}	7.73×10^{-1}		1.57×10^3
333	2.34×10^{-6}	3.12×10^{-1}	7.99×10^2	5.71×10^{-4}	7.88×10^{-1}		7.99×10^2

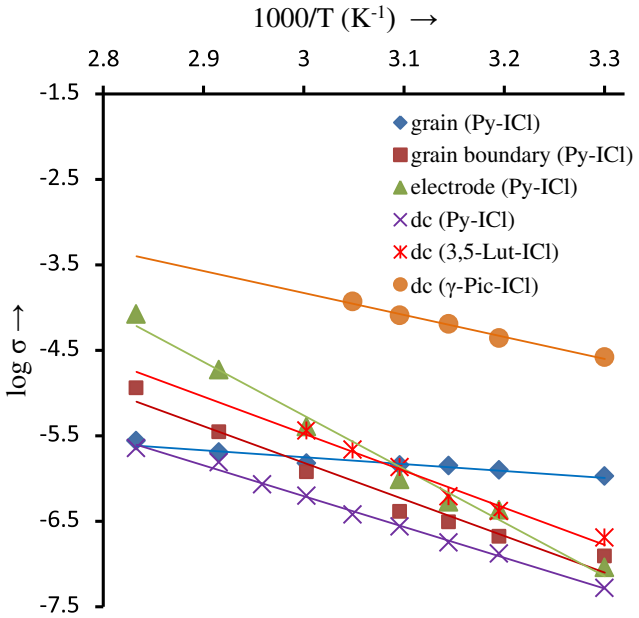

Fig. 5 Arrhenius plots of σg, σgb and σel for pyridine-ICl and σdc of the three complexes

are observed. In case of pyridine-ICl and 3,5-dimethylpyridine-ICl complex, the absence of the first low frequency regime attributed that there is no/negligible interfacial polarisation. In the low frequency region, conductivity increases with the increase in frequency which is attributed to the polarization at the electrode-sample interface. Here, flow of the charges accumulated at the interface is responsible for increase in conductivity. In the intermediate plateau region, conductivity is almost frequency independent and is equal to the bulk or d.c. conductivity of the sample. The higher frequency dispersion region can be explained by Jonscher's universal power law [43]

$$\sigma_{ac} = \sigma_{dc} + A\omega^{s} \tag{6}$$

where σ_{ac} and σ_{dc} are the a.c. and d.c. conductivity, respectively, ω is the angular frequency which equals to $\omega = 2\pi f$, A is a constant and S is the frequency exponent having values between 0 and 1. From the slope of the plot between logσ versus logω, the frequency exponent S can be obtained and the intercept of the horizontal portion on the vertical axis equals to $\log\sigma_{dc}$.

It is seen that as temperature increases, conductivity increases at all frequencies which attributes to thermal activation. It is also observed that the characteristic frequency, (the frequency at which dispersion region started to deviate from the d.c. conductivity plateau) at which relaxation effect begins to appear, shifted to the higher frequency with increase in temperature and arrived at a position beyond the measured frequency window limit. Another interesting observation is that the dispersion is more prominent at lower temperature, which is reflected in the value of S which decreases with the rise of temperature as shown in Fig. 7. All these observations

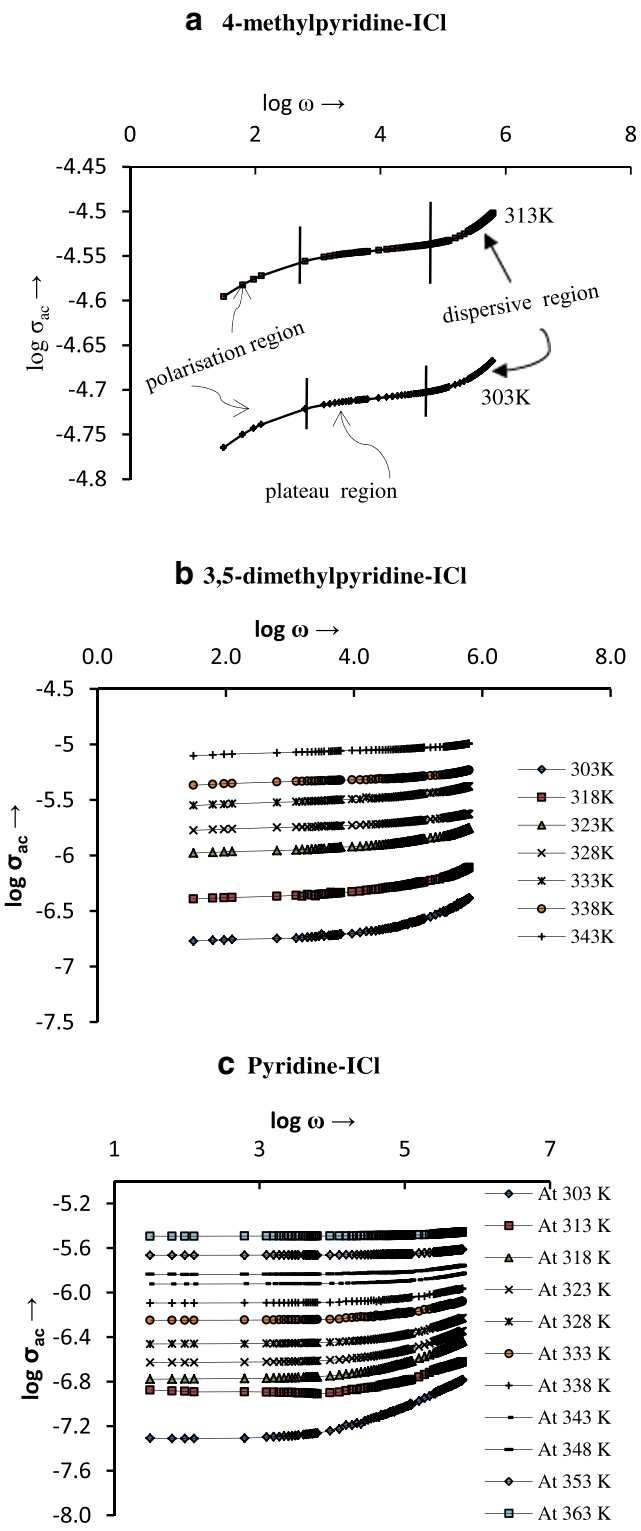

Fig. 6 Variation of a.c. conductivity with frequency for **a** 4-methylpyridine-ICl, **b** 3,5-dimethylpyridine-ICl and **c** pyridine-ICl complexes at various temperatures

indicate that the tested materials exhibit semiconducting behaviour and the a.c. conduction mechanism is due to barrier hopping [44, 45].

Table 7 Total conductivity and d.c. conductivity of the complexes at various temperatures

T (K)	$R_{total}(\Omega^{-1})$ (from Nyquist semicircle)	$\sigma_T = \frac{1}{R_{total}} \times \frac{t}{A}$ (Ω^{-1} cm^{-1})	$\sigma_{dc}(\Omega^{-1}$ cm$^{-1})$ (from intercept of the linear portion of logσ_{ac} vs logω plot by LCR meter)	$\sigma_{dc}(\Omega^{-1}$ cm$^{-1})$ (from the slope of the I/V plots by source meter)
Pyridine-ICl 303	2.41×10^6	4.95×10^{-8}	5.01×10^{-8}	5.20×10^{-8}
313	9.50×10^5	1.25×10^{-7}	1.28×10^{-7}	1.32×10^{-7}
318	7.14×10^5	1.67×10^{-7}	1.69×10^{-7}	1.77×10^{-7}
323	5.05×10^5	2.36×10^{-7}	2.38×10^{-7}	2.74×10^{-7}
328	–	–	3.48×10^{-7}	3.76×10^{-7}
333	2.11×10^5	5.64×10^{-7}	5.66×10^{-7}	6.25×10^{-7}
338	–	–	8.09×10^{-7}	8.50×10^{-7}
343	9.97×10^4	1.19×10^{-6}	1.19×10^{-6}	1.54×10^{-6}
353	5.50×10^4	2.16×10^{-6}	2.17×10^{-6}	2.26×10^{-6}
3,5-dimethylpyridine-ICl				
303	1.36×10^6	1.76×10^{-7}	1.80×10^{-7}	2.03×10^{-7}
318	5.59×10^5	4.29×10^{-7}	4.30×10^{-7}	4.14×10^{-7}
323	2.11×10^5	1.14×10^{-6}	1.11×10^{-6}	1.35×10^{-6}
328	1.33×10^5	1.80×10^{-6}	1.79×10^{-6}	2.16×10^{-6}
333	7.74×10^4	3.09×10^{-6}	3.01×10^{-6}	3.63×10^{-6}
4-methylpyridine-ICl				
303	6.37×10^3	1.97×10^{-5}	1.95×10^{-5}	2.62×10^{-5}
313	4.36×10^3	2.87×10^{-5}	2.86×10^{-5}	4.37×10^{-5}
318	2.21×10^3	5.67×10^{-5}	5.59×10^{-5}	6.41×10^{-5}
323	1.54×10^3	8.13×10^{-5}	7.99×10^{-5}	8.07×10^{-5}
328	1.06×10^3	1.18×10^{-4}	1.19×10^{-4}	1.17×10^{-4}

Measurement of ionic transport number

From the current vs time plots (Fig. 8) at room temperature, the total ionic transport number (t_{ion}) of the complexes were calculated using the Eq. 1. The values of t_{ion} (Table 2) imply that the conduction mechanism in pyridine-ICl complex (t_{ion} = 0.11) is predominantly electronic, in 3,5-dimethyl-ICl complex (t_{ion} = 0.58) is mixed ionic-electronic and in 4-methylpyridine-ICl complex (t_{ion} = 0.95) is mainly ionic as came across from impedance spectra.

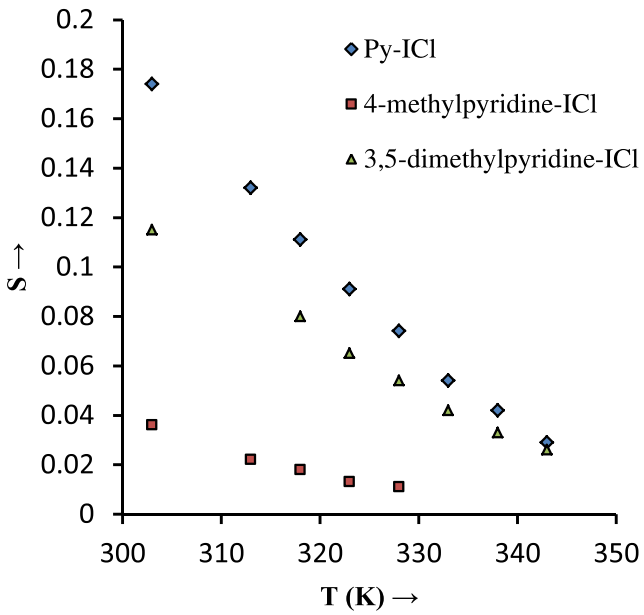

Fig. 7 Variation of frequency exponent(s) with temperature

DC conductivity measurement

The current-voltage characteristics of the samples in the pellet form recorded at various temperatures by using Keithley 2400 source meter are shown in Fig. 9 (S6a, b). It is observed that the I/V curves are linear indicating the ohmic behaviour. From the slope of the I/V curve d.c. conductivity can be calculated by using the following relation

$$\sigma_{dc} = \text{slope} \times \frac{t}{A} \tag{7}$$

where t is the thickness and A is the surface area of the sample. The d.c. conductivities measured from the I/V curves (using source meter) are well agreement to those calculated from the intercept of logσ versus logω plot (Table 7). Further, total conductivity, σ_{Total}, measured from the experimental Nyquist

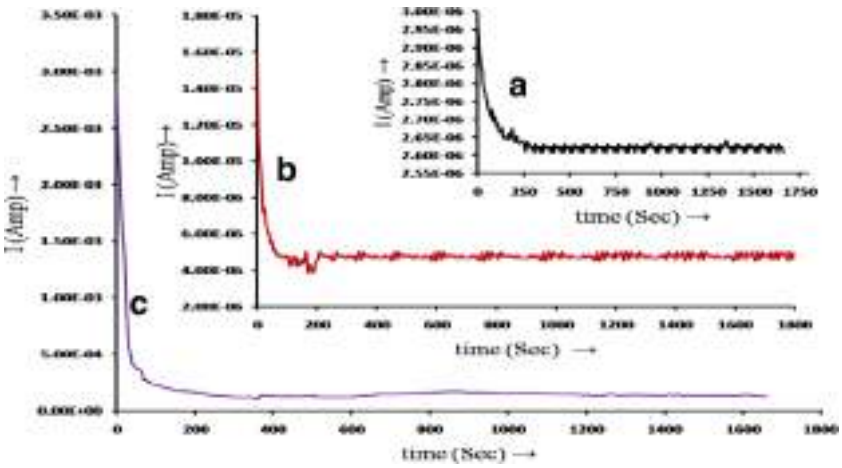

Fig. 8 Current vs time plots of **a** pyridine-ICl, **b** 3,5-dimethylpyridine-ICl and **c** 4-methylpyridine-ICl complex at 303 K

plots nearly equals to the σ_{dc} values and follows the Arrhenius law (Fig. 5). The activation energy for d.c. conductivity, calculated from the Arrhenius plots are 0.51, 0.71 and 0.86 eV for 4-methylpyridine-ICl, pyridine-ICl and 3,5-dimethylpyridine-ICl, respetively.

The increasing order of conductivity at any particular temperature is pyridine-ICl < 3,5-dimethylpyridine-ICl << 4-methylpyridine-ICl. Among the three, the highest conductivity of 4-methylpyridine-ICl complex is due to the higher ionisation (t_{ion} = 0.95) and lower band gap (E_g = 2.21 eV); on the contrary, pyridine-ICl complex with lower ionisation (t_{ion} = 0.11) and higher band gap (E_g = 2.85 eV) reveals lowest conductivity.

Conclusion

The investigations of the three charge transfer complexes by complex impedance spectra and ionic transport number measurements confirm that 4-methylpyridine-ICl can be considered purely ionic which originates from $(\gamma\text{-Pic}_2\text{-I})^+$ and ICl_2^- ions, while 3,5-dimethylpyridine-ICl is a mixed ionic-electronic conductor and pyridine-ICl is predominantly electronic in nature. The electrical properties of pyridine-ICl and 4-methylpyridine-ICl can be described by equivalent circuits –(RC)–(RC)–(RC)– and –(Rcpe)–(cpe)– respectively. The former circuit corresponds to grain, grain boundary and electrode contributions whereas the latter circuit corresponds to bulk resistance and double layer capacitance of electrode-material interface. Interestingly, electrical properties of 3,5-dimethylpyridine-ICl complex fits in both the equivalent circuits. At low temperature, it corresponds to that of –(RC)–(RC)–(RC)– and at high temperature it corresponds to –(Rcpe)–(cpe)–. The nature of the variation of d.c. conductivity with temperature suggests semiconducting behaviour with activation energy 0.71, 0.51 and 0.86 eV for pyridine-ICl, 4-methylpyridine-ICl and 3,5-dimethylpyridine-ICl complexes, respectively. The frequency dependence of a.c. conductivity obeys the Jonscher's power law.

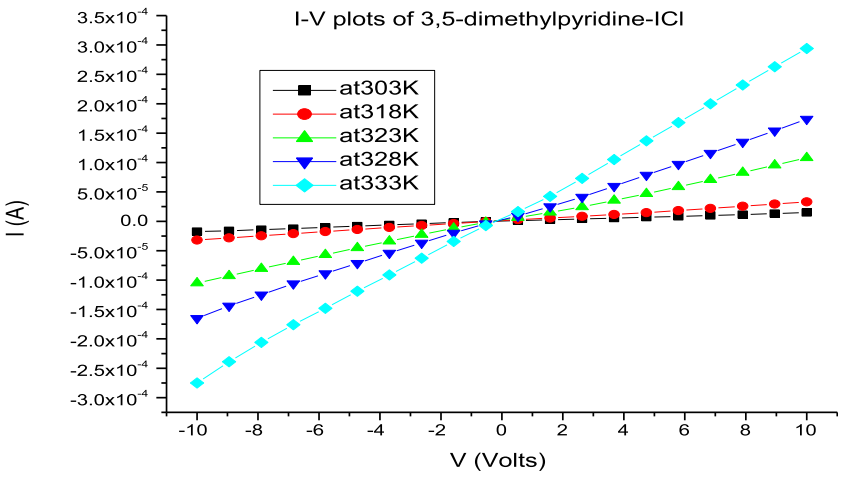

Fig. 9 Current-voltage plots of 3,5-dimethylpyridine-ICl complex at different temperatures

Acknowledgments Authors U. Mohan and P. Gogoi gratefully acknowledge U.G.C., NERO for the FIP Grant. The authors are thankful to Sudarsan Gogoi, Tezpur University for simulating the impedance data and Dr. Abhijit Gogoi, IIT, Guwahati, for his valuable discussions on indexing the powder XRD data.

References

1. Mulliken RS (1950) Structures of complexes formed by halogen molecules with aromatic and with oxygenated solvents. J Am Chem Soc 72:600–608
2. Mulliken RS (1952) Molecular compounds and their spectra II. J Am Chem Soc 74:811–824
3. Mori H (2008) Introduction of organic superconducting materials. In: Sun SS, Dalton LR (eds) Introduction to organic electronic and optoelectronic materials and devices. CRC, New York, pp. 263–286
4. Okamoto H, Mitani T, Tokura Y, Koshihara S, Komatsu T, Iwasa Y, Koda T, Saito G (1991) Anomalous dielectric response in tetrathiafulvalene-p-chloranil as observed in temperature- and pressure-induced neutral-to-ionic phase transition. Phys Rev B 43: 8224–8232
5. John Ferraris DO, Cowan V, Jr W, Perlstein JH (1973) Electron transfer in a new highly conducting donor-acceptor complex. J Am Chem Soc 95:948–949. doi:10.1021/ja00784a066
6. Coleman LB et al. (1973) Superconducting fluctuations and the peierls instability in an organic solid. Sol State Commun 12: 1125–1132
7. Jurchescu OD, Goetz KP, et al. (2014) Charge-transfer complexes: new perspectives on an old class of compounds. J Mater Chem C 2: 3065–3076. doi:10.1039/c3tc32062f
8. Gutmann F, Lyons LE (1967) Organic semiconductors. John Wiley and Sons Inc., New York
9. Ashwell GJ (ed) (1992) Molecular electronics. Research Studies Press, Taunton
10. Akamatu H, Inokuchi H, Matsunaga Y (1954) Electrical conductivity of the perylene-bromine complex. Nature 173:168–169
11. Akamatu H, Inokuchi H, Matsunaga Y (1956) Organic semiconductors with high conductivity. I. Complexes between polycyclic aromatic hydrocarbons and halogens. Bull Chem Soc Jpn 29:213–218
12. Nisizaki S, Kusakawa H (1963) The electrical conduction of the p-Phenylenediamine iodine complex. Bull Chem Soc Jpn 36: 1681–1683
13. Singh RA, Singh VK (1997) Mixed conduction in charge transfer materials based on aromatic diamines and iodine having different mole ratios. Bull Mater Sci 20(3):305–315
14. Mulliken RS, Person WB (1969) Molecular complexes—a lecture and reprint volume. Wiley, New York
15. Foster R (1969) Organic charge transfer complexes. Academic Press, London
16. Gur'yanova EN, Gol'dshtein IP, Romm IP (1975) Donor-acceptor bond. Keter Publishing House, Jerusalem
17. Akutagawa T, Uchigata M, Hasegawa T, Nakamura T, Nielsen KA, Jeppesen JO, Brimert T, Becher J (2003) Langmuir-Blodgett films of charge-transfer complexes between an Amphiphilic Monopyrrolo-TTF and TCNQ derivatives. J Phys Chem B 107:13929–13938
18. Carlin RL (1985) Magnetochemistry. Springer-Verlag, New York
19. Kahn O (1993) Molecular magnetism. VCH, Weinheim
20. Saito G (2008) Murata T (2008) Mixed valency in organic charge transfer complexes. Phil Trans R Soc A 366:139–150. doi:10.1098/rsta.2007.2146
21. Macdonald JR (1987) Impedance spectroscopy. Wiley, New York
22. Macdonald JR (1987) Impedance spectroscopy: emphasizing solid materials and systems. Wiley, New York
23. Barsoukov E, Macdonald JR (2005) Impedance sprectroscopy: theory, experiment, and applications, 2nd edn. Wiley-Interscience, New York
24. MEISP, March, 2002.Korea: Kumho Chemical Laboratories
25. Huggins RA (2002) Simple method to determine electronic and ionic components of the conductivity in mixed conductors a review. Ionics 8:300–313
26. Gogoi A, Sarma SN (2015) Conductivity study of poly(acrylonitrile-co-2-vinylpyridine) complexed with vinyl acetic acid and 4-pentenoic acid. Ionics 22(1):77–84. doi:10.1007/s11581-015-1529-5
27. Goswami S, Dutta A (2011) Measurement of ionic conductivity of poly (N-vinylimidazole) and its fluoroborate salt in solid state. Ionics 17(7):627–632. doi:10.1007/s11581-011-0554-2
28. Gabes W, Stufkens DJ (1973) Electronic absorption spectra of symmetrical and asymmetrical trihalide ions. Spectrochemica Acta 30A:1835–1841
29. Tauc J, Grigorovici R, Vancu A (1966) Optical properties and electronic structure of amorphous germanium. Phys Status Sol 15: 627–637
30. Vennila P, Govindaraju M, Venkatesh G (2013) Scaled quantum chemical studies of the structure, vibrational spectra, force constants and first-order Hyperpolarizability of 3,5-dimethylpyridine. Elixir Vib Spec 65B:20204–20211
31. Marcos JI, Oter JC, Tocon IL, Arenas JF (1999) Vibrational spectra of methylpyridines. J Mol Struct 476:139–150
32. Akyiiz S, Dempster AB, Morehouse RL, Suzuki S (1973) An infrared and Raman spectroscopic study of some metal pyridine tetracyanonickelate complexes. J Mol Struct 17(1):105–125. doi:10.1016/00222860(73)850471
33. Kantarci Z, Bayrak C, Bayari S (1997) An infrared and Raman spectroscopic study on the Hofmann-td-type complexes: $ML_2M'(CN)_4$, M = Mn or Zn, M' = Zn, Cd or Hg, L = pyridine, α-, β- or γ-picoline. J Mol Struct 407:155–163
34. Akyuz S, Pasaoglu H, Davies JED (1994) A vibrational spectroscopic study of Hofmann type complexes of 3- and 4-methylpyridines. J Mol Struct 317(3):215–221
35. Person WB, Humphrey RE, Deskin WA, Popov AI (1958) Infrared spectra of iodine monochloride charge-transfer complexes. J Am Chem Soc 80:2049–2053
36. Ginn SGW, Haque I, Wood JL (1968) The vibration spectra of the complexes pyridine—bromine, and pyridine—bromine chloride. Spectrochim Acta A: Mol Spectrosc 24(10):1531–1542
37. Katcka M, Urbanski T (1968) NMR spectra of pyridine, picolines and hydrochlorides and of their hydrochlorides and methiodides. Bulletin de L'academie Polonaise des Sciences XVI(7):347–350
38. Romming C (1972) Refinement of the crystal structure of charge transfer compound pyridine-iodomonochloride. Acta Chem Scand 26:1555–1560
39. Alexaner L, Klug HP (1950) Determination of crystallite size with the X-ray spectrometer. J Appl Phys 21:137–142. doi:10.1063/1.1699612
40. Hafidi E, Omari ME, Omari ME, Bentayeb A, Bennazha J, Maadi AE, Chehbouni M (2013) Arab J Chem 6:253–263. doi:10.1016/j.arabjc.2011.01.028
41. Bauerle JE (1969) Study of solid electrolyte polarization by a complex admittance method. J Phys Chem Solids 30:2657–2670
42. Yang X, Tan S, Liang T, Wei B, Wu Y (2016) Synthesis, characterization, and electrochemical properties of smectic pyridinium salts with inorganic dihydrogen phosphate ions. Ionics 22(1):85–92. doi:10.1007/s11581-015-1524-x
43. Jonscher AK (1977) The 'universal' dielectric response. Nature 267:673–679. doi:10.1038/267673a0
44. Elliott SR (1977) A theory of a.c. conduction in chalcogenide glasses. Philos Mag 36:1291–1304. doi:10.1080/14786437708238517
45. Ali AA, Shaaban MH (2010) Electrical properties of LiBBaTe glass doped with Nd_2O_3. Solid State Sci 12:2148–2154. doi:10.1016/j.solidstatesciences.2010.09.016

Journal of Molecular Structure 1131 (2017) 114–123

Contents lists available at ScienceDirect

Journal of Molecular Structure

journal homepage: http://www.elsevier.com/locate/molstruc

UV–Vis spectroscopy and density functional study of solvent effect on the charge transfer band of the n → σ* complexes of 2-Methylpyridine and 2-Chloropyridine with molecular iodine

Pallavi Gogoi [a, *], Uttam Mohan [b], Manash Protim Borpuzari [c], Abhijit Boruah [c], Surjya Kumar Baruah [c]

[a] Department of Chemistry, Tinsukia College, Tinsukia, Assam, 786125, India
[b] Department of Chemistry, D.H.S.K. College, Dibrugarh, Assam, 786001, India
[c] Department of Chemistry, Dibrugarh University, Dibrugarh, Assam, 786004, India

ARTICLE INFO

Article history:
Received 26 August 2016
Received in revised form
2 November 2016
Accepted 13 November 2016
Available online 15 November 2016

Keywords:
Multiple linear regression theory (MLRT)
Hansen parameter
Catalan parameter
Tauc plot
TDDFT

ABSTRACT

UV–Vis spectroscopy has established that Pyridine substitutes form n→σ* charge transfer (CT) complexes with molecular Iodine. This study is a combined approach of purely experimental UV–Vis spectroscopy, Multiple linear regression theory and Computational chemistry to analyze the effect of solvent upon the charge transfer band of 2-Methylpyridine-I_2 and 2-Chloropyridine-I_2 complexes. Regression analysis verifies the dependence of the CT band upon different solvent parameters. Dielectric constant and refractive index are considered among the bulk solvent parameters and Hansen, Kamlet and Catalan parameters are taken into consideration at the molecular level. Density Functional Theory results explain well the blue shift of the CT bands in polar medium as an outcome of stronger donor acceptor interaction. A logarithmic relation between the bond length of the bridging atoms of the donor and the acceptor with the dielectric constant of the medium is established. Tauc plot and TDDFT study indicates a non-vertical electronic transition in the complexes. Buckingham and Lippert Mataga equations are applied to check the Polarizability effect on the CT band.

1. Introduction

Solvatochromism signifies the medium dependence of electronic absorption spectrum of a system. It is an outcome of type of electronic transition and the nature of the chromophore involved [1]. Again the response of the molecular orbitals involved in electronic transition towards the medium is governed by their polarity. Depending on the polarity of the solvent and the corresponding molecular orbitals, energy reshuffling of the molecular orbitals takes place. Energy reshuffling sometimes leads to increase in energy gap between the molecular orbitals involved in transition or it also may lead to decease in energy gap between them. Either way we obtain a shift of the absorption maximum of the corresponding system in terms of blue shift or red shift [2].Moreover specific (e.g. hydrogen bonding) and non-specific (dielectric enrichment) interactions between the solute and solvent molecules result in the variation of geometry of the complex which changes the properties like dipole moment, molecular orientation, energy of different molecular orbitals etc. Compounds like everyday life drugs and dyes are medium dependent which makes solvatochromic study very important to understand solution chemistry involved with essential chemicals in different environment [3,4].

Pyridine substitutes, 2-Methylpyridine and 2-Chloropyridine have wide applications in agriculture and medicinal sector [5–7]. They form n→σ* charge transfer complexes with molecular iodine. The charge transfer bands of 2-Methylpyridine-I_2 and 2-Chloropyridine-I_2 are susceptible to polarity of the solvent medium. A prominent blue shift of these two CT bands is observed in solvents with higher dielectric constant values. Dielectric constant, refractive index and polarizability are bulk properties of solvents. Many other solvent parameters have been assigned which explain the solute solvent interaction at the molecular level [8–13]. Hansen parameter is a 3-dimensional solvent parameter system. In this system solubility parameter is a vector with the components of dispersion forces (∂d), polar forces (∂p), and hydrogen bonding (∂h).

* Corresponding author.
E-mail address: gogoipallavi@yahoo.com (P. Gogoi).

http://dx.doi.org/10.1016/j.molstruc.2016.11.040
0022-2860/

Catalan further developed a four parameter solvent scale based on specific interaction (SA and SB terms) and non specific interaction (SP and SDP terms).

UV–Vis study of many CT complexes considering the impact of solvent parameters upon spectroscopic properties is already reported [14–19]. Kamlet and Taft are the pioneers in this field [10].

The linear solvation energy relationship (LSER) as proposed by Kamlet is given by Equation (1)

$$XYZ = XYZ_0 + \ Solvent\ polarity\ or\ Polarizability\ effect + a\alpha + b\beta \quad (1)$$

Here XYZ is any spectroscopic property. α and β are the hydrogen bond donor acidity and hydrogen bond acceptor basicity. In Equation (1) α and β are microscopic level parameters whereas the polarizability term is a bulk physical phenomenon. This term was later replaced by π^* value which is a measure of the polarizability of a medium. In systems like 2-methylpyridine-I_2 and 2-Chloropyridine-I_2 there exists no hydrogen bonding between the complex and the solvent and so the hydrogen bonding terms can be neglected giving Equation (2).

$$XYZ = XYZ_0 + \ s\pi^* \quad (2)$$

On the basis of Linear Solvation Energy model considering bulk and molecular level solvent parameters we have designed some equations to study the solvent effect upon the title charge transfer complexes. For spectroscopic property XYZ we have substituted the wavelength of maximum absorbance (λ_{max}) of the CT band. Equation (3), Equation (4) and Equation (5) are designed for 2-methylpyridine-I_2 and 2-Chloropyridine-I_2 complexes.

$$\lambda_{max} = \lambda_0 + \ a\varepsilon + bn + s\pi^* \quad (3)$$

$$\lambda_{max} = \lambda_0 + \ \partial d + \ \partial p + \ \partial h \quad (4)$$

$$\lambda_{max} = \lambda_0 + \ aSP + bS\partial P + cSA + dSB \quad (5)$$

In Equation (3) ε and n are the dielectric constant and refractive index values of the experimental solvents respectively. π^* is the corresponding polarizability value. a, b and s are the respective coefficients showing individual contribution of each parameter upon the observed result. Equation (4) and Equation (5) explain the effect of Hansen and Catalan parameters upon λ_{max} respectively.

In order to establish our proposed equations we have applied multiple linear regression method. It helps to examine the dependence of a parameter upon several other independent parameters considering all at a time. The validity of a regression model can be examined by the correlation plot of the experimental value of the parameter and the calculated value of the same, predicted by the regression model. If the correlation plot stands well resulting in a good linear plot then the linear regression model is valid. We have applied MLRT to check the dependence of λ_{max} (CT) upon various solvent parameters for 2-Methylpyridine-I_2 and 2-Chloropyridine-I_2 complexes in solvents within the dielectric constant range of 1.89–9.08. The regression model successfully explains the dependence of λ_{max} (CT) upon the solvent parameters under consideration.

Besides all these equations Buckingham equation (S1) and Lippert Mataga equation (S2) (See supplementary information) also explain the dependence of a spectroscopic property on solvent parameters. These solvent parameters discussed so far are widely used to study different systems like dyes, amides, drugs and flavones [4,13,20–22].

Recently Density Functional Studies have been widely applied to study weak donor acceptor interaction between organic n and π donors with halogen and interhalogen acceptors. Density functional theory at the B3LYP level of theory has predicted good intermolecular distances and intermolecular interaction energy as well [23–29]. Theoretical investigations of similar complexes have been done to study the structure of the complex, CT transition energy, solvent effect on polarity etc. [30–52] The experimental blue shift of 2-Methylpyridine-I_2 and 2-Chloropyridine-I_2 CT band with solvent polarity is analyzed theoretically with the help of Density Functional Study. TDDFT study at different levels of theory is also widely applied these days to investigate the energy states involved in electronic transition in complexes [53].

2-Chloropyridine-ICl charge transfer complex is recently studied combining UV–Vis spectroscopy and density functional study. It gave good insight into the trend of charge transfer interaction and bond length variation as a function of solvent dielectric constant values [54].

2. Experimental details

UV–Visible spectra of the charge transfer complexes are recorded in a Shimadzu UV–Visible Spectrophotometer, UV-240 with quartz cells of 1 cm path length. All the solvents used are from Merck with percentage purity of 97–99%. 2-Chloropyridine used is from Fluka (98%) with a density of 1.209 g/dm^3. 2-Methylpyridine is from Merck (98%) with a density of 0.9 g/dm^3. Percentage purity and density values are included in the calculations while preparing solutions of the compounds in order to minimize errors.

Previous workers in the field are followed to prepare sample solutions [31,55–59]. Kosower's solvent parameter [60] corresponding to maximum absorption, Z value, is calculated from the spectral data of the title compounds in each solvent system. Different solvent parameters applied during the study are listed in S4 and S5 (See supplementary information).

3. Computational details

2-Methylpyridine-I_2 and 2-Chloropyridine-I_2 are optimized using B3LYP and ωB97XD [61–64] functional with 6–311++G** basis set for main group elements and 6-311G** for Iodine. Frequency calculations at the same level of theory are performed to confirm the stationary point as minimum. For the calculations in the solvent medium the conductor like screening model (COSMO) [65] is used. Geometry optimization and frequency calculations are performed using GAMESS software [66]. The TD-DFT calculations are performed using ωB97X functional on the optimized geometries obtained from ωB97XD calculations [67].

4. Results and discussion

4.1. Experimental analysis

4.1.1. Formation of 1:1 charge transfer complexes of 2-Methylpyridine-I_2 and 2-Chloropyridine-I_2

Appearance of a new absorption band with those of the acceptor and donor bands in UV–Vis spectra confirms the formation of a CT complex. For 2-Methylpyridine, 2-Chloropyridine and molecular Iodine absorption bands occur at 254.8 nm, 256.2 nm and 506 nm respectively in chloroform. When molecular iodine is added to the solution of 2-Methylpyridine a new band appears at 396 nm and when it is added to 2-Chloropyridine appearance of a new band at 425.25 nm is observed (See Supplementary Fig. S6). These new bands are in confirmation with the formation of charge transfer complexes of 2-Methylpyridine-I_2 and 2-Chloropyridine-I_2 [57]. The formation of 2-Methylpyridine-I_2 and 2-Chloropyridine-I_2

complexes in the ratio of 1:1 is confirmed from the Benesi Hildebrand plots [58]. (See Supplementary Fig. S7).

4.1.2. Formation of $n \rightarrow \sigma^*$ CT complex and the physical parameters of 2-Methylpyridine-I_2 and 2-Chloropyridine-I_2

Iodine forms CT complexes by $n \rightarrow \sigma^*$ transition with lone pair donors which is indicated by prominent blue shift of the CT band in polar solvents [38,40,67,68]. Blue shift for 2-Methylpyridine-I_2 and 2-Chloropyridine-I_2 CT bands are seen in polar solvents indicating charge transfer from the lone pair on nitrogen atoms of the donors to the σ^* orbitals of the acceptor iodine molecule [Table 1]. The Ionisation potential values of the donors in the complexes match well with the values previously calculated by electron impact method [69,70] [Table 1 & Table 4].

Table 1 lists the physical parameters associated with 2-Methylpyridine-I_2 and 2-Chloropyridine-I_2 CT complexes in different solvents. These include the position of the CT bands (λ_{max}), Frequency shift of the CT band from free Iodine band ($\Delta\bar{\upsilon}$), Ionisation potential of the donor in the CT complex (IP), Energy of charge transfer (ΔE_{CT}), Dipole Moment (μ), Oscillator Strength (f) Extinction coefficients (ε_C), Formation constant (K_C) and Gibbs free energy change at the experimental temperature (ΔG) of the two complexes in the corresponding solvents. These are calculated using established equations given at S8 [58]. (See supplementary information).

4.1.3. Effect of solvent parameters on the wavelength of CT band (λ_{max} CT)

Multiple Linear Regression Theory is applied using Microsoft Excel 2007 at 95% of confidence level. MLRT is performed considering different solvent parameters taken three at a time (Fig. 1).

Initially regression analysis is done considering *dielectric constant* and *refractive index* as independent parameters for the dependent parameter λ_{max}CT It shows good correlation between the calculated and experimental CT bands with R^2 values of 0.86 for 2-Chloropyridine-I_2 and 0.955 for 2-Methylpyridine-I_2 complex (Fig. 1a).

Successive introduction of the *Kamlet parameter* π^* to ε and n improves the R^2 value of the λ_{max}CT(experimental) against λ_{max}CT (Calculated) correlation plots to 0.917 and 0.979 for 2-Chloropyridine-I_2 and 2-Methylpyridine-I_2 respectively (Fig. 1b). It shows that not only dielectric constant and refractive index of the medium but also this Kamlet parameter which is a measure of solvent polarity-polarizability effect, affects the position of the CT band upto a large extent.

On analyzing the dependence of λ_{max} **CT** upon *Hansen solubility parameter* we obtained a correlation plot with R^2 value of 0.830 for 2-Chloropyridine-I_2. The same value obtained for 2-Methylpyridine-I_2 is 0.901 (Fig. 1c).

Consideration of Catalan parameter shows that λ_{max}**CT** also depends on Catalan parameter. This time correlation plot of λ_{max} **CT** (Calculated) against λ_{max} **CT** (Experimental) gives R^2 value of 0.801 for 2-Chloropyridine-I_2 and 0.989 for 2-Methylpyridine-I_2 complex (Fig. 1d).

Summarizing we can conclude that application of MLRT strongly reveals the dependence of λ_{max} **CT** upon the solvent parameters discussed herein with considerable high R^2 values (Table 2). It is recently reported that in case 2-Chloropyridine-ICl CT complex correlation plot of λ_{max}**CT** (Calculated) against λ_{max}**CT** (Experimental) gives R^2 value as high as 1 for Hansen solubility parameter [54].

Table 1
Physical parameters of (A) 2-Methylpyridine-I_2 and (B) 2-Chloropyridine-I_2.

Complex	A								B							
Solvents	n-C_6H_{14}	n-C_7H_{16}	Cyclo-C_6H_{14}	Iso-C_8H_{18}	CCl_4	C_6H_6	$CHCl_3$	CH_2Cl_2	n-C_6H_{14}	n-C_7H_{16}	Cyclo-C_6H_{14}	Iso-C_8H_{18}	CCl_4	C_6H_6	$CHCl_3$	CH_2Cl_2
λ_{max} of iodine (nm) in complex	516	515.69	516.16	515.97	512	492.17	503.97	500	523.63	515.69	511.72	511.72	507.6	488.47	506	500
λ_{max} of complex (nm)	438.61	432.04	437.37	430	432	431.37	425.25	416	417.65	413.73	415.69	413.73	408	396.15	396	380
$\Delta\bar{\upsilon}$ ($\times 10^3$ cm^{-1})	3.56	3.69	3.596	3.88	3.62	2.86	3.52	4.04	4.85	4.78	4.5	4.63	4.82	4.77	5.49	6.32
Z values of iodine (kcal/mol)	55.41	55.44	55.39	55.41	55.84	58.09	56.73	57.18	54.6	55.44	55.87	55.87	56.28	58.53	56.5	57.18
Z (kcal/mol)	65.57	65.98	65.67	66.49	66.18	66.28	66.8	68.73	68.45	69.1	68.78	69.1	70.07	72.17	72.19	75.24
K_c ($\times 10^3 dm^3/mol$)	58.4	50.87	25.5	60.61	8.04	40	30	24.4	1.6	1.86	1.528	2.14	1.88	0.992	0.98	1.07
ε_c (m^2/mol)	136.99	131.06	111.11	125	135.5	125	133.33	180.51	181.82	161.29	160	142.86	208.33	212.77	167.67	666.67
$-\Delta G$ (kj/mol)	10.08	9.74	8.02	10.17	9.01	9.14	8.43	7.91	18.28	18.65	18.17	18.99	18.68	17.09	17.07	17.29
f (mol/dm^3)	12.28	12.46	8.88	12.38	11.81	12.39	14.66	14.52	14.1	13.44	12.42	12.86	19.27		12.49	56.04
μ (mol/dm^3 cm)	26.77	39.83	34.31	39.67	31.58	41.29	43.7	43.67	41.47	40.49	39.55	39.66	49.43		38.98	80.25
ΔE_{CT} ($\times 10^{-19}$)joule	4.53	4.6	4.54	4.62	4.6	4.61	4.67	4.78	4.76	4.8	4.78	4.8	4.87	5.01	5.02	5.23
ΔE (eV)	2.83	2.87	2.84	2.88	2.87	2.88	2.92	2.98	2.97	2.99	2.98	2.99	3.04	3.13	3.13	3.26
IP (eV)	9.23	9.28	9.24	9.29	9.28	9.28	9.33	9.41	9.399	9.434	9.417	9.434	9.485	9.597	9.598	9.76
W (eV)	3.34	3.35	3.34	3.35	3.35	3.35	3.36	3.37	3.37	3.38	3.37	3.38	3.39	3.41	3.41	3.44

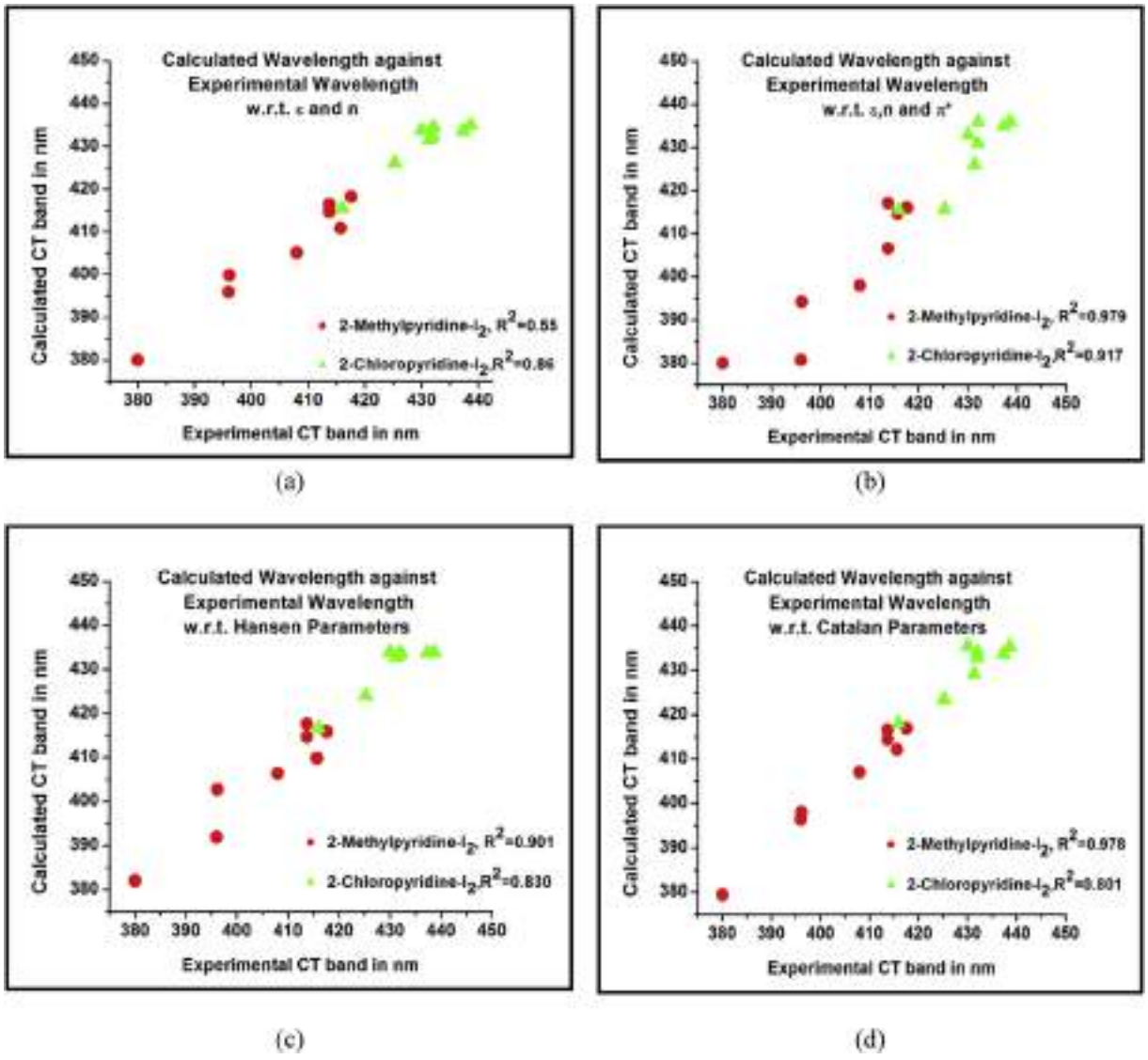

Fig. 1. Multiple Linear Regression Analysis for CT band of 2-Chloropyridine-I_2 & 2-Methylpyridine-I_2 in different solvents (a) Calculated λ_{max} against experimental λ_{max} w.r.t. dielectric constant,ε and refractive index, n (b) Calculated λ_{max} against experimental λ_{max} w.r.t. dielectric constant,ε, refractive index, n and π^* (c) Calculated λ_{max} against experimental λ_{max} w.r.t. Hansen Parameter (d) Calculated λ_{max} against experimental λ_{max} w.r.t. Catalan Parameter.

4.1.4. Solvent parameter dependence of frequency shift (Δῡ) of CT band

Frequency shift of the CT band is also studied using same methodology in different media (Fig. 2a and b, Table 2). Δῡ value is also strongly dependent on the bulk solvent parameters under study as well as Hansen parameter.

Table 2
Result of regression analysis for (A) 2-Methylpyridine-I_2 and (B) 2-Chloropyridine-I_2.

Dependent parameter	Independent parameters	Linear equation	R^2	Comment
A				
λ_{max} CT	ε,n	Linear equation	R^2	Comment
	ε,n,π*	$\lambda_{max} = 608.23 - 4.424\varepsilon - 132.119n$	0.955	Regression valid
	Hansen parameters	$\lambda_{max} = 419.71 - 1.624\varepsilon - 1.232n - 27.443\pi^*$	0.979	Regression valid
	Catalan parameters	$\lambda_{max} = 460.64 - 3.001\delta D - 2.557\delta P - 1.275\delta H$	0.901	Regression valid
Δῡ	ε,n,π*	$\lambda_{max} = 470.511 - 95.523SPP - 70.764SB + 129.552SA$	0.978	Regression valid
	Hansen parameters	$\Delta\bar{\nu} = 14.33 + 0.098\varepsilon - 6.974n - 1.269\pi^*$	0.989	Regression valid
B				
λ_{max} CT	ε,n	$\lambda_{max} = 465.88 - 2.576\varepsilon - 18.947n$	0.859	Regression valid
	ε,n,π*	$\lambda_{max} = 453.27 - 2.202\varepsilon - 9.657n - 4.674\pi^*$	0.917	Regression valid
	Hansen parameters	$\lambda_{max} = 433.99 - 0.005\delta D - 2.261\delta P - 0.500\delta H$	0.83	Regression valid
	Catalan parameters	$\lambda_{max} = 50.96 - 26.171SPP - 34.949SB - 93.896A$	0.801	Regression valid
Δῡ	ε,n,π*	$\Delta\bar{\nu} = 2.161 + 0.263\varepsilon + 3.748 - 1.828\pi^*$	0.888	Regression valid
	Hansen parameters	$\Delta\bar{\nu} = 5.06 - 0.089\delta D + 0.255\delta P - 0.156\delta H$	0.778	Average

Table 3
Frequency shift corresponding to Orientation Polarizability for (A) 2-Methylpyridine-I_2 and (B) 2-Chloropyridine-I_2.

Solvents	ε	$f(\varepsilon)=\frac{(\varepsilon-1)}{(2\varepsilon+1)}$	n	$f(n)=\frac{(n^2-1)}{(2n^2+1)}$	$\Delta f\ (\varepsilon,\ n)$	*Frequency shift*, $\Delta\bar{\upsilon}\times\ 10^3\ cm^{-1}$	
						A	B
n-C_6H_{14}	1.89	0.186192	1.3749	0.186238	−4.59497E-05	4.85	3.56
n-C_7H_{16}	1.924	0.190594	1.3876	0.190777	−0.000182901	4.78	3.69
Cyclo-C_6H_{14}	2.023	0.202735	1.4262	0.204031	−0.001295841	4.5	3.596
Iso-C_8H_{18}	2.2	0.222222	1.3915	0.192153	0.03006959	4.63	3.88
CCl_4	2.238	0.226077	1.463	0.215949	0.010128635	4.82	3.62
C_6H_6	2.284	0.230603	1.5011	0.2276	0.003003721	4.77	2.86
$CHCl_3$	4.806	0.358651	1.4457	0.21043	0.148220452	5.49	3.52
CH_2Cl_2	9.08	0.421712	1.4235	0.203129	0.218582615	6.32	4.04

4.1.5. Validity of Buckingham equation

A 3-D plot of $\Delta\bar{\upsilon}$ against f (ε) and f (n) is drawn for 2-Methylpyridine-I_2 and 2-Chloropyridine-I_2 (Table 3, Fig. 3). Since the corresponding points in space are not coplanar, they certainly simultaneously vary with respect to f(ε) and f(n) establishing the validity of Buckingham equation in the considered complexes under study.

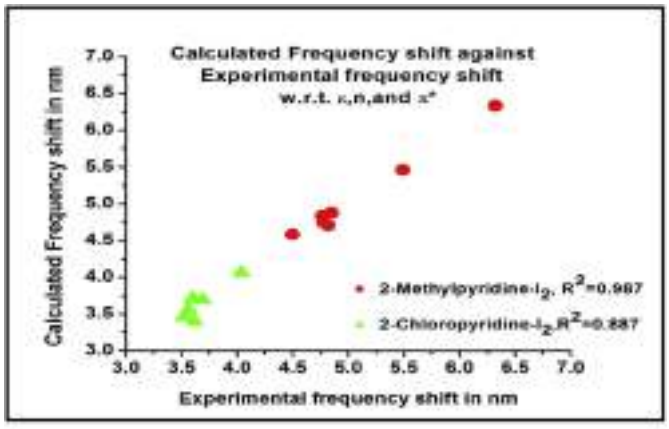

(a)

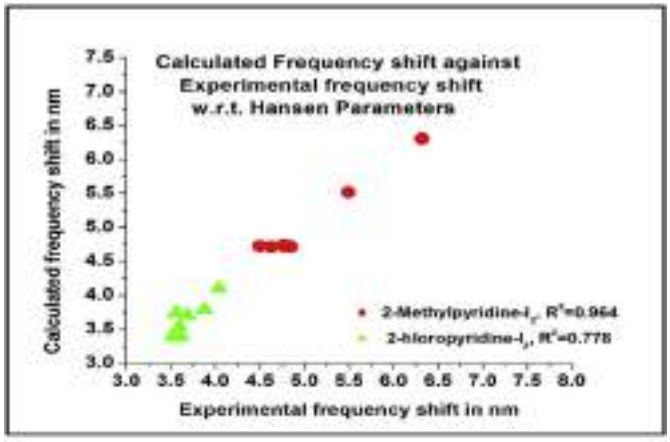

(b)

Fig. 2. Multiple Linear Regression Analysis for shift in CT band for 2-Chloropyridine-I_2 & 2-Methylpyridine-I_2 (a) Calculated $\Delta\bar{\upsilon}$ against experimental $\Delta\bar{\upsilon}$ w.r.t. dielectric constant,ε, refractive index, n and π^* (b) Calculated $\Delta\bar{\upsilon}$ against experimental $\Delta\bar{\upsilon}$ w.r.t. Hansen Parameter.

4.1.6. Application of Lippert Mataga equation to correlate frequency shift ($\Delta\bar{\upsilon}$) and

Orientation Polarizability (Δf) of the solvents Lippert Mataga equation [71] relates frequency shift with the orientation Polarizability linearly. In case of 2-Methylpyridine-I_2 complex, R^2 value obtained is 0.932 while for 2-Chloropyridine-I_2 the value is 0.204 (Table 3, Fig. 4).

4.1.7. Tauc plot for the complexes and type of transition involved

Electronic transitions observed in UV–Vis spectroscopy may be direct transitions or indirect. Among direct transitions we have the direct allowed and direct forbidden. Likewise in case of indirect transitions we have the indirect allowed and indirect forbidden transitions. Tauc, David and Mott have given a nice relation to determine the type of electronic transition (See supplementary information). In case of 2-Methylpyridine-I_2 and 2-Chloropyridine-I_2 complexes the transition type is Indirect allowed as can be seen from Fig. 5.

4.2. Computational analysis

4.2.1. Equilibrium geometries of 2-Methylpyridine-I_2 and 2-Chloropyridine-I_2 in different solvents

The complexes are optimized using B3LYP and ωB97XD functional. The optimized geometries of the two complexes at both functional show that the I_2 molecule stays away from the substituent groups at α position of the Pyridine moiety (See supplementary information, Fig: S9 and S10). It may be an outcome of steric repulsion between $-CH_3$ and $-Cl$ groups and the Iodine molecule. The N–I bond distances ($r_{N\text{-}I}$) in the gas phase obtained for 2-Methylpyridine-I_2 and 2-Chloropyridine-I_2 are comparable to the previously reported value for Pyridine-I_2 CT complex [72]. From Table 4 and S11 (See supplementary information) it is seen that I–I bond distances (r_{I-I}) in the gas phase are more than free I_2 molecule. It indicates elongation of I–I bond upon complexation. This increase in bond length lies within the range of 0.05–0.07 as reported earlier [72].

4.2.2. Solvatochromism is an outcome of change in molecular geometry with solvent polarity

Analysis of Lowdin population on the donor N atom shows building up of electron density around it with the increasing polarity of the solvents (Table 5). Polar solvent stabilizes the charge separation in donor acceptor molecule [$A^{\delta-}$ $D^{\delta+}$] [73]. It signifies a stronger CT interaction in polar medium.

There is also a significant change in the bond length of bridging atoms and the acceptor molecule. It is observed that r_{N-I} decrease with the polarity of the solvents while r_{I-I} increases with it (Table 4 and S11). It is in accordance with the earlier findings that r_{N-I} in such complexes decreases with increase in complexation while that of r_{I-I} increases [37,41]. **T**he electric field of the solvent

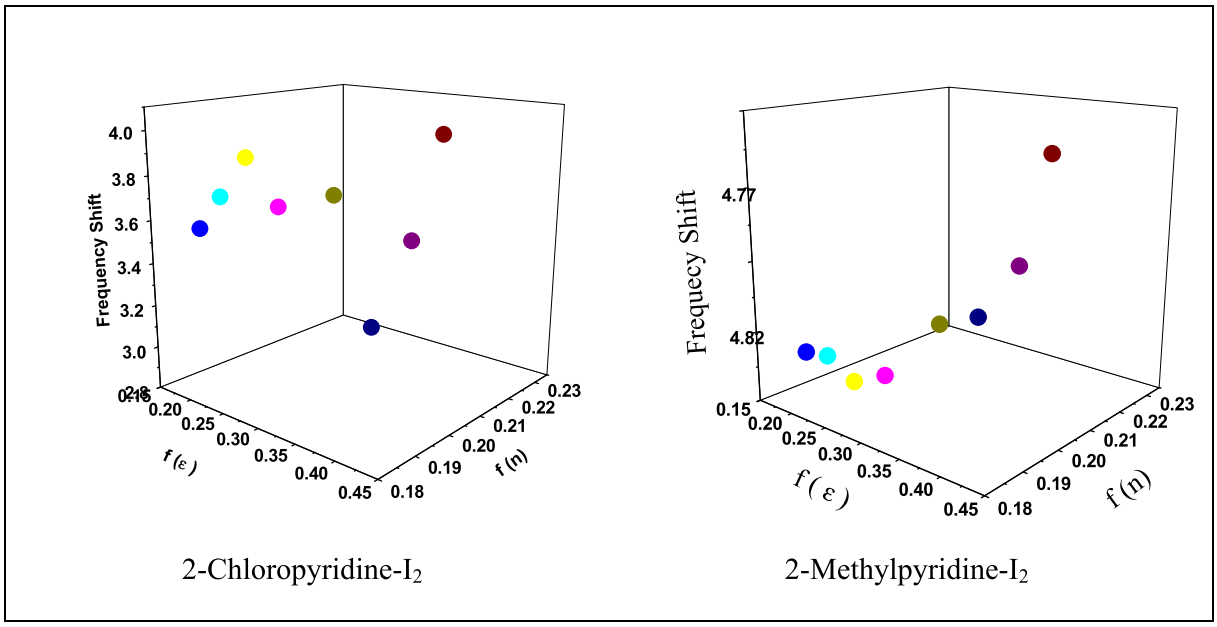

Fig. 3. 3D plot for $\Delta\bar{\upsilon}$, f(ε) and f(n) for Buckingham Equation.

also plays a role in contraction of the N–I bond [72].

Therefore from the bond length analysis and also the electron density analysis we can conclude that solvent polarity leads to structural changes within the molecule, stabilizes the charge separation and leads to a stronger donor acceptor interaction. Thus the UV–Vis spectra show a prominent blue shift of the CT band in polar medium.

4.2.3. Quantitative relation between dielectric constant of medium and bond length

We proposed a logarithmic relation between the bond length of the bridging atoms of donor and acceptor molecules and Dielectric constant of the corresponding media for 2-Chloropyridine-ICl CT complex [54]. Same logarithmic relation equally holds in these two complexes too. It is observed from Fig. 6. Earlier it is reported that the changes observed by solvent variation in complexes is largely dependent on the dielectric constant upto a value of ~10. Thus we have selected the solvents within this range and tried to find a quantitative relation between the dielectric constant of solvents and the bond length [74].

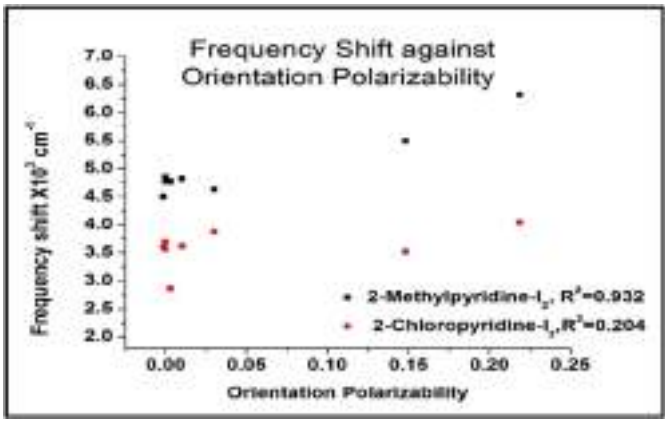

Fig. 4. Lippert Mataga equation for 2-Methylpyridine-I_2 and 2-Chloropyridine-I_2.

4.2.4. Molecular orbitals involved in transition

Although Pyridine has both π electron system and an n-pair, Pyridine and halogens form $n \rightarrow \sigma^*$ charge transfer complex [33,39]. We have tried to visualize the molecular orbitals of the two compounds after fully optimizing them in the gas phase and it is seen that the transition in 2-Methylpyridine-I_2 complex occurs from HOMO-2 to LUMO of the complex and in case of 2-Chloropyridine-I_2 complex it occurs from HOMO-5 to LUMO of the complex (Fig. S12). (See supplementary information).

4.2.5. TD-DFT studies

We have performed TDDFT using long range corrected functional ωB97X since the preference of using LC functional over other hybrid functional has been widely discussed by previous workers [75–77]. However both the success and failure of TDDFT in explaining CT states have been already reported [78,79]. It is seen from Table 5 that λ_{max} values increase with increase in solvent polarities, which is in contradiction with experimental values. This contradiction can be due to either improper asymptotic behavior of the density functional or experimental transition may not be vertical. Since ωB97X functional is range-separated functional with proper asymptotic form, therefore, the main reason of this contradiction is that experimental transition as we have already seen while considering the Tauc plot is not vertical. Moreover, it should be noted that the difference between theoretical and experimental λ_{max} is very large, which also support our conclusion that experimental transition is not vertical.

4.3. Substituent effect

Position of the CT band from the experimental analysis, bond length study and Lowdin population analysis strongly suggest the substituent effect of the $-CH_3$ and $-Cl$ groups present in the two systems.

The experimental results show that the CT band for 2-Methylpyridine-I_2 appears at a lower wavelength as compared to that of 2-Chloropyridine-I_2 band. The positive inductive effect methyl group on the pyridine ring increases the electron density at the donor N atom while the chlorine atom does just the opposite.

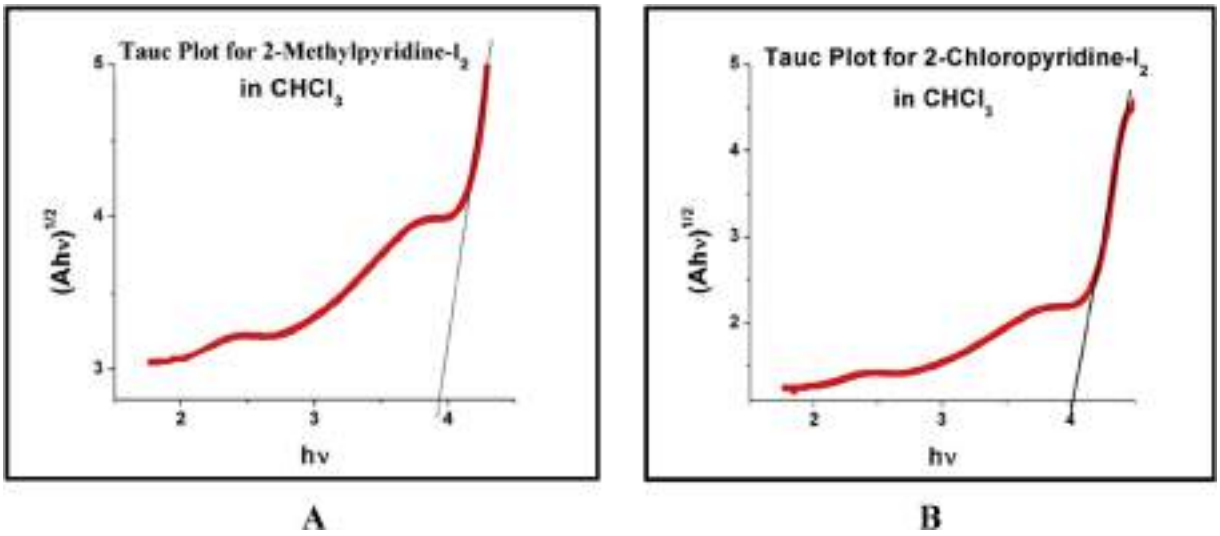

Fig. 5. Tauc plot for (A) 2-Methylpyridine-I_2 and (B) 2-Chloropyridine-I_2.

The lone pair on N atom in 2-Methylpyridine becomes more labile facilitating bond formation with Iodine more than that of 2-Chloropyridine molecule. As a whole the 2-Methylpyridine-I_2 complex gets stabilized more and thus the energy gap between the charge transfer transition states becomes more. As a result we get lower values of $\lambda_{(max)CT}$ for 2-Methylpyridine-I_2 complex as compared to the corresponding values for 2-Chloropyridine-I_2 CT complex (Table 1).

From bond distance analysis it is seen that (Table 4 and S11).

$r_{N\text{-}I}$ (2-Methylpyridine-I_2)<$r_{N\text{-}I}$ (2-Chloropyridine-I_2)

and

$r_{I\text{-}I}$ (2-Methylpyridine-I_2)>$r_{I\text{-}I}$ (2-Chloropyridine-I_2)>$r_{I\text{-}I}$(Iodine Molecule)

This clearly indicates that there is more Charge transfer interaction between 2-Methylpyridine and I_2 molecule as compared to 2-Chloropyridine and I_2 molecule.

The optimized geometries in the gas phase show that Lowdin population on the donor N atom of 2-Methylpyridine-I_2 is less than that of donor N atom of 2-Chloropyridine-I_2 complex (Table 4 and S11). Thus we may conclude that better electron transfer occurs in case of 2-Methylpyridine-I_2 indicating stronger donor acceptor interaction in this complex. The Binding energy values also support this fact (S13). (See supplementary information).

5. Conclusion

Multiple linear regression method helps in establishing the Linear solvation energy relationship and explains well the dependence of λ_{max}(CT) of the two complexes on different solvent

Table 4
Bond length and population analysis from theoretical data for (A) 2-Methylpyridine-I_2, (B) 2-Chloropyridine-I_2complex in gas phase and different solvents for ωB97XD functional.

Medium	∈	$r_{I\text{-}I}$ Å		$\Delta r_{I\text{-}I}$ Å	$r_{N\text{-}I}$ Å	Lowdin population and charge on			
					In CT complex	N atom		I atom	
		Free iodine	In CT complex			Population	Charge	Population	Charge
A									
Gas	1	2.7035	2.7544	0.0509	2.7466	7.377956	0.377956	52.379904	0.620096
n-C_6H_{14}	1.89	2.7046	2.7686	0.064	2.6804	7.252789	−0.252789	52.720560	0.279440
n-C_7H_{16}	1.924	2.7046	2.7692	0.0646	2.6776	7.257561	−0.257561	52.705096	0.294904
Cyclo-C_6H_{14}	2.023	2.7047	2.7704	0.0657	2.6721	7.255883	−0.255883	52.713254	0.286746
Iso-C_8H_{18}	2.2	2.7048	2.7727	0.0679	2.6631	7.253512	−0.253512	52.720708	0.279292
CCl_4	2.238	2.7048	2.7732	0.0684	2.6615	7.253594	−0.253594	52.720724	0.279276
C_6H_6	2.284	2.7049	2.7738	0.0689	2.6587	7.259191	−0.259191	52.701244	0.298756
$CHCl_3$	4.806	2.7057	2.7889	0.0832	2.6154	7.262663	−0.262663	52.697926	0.302074
CH_2Cl_2	9.08	2.7061	2.8026	0.0965	2.5772	7.265322	−0.265322	52.686178	0.313822
B									
Gas	1	2.7035	2.7327	0.0292	2.88	7.387995	−0.387995	52.386292	0.613708
n-C_6H_{14}	1.89	2.7046	2.7371	0.0325	2.8571	7.249224	−0.249224	52.764287	0.235713
n-C_7H_{16}	1.924	2.7046	2.7373	0.0327	2.8562	7.249349	−0.249349	52.764347	0.235653
Cyclo-C_6H_{14}	2.023	2.7047	2.7377	0.033	2.8538	7.249696	−0.249696	52.764515	0.235485
Iso-C_8H_{18}	2.2	2.7048	2.7383	0.0335	2.8504	7.250259	−0.250259	52.764786	0.235214
CCl_4	2.238	2.7048	2.7384	0.0336	2.8497	7.248393	−0.248393	52.769229	0.230771
C_6H_6	2.284	2.7049	2.7385	0.0336	2.8491	7.246357	−0.246357	52.770331	0.229669
$CHCl_3$	4.806	2.7057	2.7454	0.0397	2.8038	7.254425	−0.254425	52.766768	0.233232
CH_2Cl_2	9.08	2.7061	2.7513	0.0452	2.7676	7.256471	−0.256471	52.767736	0.232264

Table 5
TDDFT data (A) 2-Methylpyridine-I_2, (B) 2-Chloropyridine-I_2 complex in gas phase and different solvents for ωB97X functional.

2-Methylpyridine-I_2					2-Chloropyridine-I_2		
Medium	ε	λ_{max}	f_{osc}	State	λ_{max}	f_{osc}	State
Gas	1	210.9	1.0728	7	201.5	1.6124	8
n-C_6H_{14}	1.89	213	1.1004	7	204.2	1.6501	7
n-C_7H_{16}	1.924	213	1.1013	7	204.3	1.6519	7
Cyclo-C_6H_{14}	2.023	213.2	1.1048	7	204.5	1.6549	7
Iso-C_8H_{18}	2.2	213.4	1.1051	7	204.8	1.6597	7
CCl_4	2.238	213.4	1.8989	7	204.9	1.6602	7
C_6H_6	2.284	213.5	1.1059	7	204.9	1.6614	7
$CHCl_3$	4.806	215.5	1.0765	7	207.1	1.7313	7
CH_2Cl_2	9.08	216.5	1.0339	7	208.6	1.7887	7

parameters both at the bulk and molecular levels. Theoretical investigation of the geometry of the complexes strongly suggests that solvatochromism is a result of change in geometric and electronic arrangement within the complex in different media.

Molecular orbital analysis implies that electronic transition in 2-Methylpyridine-I_2 occurs from HOMO-2 to LUMO and in 2-Chloropyridine-I_2 it occurs from HOMO-5 to LUMO of the complex. Thus charge transfer transition is not strictly confined to the frontier orbitals only. A logarithmic relation between the dielectric constant of the medium and the Donor-Acceptor bond distance is found to exist upto a dielectric constant value of 10. Substituent effect is seen to play an important role in the position of the CT bands. All the results obtained propose a stronger donor acceptor interaction in 2-Methylpridine-I_2 than 2-Chloropyridine-I_2 with the increase in the solvent polarity. Tauc plot from UV–Vis study and TDDFT studies suggest an indirect allowed transition in 2-Methylpyridine-I_2 and 2-Chloropyridine-I_2 charge transfer complexes.

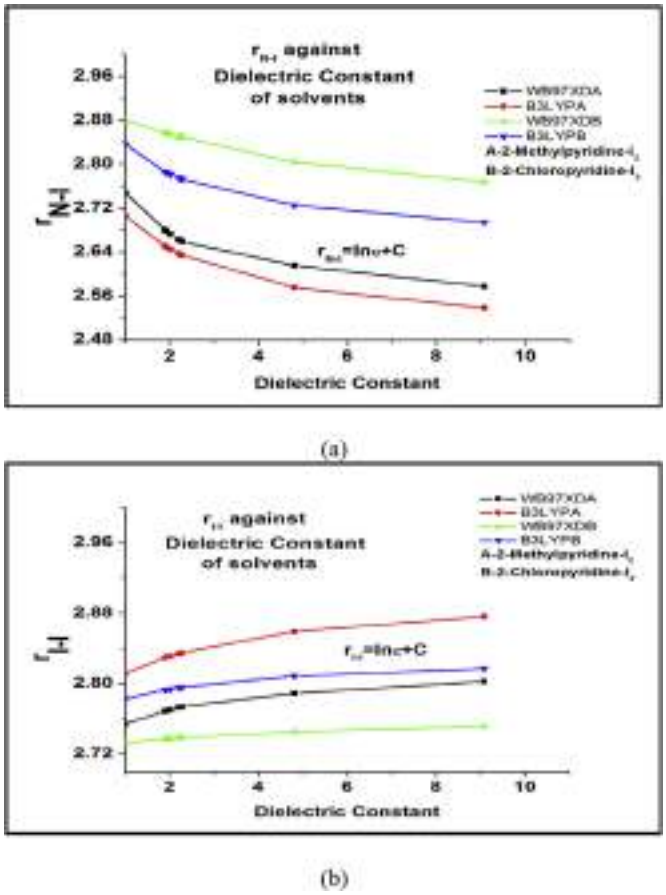

Fig. 6. Variation of Bond length with Dielectric Constant of solvents, (a)$r_{N\text{-}I\ against}$ Dielectric constant (b)$r_{I\text{-}Cl}$ against Dielectric constant.

Acknowledgement

PG and UM acknowledge the University Grants Commission for granting leave on Faculty Development Program to conduct this research work. MPB acknowledges the Council of Scientific and Industrial Research (CSIR), New Delhi.

Appendix A. Supplementary data

Supplementary data related to this article can be found at http://dx.doi.org/10.1016/j.molstruc.2016.11.040.

References

[1] P.K. Behera, A. Xess, S. Sahu, Solvent effects on the electronic spectra of some heterocyclic azo dyes, Bull. Korean Chem. Soc. 35 (2) (2014) 610–616.
[2] M.I. Sancho, M.C. Almandoz, S.E. Blanco, E.A. Castro, Spectroscopic study of solvent effects on the electronic absorption spectra of flavone and 7-hydroxyflavone in neat and binary solvent mixtures, Int. J. Mol. Sci. 12 (2011) 8895–8912.
[3] M.S. Zakerhamidi, A. Ghanadzadeh, M. Moghadan, Solvent effects on the UV/visible absorption spectra of some aminobenzene dyes, Chem. Sci. Trans. 1 (1) (2012) 1–8.
[4] A. Dawoud, B. Yaseen, M. Al-Balawi, The solvatochromic, spectral, and geometrical properties of nifenezone: a DFT/TD-DFT and experimental study, Phys. Chem. Chem. Phys. 16 (2014) 15519–15526.
[5] C. Botteghi, G. Chelucci, G.D. Ponte, M. Marchetti, S. Paganellit, New synthetic route to pheniramines via hydroformylation of functionalized olefins, J. Org. Chem. 59 (1994) 7125–7127.
[6] S. Shimizu, N. Watanabe, T. Kataoke, T. Shoje, N. Abe, S. Morishita, H. Ichimura, Pyridine and alkylpyridines, in: Ullmann's Encyclopedia of Industrial Chemistry, vol. 30, Wiley-VCH. Verlag GmbH & Co, KGaA, Weinhem, 2012, pp. 557–589.
[7] C. Manansala, G.K. Tranmer, Flow synthesis of 2-methylpyridines via alpha-methylation, Molecules 20 (2015) 15797–15806.
[8] M.S. Refat, T.A. Sharshar, A.M. Adam, K.M. Elsabawy, O.M. Hemeda, Chemical and physical investigations on the charge transfer interaction of organic donors with iodine and its application as non-traditional organic conductors, J. Mol. Struct. 1074 (2014) 27–32.
[9] A.D. Buckingham, A theory of the dielectric polarization of polar substances, in: Proceedings of the Royal Society of London, Series A, Mathematical and Physical Sciences, 238 (1213), 1956, pp. 235–244.
[10] M.J. Kamlet, R.W. Taft, Linear solvation energy relationships. Part 1.1 solvent polarity-polarizability effects on infrared spectra, J.C.S. Perkins II. (1979) 349–356.
[11] M.J. Kamlet, M.E. Jones, R.W. Taft, J.L. Abboud, Linear solvation energy relationships. Solvent polarity? Polarizability effects on infrared spectra, J.C.S. Perkins II 3 (1979) 342–348.
[12] R.W. Taft, M.J. Kamlet, The solvatochromic comparison method. 2. The alpha-scale of solvent hydrogen-bond donor(HBD) acidities, J. Am. Chem. Soc. 98 (10) (1976) 2886–2894.
[13] J. Catalan, Toward a generalized treatment of the solvent effect based on four empirical scales: dipolarity(sdp, a new scale), polarizability (SP), acidity(SA), and basicity (SB) of the medium, J. Phys. Chem. B 113 (2009) 5951–5960.
[14] C.M. Hansen, The Three Dimensional Solubility Parameter and Solvent Diffusion Coefficient-Their Importance in Surface Coating Formulation, Danish Technical Press, Copenhagen, 1967.
[15] I. Bratu, R. Grecu, R. Constantinescu, T. Iliesco, Molecular relaxation processes of 2-bromopropane in solutions from IR ν(C-Br) band shape analysis, Spectrochim. Acta Part A Mol. Biomol. Spectrosc. 54 (3) (1998) 501–506.
[16] J. Basavaraja, S.R. Inamdar, H.M.S. Kumar, Solvents effect on the absorption and fluorescence spectra of 7-diethylamino-3-thenoylcoumarin: evaluation and correlation between solvatochromism and solvent polarity parameters, Spectrochim. Acta Part A Mol. Biomol. Spectrosc. 137 (2015) 527–534.
[17] U.P. Raghavendraa, M. Basanagouda, R.M. Melavankic, R.H. Fattepurd, J. Thipperudrappae, Solvatochromic studies of biologically active iodinated 4-aryloxymethyl coumarins and estimation of dipole moments, J. Mol. Liq. 202 (2015) 9–16.
[18] J.M. Markovic, N.P. Trisovic, D. Mutavdzic, K. Radotik, I.O. Juranicc, B.J. Drakulic, A.D. Marinkovic, Solvatochromism of symmetrical 2,6-distyrylpyridines. An experimental and theoretical study, Spectrochim. Acta Part A Mol. Biomol. Spectrosc. 135 (2015) 435–446.
[19] Y.G. Sidir, I. Sidir, H. Berber, G. Turkuglu, Solvatochromic behaviour and

electronic structure of some symmetric 2-aminophenol Schiff base derivatives, J. Mol. Liq. 199 (2014) 57–66.
[20] K. Aggarwal, J.M. Khurana, Effect of hydroxyl group on the photopysical properties of benzo(a)xanthenes-solvatochromic studies and estimation of dipole moment, J. Photochem. Photobiol. A Chem. 276 (2014) 71–82.
[21] A. Alimmari, B. Bozic, D. Mizin, A. Marinkovic, N. Valentic, G. Uscumlic, Synthesis, structure and Solvatochromic properties of some novel 5-arylazo-6-hydroxy-4-(4-methoxyphenyl)-3-cyano-2-pyridone dyes: hydrazone-azo tautomeric analysis, Arab. J. Chem. 8 (2015) 269–278.
[22] B. Jovie, A. Nikolic, S. Petrovic, B. Kordic, T. Dakovic-Sekulie, N. Stojanoic, FTIR investigation of solvent effects of N-methyl and N-tert-butyl benzamide, J. Struct. Chem. 55 (88) (2014) 1616–1622.
[23] A. Garcia, J.M. Elorza, J.M. Ugalde, Density functional studies of the pseudo-π.aσ charge-transfer complex between cyclopropane and chlorine monofluoride, Phys. Chem. Chem. Phys. 1 (1999) 2203–2207.
[24] A. Garcia, E.M. Cruz, C. Sarasola, J.M. Ugalde, Density functional studies of the bπ.aσ charge-transfer complex formed between ethyne and chlorine monofluoride, J. Phys. Chem. A 101 (1997) 3021–3024.
[25] A. Garcia, J.M. Elorza, J.M. Ugalde, Density functional studies of the n.aσ charge-transfer complexes between NH_3 and BrX(X= Cl, Br), J. Mol. Struct. Theochem. 501–502 (2000) 207–214.
[26] R. Longuinhos, A.D. Lucio, H. Chancham, S.S. Alexandre, Charge transfer optical absorption mechanism of DNA: Ag-nanocluster complexes, Phys. Rev. E 93 (2016) 052413.
[27] A. Garcia, J.M. Elorza, J.M. Ugalde, Density functional studies of the n.a charge-transfer complex between sulphur dioxide and chlorine monofluoride, J. Phys. Chem. A 102 (1998) 8974–8978.
[28] L.T. Tang, Y. Wei, Y. Wang, S.W. Hu, X.Q. Liu, T.W. Chu, X.Y. Wang, A density functional study on the formation of charge transfer complexes between alkaloids and iodine monochloride, J. Mol. Struct. 686 (2004) 25–30.
[29] S.B. Chattaraj, A. Chakrabortty, S.P. Sharma, S.C. Lahiri, Spectrophotometric, FTIR and theoretical studies of the charge-transfer complexes between nicotinamide and the acceptors(p-chloranil, chloranilic acid and DDQ) in acetonitrile, their association constants, thermodynamic properties and other related properties, J. Solut. Chem. 44 (12) (2015) 2357–2382.
[30] S.F. Hmuda, N.R. Banjac, N.P. Trisovic, B.D. Bojic, N.V. Valentic, G.S. Uscumlic, Solvent effect on the absorption spectra of potentially pharmacologically active 5-alkyl-5arylhydantoins: a structure-property relationship study, J. Serb Chem. Soc. 78 (5) (2013) 627–637.
[31] W.J. Mckinney, A.I. Popov, Studies on the chemistry of halogens and of polyhalides, XXX. The influence of solvent properties on the formation of pyridine-iodine charge transfer complexes, J. Am. Chem. Soc. 91 (1969) 5215–5218.
[32] G.A. Olah, J.M. Bollinger, A.M. White, Solvent effects on the iodine-pyridine charge transfer complex, J. Am. Chem. Soc. (1969) 3669–3670.
[33] B.F. Levine, C.G. Bethea, Hyperpolarizability of the pyridine-iodine charge transfer complex, J. Chem. Phys. 85 (6) (1976) 2439–2442.
[34] S.N. Rajkhowa, S.K. Baruah, Study on comparison of polar and non-polar solvents on the blue-shifted iodine band of a-picoline-iodine complex, Asian J. Chem. 16 (1) (2004) 190–196.
[35] S.K. Baruah, Linear solvation energy concept on infrared spectra of donors on complex formation with halogens and interhalogens, Int. J. Chem. Sci. 1 (3) (2003) 187–192.
[36] K.M.C. Davis, M.C.R. Symons, Charge-transfer complexes. Part I. interaction with tolvent, J. Chem. Soc. (1965) 2079–2083.
[37] A.S. Tiwary, A.K. Mukherjee, Calculation of the charge transfer transition energy of the mesitylene-ICl complex by *ab initio* and TDDFT methods: comparison with other methylbenzene-ICl complexes, Mol. Phys. 107 (19) (2009) 2063–2070.
[38] H. Kusama, H. Sugihara, Theoretical studies of 1:1 charge-transfer complexes between nitrogen-containing heterocycles and I_2 molecules, and implications on the performance of dye-sensitized solar cell, J. Photochem. Photobiol. A Chem. 181 (2–3) (2006) 268–273.
[39] B. Raimondi, G.L. Manna, Structure and spectroscopic study of rthe Br_2–-3-Br-pyridine complex by DFT calculations, Spectrochim. Acta Part A Mol. Biomol. Spectrosc. 69 (3) (2008) 933–938.
[40] H. Kusama, H. Sugihara, Density functional study of alkylpyridine–iodine interaction and its implications in the open-circuit photovoltage of dye-sensitized solar cel, Sol. Energy Mater. Sol. Cells 90 (7–8) (2006) 953–966.
[41] A.S. Tiwary, P.S. Sengupta, A.K. Mukherjee, Modelling the ground state geometry and estimating the charge transfer transition energy of the toluene-ICl molecular complex by ab initio and DFT methods, J. Theor. Comput. Chem. 7 (3) (2008) 331–346.
[42] O.K. Poleshchuk, J. Koput, J.N. Latosinska, B. Nogaj, ab initio study of the bonding and nuclear quadrupole coupling in the Py-ICl complex, J. Mol. Struct. 513 (1–3) (1999) 29–34.
[43] M. Esseffar, W. Bouab, A. Lamsabhi, J.L.M. Abboud, R. Notario, M. Yenez, An experimental and theoretical study on some thiocarbonyl-I2 molecular complexes, J. Am. Chem. Soc. 122 (2000) 2300–2308.
[44] P.L. Anto, R.J. Anto, H.T. Varghese, C.Y. Panicker, D. Philip, G.F.S. Andrade, G.B. Alexandre, Spectroscopic investigations and computational study of sulfur trioxide-pyridine complex, J. Raman Spectrosc. 42 (2011) 1812–1819.
[45] S. Reiling, M. Besnard, A.P. Bopp, Theoretical studies on the pyridine-I_2 charge transfer complex. 1. Ab-initio calculations on I_2 and pyridine-I_2, J. Phys. Chem. A 101 (1997) 4409–4415.
[46] Z. Wang, B. Zheng, X. Yu, X. Li, P. Yi, Structure, properties and nature of the pyridine-XY (X, Y= F, Cl, Br) complexes: an ab initio study, J. Chem. Phys. 132 (2010) 164104 (1-5).
[47] N.A. Al-Hashimi, Y.H.A. Hussein, Ab initio study on the formation of triiodide CT complex from the reaction of iodine with 2,3-diaminopyridine, Spectrochim. Acta Part A 75 (2010) 198–202.
[48] Y. Danten, B. Guillot, Y. Guissani, Investigation of charge transfer complexes by computer simulation. II. Iodine in pyridine solution, J. Chem.Phys. 96 (5) (1992) 3795–3810.
[49] I. Jano, Molecular orbital calculations for iodine complexes 2. Ammonium iodine and pyridine iodine, Theor. Chim. Acta. 71 (1987) 305–314.
[50] F.C. Grozema, R.W.J. Zijlstra, M. Swart, T.H. Piet, V. Duijnen, Iodine-Benzene charge-transfer complex: potential energy surface and transition probabilities studied at several levels of theory, Int. J. Quantum Chem. 75 (1999) 709–723.
[51] M. Oftadeh, M. Moghadary, M. Solimannejad, A. Semnani, A study of donor-acceptor in the charge transfer molecular complexes of some thiacrown ethers with dihalogen molecules by DFT method, Acta Chim. Slov. 60 (2013) 95–104.
[52] D. Sutradhar, T. Zeegers-Huyskens, A.K. Chandra, Theoretical study of the interaction between pyridine derivatives and atomic chlorine. Substituent effect and nature of bonding, Mol. Phys. 1–9 (2015), http://dx.doi.org/10.1080/00268976.2015.1014440.
[53] F. Muniz-Miranda, A. Pedone, G. Battistelli, M. Montalti, J. Bloino, Benchmarking TD-DFT against vibrationally resolved absorption spectra at room temperature: 7-aminocoumarins as test cases, J. Chem. Theory Comput. 11 (2015) 5371–5384.
[54] P. Gogoi, U. Mohan, M. Protim Borpuzari, A. Boruah, S. Kumar Baruah, UV-visible spectroscopy and density functional study of solvent effect on halogen bonded charge-transfer complex of 2-chloropyridine and iodine monochlor ide, Arab. J. Chem. (2016), http://dx.doi.org/10.1016/j.arabjc.2016.07.011.
[55] Z. Lyatajka, H. Ratajozaka, W.J. Orville-Thomas, A study of the properties of charge transfer complexes in systems composed of pyridine derivatives and chloride by the CNDO/2 Method, Theor. J. Eksperimental'naya Khimiya 13 (4) (1977) 518–521.
[56] A.V. Vasilyev, S.V. Lindeman, J.K. Kochi, Molecular structure of the metastable charge-transfer complexes of benzene (and toluene) with bromine as the pre-reactive intermediates in electrophilic aromatic bromination, New. J. Chem. 26 (2002) 582–592.
[57] E. Augdahl, P. Klaeboe, Spectroscopic studies of charge transfer complexes, Acta Chem. Scand. 19 (4) (1965) 807–816.
[58] M.S. Subhani, S. Aslam, R. Qureshi, A. Rahman, UV spectroscopic studies of charge transfer complxes of 2-hydroxy-1,4-naphthoquinone, J. Chem. Soc. Pak. 30 (2) (2008) 232–236.
[59] M.S. Refat, M.Y. El-Sayed, A.M.A. Adam, H.A. Saad, H.H. Eldaroti, Charge transfer complexes as a semiconductor models: outline of spectroscopic studies on electron donor-acceptor complexes of hexane-1,6-diol with different π-acceptors, Int. J. Electrochem. Sci. 8 (2013) 4234–4259.
[60] E.M. Kosower, An Introduction to Physical Organic Chemistry, Wiley International, 1968.
[61] A.D. Becke, Density-functional exchange-energy approximation with correct asymptotic behavior, Phys. Rev. A 38 (1988) 3098.
[62] A.D. Becke, Density functional thermochemistry. III. The role of exact exchange, J. Chem. Phys 98 (1993) 5648.
[63] C. Lee, W. Yang, R.G. Parr, Development of the colle-salvetti correlation-energy formula into a functional of the electron density, Phys. Rev. B 37 (1988) 785.
[64] J.-D. Chai, M. Head-Gordon, Long-range corrected hybrid density functionals with damped atom–atom dispersion corrections, Phys. Chem. Chem. Phys. 10 (2008) 6615–6620.
[65] A. Klamt, G. Schüürmann, COSMO: a new approach to dielectric screening in solvents with explicit expressions for the screening energy and its gradient, J. Chem. Soc. Perkin Trans. 2 (5) (1993) 799–805.
[66] M.W. Schmidt, K.K. Baldridge, J.A. Boatz, S.T. Elbert, M.S. Gordon, J.H. Jensen, S. Koseki, N. Matsunaga, K.A. Nguyen, S.J. Su, T.L. Windus, M. Dupuis, J.A. Montgomery, General atomic and molecular electronic structure system, J. Comput. Chem. 14 (1993) 1347–1363.
[67] J.-D. Chai, M. Head-Gordon, Systematic optimization of long-range corrected hybrid density functionals, J. Chem. Phys. 128 (1–15) (2008) 084106.
[68] H. Razzaq, R. Qureshi, N.K. Janjua, F. Saira, S. Saleemi, Charge transfer complexes of picolines with σ-and π-acceptors, Spectrochim. Acta Part A 70 (2008) 1034–1040.
[69] H.M. Salmana, U.M. Rabie, E.M. Abd-Alla, Charge transfer complexes of some pyrimidines with π- and σ-acceptors, Can. J. Anal. Sci. Spectrosc. 49 (1) (2004) 1–7.
[70] M. Basila, D. Clancy, The ionisation potentials of monosubstituted pyridines by electron impact, J. Phys. Chem. 67 (7) (1963) 1551–1554.
[71] C. Reichardt, T. Welton, Solvents and Solvent Effects in Organic Chemistry, fourth ed., WILEY-VCH Verlag GmbH & Co. KGaA, Weinheim, London, 2011.
[72] S. Reiling, M. Besnard, P.A. Bopp, Theoretical studies on the pyridine–I_2 charge-transfer complex. 1. Ab-initio calculations on I_2 and pyridine–I_2, J. Phys. Chem. A 101 (24) (1997) 4409–4415.
[73] C. Reid, R.S. Mulliken, Molecular compounds and their spectra. IV. The pyridine-iodine System[1], J. Am. Chem. Soc. 76 (15) (1954) 3869–3874.
[74] A. Chen, X. Pu, S. He, Y. Guo, Z. Wen, M. Li, N.B. Wong, A. Tian, Solvent effects on isolated formamide and its monohydrated complex: observations from

PCM study, New J. Chem. 33 (2009) 1709–1719.
[75] A. Dreuw, M. Head-Gordon, Failure of time-dependent density functional theory for long-range charge transfer excited states: the zincbacteriochlorin-bacteriochlorin and bacteriochlorophyll-spheroidene complexes, J. Am. Chem. Soc. 126 (2004) 4007–4016.
[76] D. Jacquemin, E.A. Perpete, G. Scalmani, M.J. Frisch, R. Kobayashi, C. Adamo, Assesment of the efficiency of long-range corrected functional for some properties of large compounds, J. Chem. Phys. 126 (1–12) (2007) 144105.
[77] B.M. Wong, M. Piacenza, F.D. Sala, Absorption and fluorescence properties of oligothiophene biomarkers from long-range-corrected time-dependent density functional theory, Phys. Chem. Chem. Phys. 11 (2009) 4498–4508.
[78] T.T. Arifioglu, M. Efecinar, N. Satiroglu, A combined first principles TDDFT and experimental study on the UV-Vis spectra properties of M(p-nitrophenyl azo resorcinol)3 complexes (M: Fe, Cr), Turk J. Chem. 38 (2014) 99–108.
[79] T.A. Niehaus, T. Hofbeck, H. Yersin, Charge-transfer excited states in phosphorescent organo-transition metal compounds: a difficult case for time dependent density functional theory, RSC Adv. 5 (2015) 63318–63329.

Arabian Journal of Chemistry (2019) **12**, 4522–4532

King Saud University

Arabian Journal of Chemistry

www.ksu.edu.sa
www.sciencedirect.com

ORIGINAL ARTICLE

UV-Visible spectroscopy and density functional study of solvent effect on halogen bonded charge-transfer complex of 2-Chloropyridine and iodine monochloride

Pallavi Gogoi *, **Uttam Mohan, Manash Protim Borpuzari, Abhijit Boruah, Surjya Kumar Baruah**

Department of Chemistry, Dibrugarh University, Dibrugarh, Assam 786004, India

Received 8 April 2016; accepted 23 July 2016
Available online 5 August 2016

KEYWORDS

MLRT;
Solvent parameter;
NBO;
NRT;
QTAIM

Abstract 2-Chloropyridine and Iodine monochloride form 1:1 $n \rightarrow \sigma^*$ charge transfer complex which is confirmed by Benesi Hildebrand plot using UV-vis spectroscopy. Multiple Linear Regression Technique (MLRT) shows that 2-Chloropyridine-ICl complex is susceptible to medium effect in reference to different solvent parameters, at both the bulk and molecular levels. Dielectric constant ($\in$), refractive index (n), Hansen parameter, Catalan parameter and Kamlet's π^* values give good linear fit equations between experimental and calculated CT bands with R^2 values as high as 1. Polarizability effect on the CT band is examined using Buckingham and Lippert Mataga equation. Formation constant of the complex in different mediais found to be linearly dependent on Hansen solubility parameter. Computational analysis defends well the blue shift in polar medium observed for 2-Chloropyridine-ICl. NBO, NRT, and QTAIM analyses explain a shift from ionic character to covalent character in polar medium. It emphasises a stronger donor acceptor interaction in polar medium and thereby explains the experimentally observed blue shift. A logarithmic relation between the bond lengths of the bridging atoms and dielectric constant is proposed.

1. Introduction

Charge transfer (CT) complexes are formed when electron transfer occurs from one compound to another. The former compound is called the donor (D) and the latter is called the acceptor (A) (Mulliken, 1952, 1956; Mulliken and Pearson, 1969). Appearance of a new band with those of donor and acceptor bands in the electronic spectra of the donor and acceptor together in solution, confirms the formation of a new CT compound which is capable of absorbing in the UV-vis region of the spectrum (Benesi and Hildebrand, 1949). Such bands are thus

* Corresponding author.
E-mail address: gogoipallavi@yahoo.com (P. Gogoi).
Peer review under responsibility of King Saud University.

ELSEVIER Production and hosting by Elsevier

http://dx.doi.org/10.1016/j.arabjc.2016.07.011
1878-5352

termed as CT bands. CT bands are formed for the electronic transition from the ground state complex [D, A] to the dative excited state [D^+, A^-] (Vasilyev et al., 2001). Depending on the type of molecular orbital involved during the electronic transition, CT complexes are classified accordingly (Guryanova et al., 1975). In the recent years, considerable interest is given to charge-transfer complexes, due to their vast application in the field of organic electronics, such as in organic solar cells and in light-emitting diodes (Walzer et al., 2007; Gunes et al., 2007).

Halogen bonds are also a kind of electron donor-acceptor interaction, in which a halogen atom X interacts with an atom, Y, with an excess of electron charge density and are denoted by RX−X···Y−RY formulae (Matter et al., 2009; Politzer et al., 2007, 2010; Lu et al., 2009). One such donor acceptor interaction is observed in case of 2-Chloropyridine and Iodine monochloride. 2-Chloropyridine is an important chemical as an insecticide, microbiocide, molluscicide, nematicide, Insect Growth Regulator, etc (Shimizu et al., 2012). It is also used in the preparation of antihistaminic agent pheniramines (Botteghi et al., 1994). Iodine monochloride is basically used in determining the Iodine number of fats, fatty acids, oils and various organic solvents by Wij's method. Moreover it is used as an iodinating agent to produce pharmaceuticals, in enhancing the conductivity of carbon nanotube wires and also in the synthesis of graphene (Xiong et al., 1999; Lahyani and Trabelsi, 2016; Janas et al., 2014; Jadaun et al., 2013). 2-Chloropyridine-ICl CT complex is formed by the transfer of electron from the lone pair on nitrogen atom of the pyridine ring to the antibonding σ^* orbital of the ICl molecule. Formation of the CT complex is confirmed by electronic spectroscopy.

Solvatochromism is a significant behaviour of CT complexes observed. Many solute-solvent interaction types are held responsible for the preferential blue or red shift observed for a CT band in polar medium (Basavaraja et al., 2015; Taft and Kamlet, 1976; Kamlet et al., 1979; Kamlet and Taft, 1979). Several solvent parameters are formulated to define the type of interaction responsible for the Solvatochromic shift (Catalan, 2009; Hansen, 1967). Kamlet's Linear Solvation Energy Relationship is a landmark in determining the partial effect of different parameters on the spectroscopic parameter of a CT band. Nowadays, it is possible to analyse simultaneous effect of different solvent parameters on the spectroscopic behaviour with the help of Multiple Linear Regression Technique (MLRT) (Hmuda et al., 2013).

Besides solvent effect study, recently, density functional theory (DFT) has been extensively used in chemistry and physics to study the ground and excited state properties of molecular systems (Kohn and Sham, 1965). In a conventional DFT calculation, Kohn-Sham (KS) equation is iteratively solved by using various exchange-correlation functionals which are of LDA, GGA and hybrid types. However, failure of conventional density functional in predicting some ground and excited state properties is recently reported (Tozer and Handy, 1998; Tozer et al., 1999; Dreuw et al., 2003). To overcome the drawback of conventional density functional, range-separated density functional is developed in which the electron–electron repulsion term is split into long-range interaction term (*first term in* Eq. (1)) which describes the long-range exchange interaction using the Hartree–Fock exchange (HF) integral and short-range interaction term (*second term in* Eq. (1)) which includes the DFT exchange functional (Savin, 1996; Leininger et al., 1997). Range-separated density functionals are found to reproduce nonlinear optical properties, reaction barrier height, charge-transfer excitation, Rydberg excitation and van der Waals interactions (Iikura et al., 2001; Tawada et al., 2004; Vydrov and Scuseria, 2006; Peverati and Truhlar, 2012; Sekino et al., 2007; Tsai et al., 2013).

$$\frac{1}{r_{12}} = \frac{\mathrm{erf}(\mu r_{12})}{r_{12}} + \frac{\mathrm{erfc}(\mu r_{12})}{r_{12}} \quad (1)$$

where μ is the range–separation parameter.

We have approached both experimentally and theoretically to study spectroscopic behaviour of 2-Chloropyridine-ICl complex in the UV-vis region in different solvent media.

2. Experimental details

UV–Visible spectra of the charge transfer complex in different media are recorded in a Shimadzu UV-1700 PharmaSpec UV-vis spectrophotometer. All the five solvents Carbon tetrachloride, Cyclohexane, *n*-Hexane, Chloroform and Dichloromethane used are from Merck with percentage purity of 97–99%. The solvents are distilled at their boiling points for spectroscopic purpose. 2-Chloropyridine used is from Fluka (98%) with a density of 1.209 gml^{-1}. Iodine monochloride (98%) is used from CDH. Percentage purity and density values are included in the calculations while preparing quantitative solutions of the compounds.

The sample solutions for recording UV-vis spectra are prepared as reported earlier (Mckinney and Popov, 1969; Lyatajka et al., 1977; Augdahl and Klaeboe, 1965; Subhani et al., 2008; Refat et al., 2013).

3. Computational details

Geometries of all the stationary points are fully optimised at gas phase and in solvent medium using LC-BLYP (Iikura et al., 2001) functional and 6-31 + + G(d,p) basis set for main group elements and LANL2DZ for I atom. This chosen basis set is recently being used to study the charge-transfer transition energy of the mesitylene-ICl complexes (Tiwary and Mukherjee, 2009). Frequency calculations are performed at the same level of theory to confirm the stationary point as minimum. The conductor like screening model (COSMO) is used for the calculations in the solvent medium. Geometry optimisation and frequency calculations are performed at GAMESS

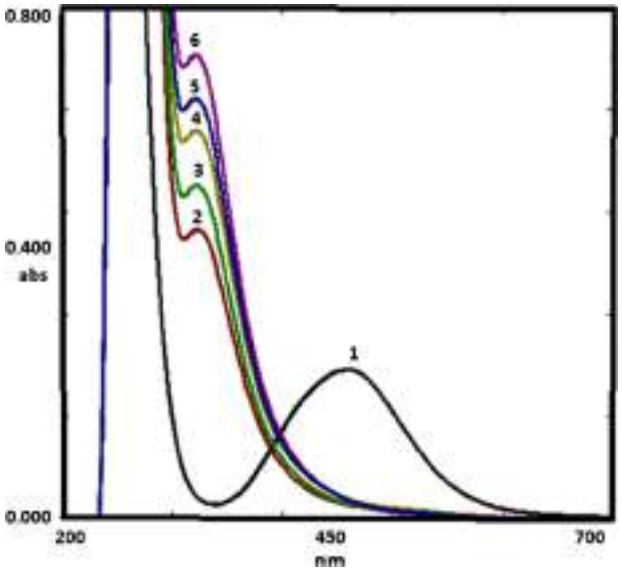

Figure 1 UV-vis spectra of 2-Chloropyridine and ICl in Chloroform at 25 °C for 1 cm cell. The concentrations of 2-Chloropyridine (M) are (1) zero; (2) 0.1054; (3) 0.3162; (4) 0.527; (5) 0.7378; (6) 0.9486.

software (Schmidt et al., 1993). Moreover, natural bond orbital (NBO) and quantum theory of atom in molecule are performed using NBO6 (Glendening et al., 2013) and multiwfn suite of program respectively.

4. Results and discussion

4.1. Experimental analysis

4.1.1. Spectral properties of the acceptor, donor and the complex formed in solution

2-Chloropyridine and ICl both are soluble in all the five solvents used in this study. Solution of 2-Chloropyridine in all the solvents is colourless while that of ICl is light brownish. Gradual addition of 2-Chloropyridine solution to the ICl solution results in lightening of brown colour of ICl up to different extents indicating the formation of a new compound (Refat et al., 2013). Pure ICl absorbs at 453.2 nm and 2-Chloropyridine absorbs at 256.2 nm in chloroform. When these two are mixed a new band appears at 324 nm which is neither the characteristic of ICl or of 2-Chloropyridine. Appearance of this band confirms the formation of the charge transfer complex between ICl and 2-Chloropyridine (Fig. 1). Similar observations are obtained for the other four solvents (Fig. 2). From the UV-vis spectra the stoichiometry of the complex formed is found to be 1:1 using the modified Benesi-Hildebrand plot which gives straight lines for all the five solvents considered (Fig. 3).

Table 1 lists the physical data such as CT absorption band wavelength (λ_{max}), Extinction coefficient (ε_{max}), Formation constant (K_C), Energy of the CT band (ΔE_{CT}), Ionisation Potential of the donor in the complex (I_p), Dissociation Energy (W), Resonance Energy of the complex in the ground state

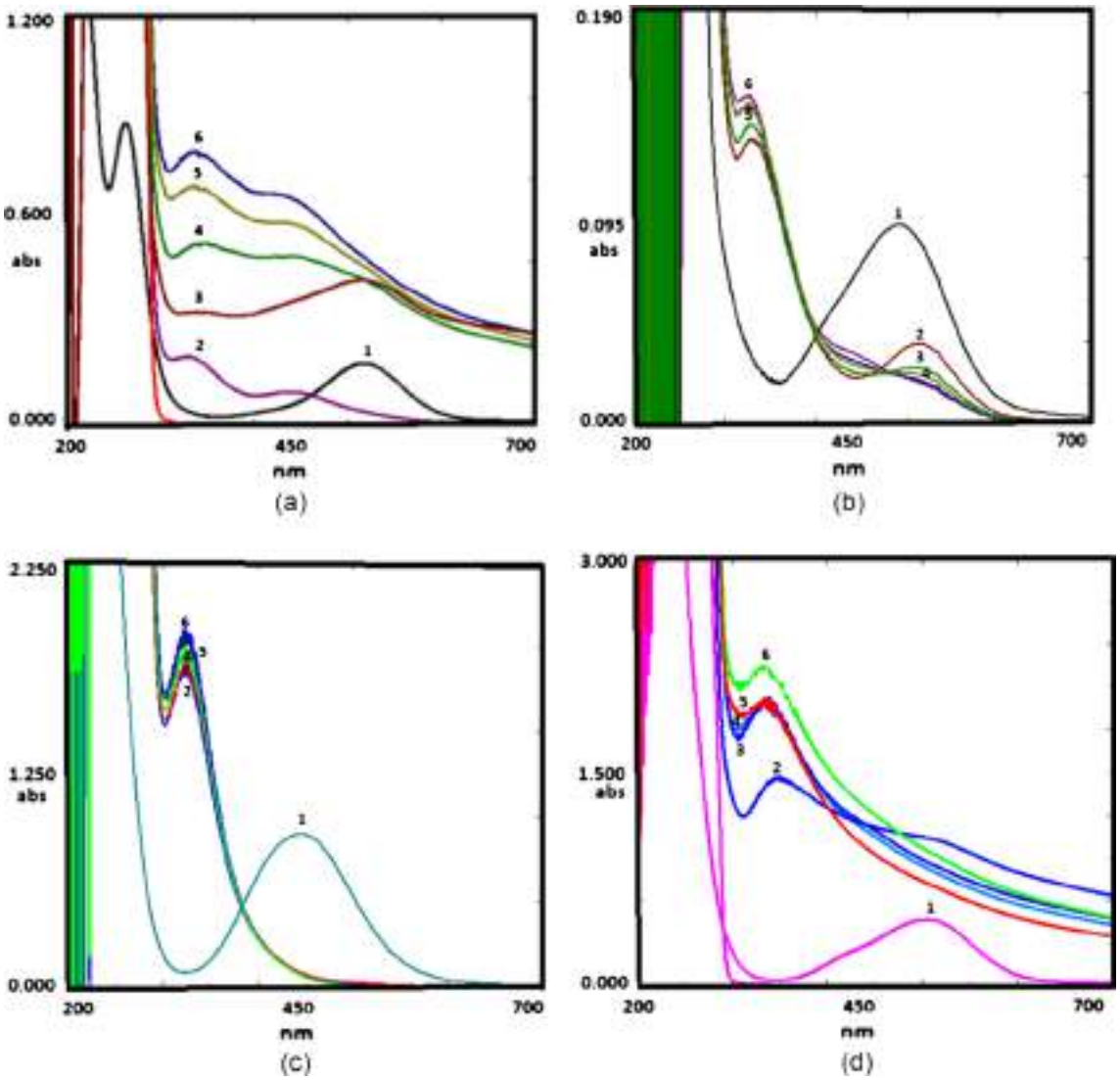

Figure 2 UV-vis spectra of 2-Chloropyridine-ICl charge transfer complex in (a) Hexane, (b) CCl_4, (c) CH_2Cl_2 and (d) Cyclohexane at 25 °C in 1 cm cell. The concentration of ICl is kept constant and that of 2-Chloropyridine is varied. The concentrations of 2-Chloropyridine (M) are (a) Hexane: (1) zero; (2) 0.06999; (3) 0.20997; (4) 0.34995; (5) 0.48993; (6) 0.62991. (b) CCl_4: (1) zero; (2) 0.0351; (3) 0.0763; (4) 0.1053; (5) 0.1755; (6) 0.3159. (c) CH_2Cl_2: (1) zero; (2) 0.1054; (3) 0.3162; (4) 0.527; (5) 0.7378; (6) 0.9486. (d) Cyclohexane: (1) zero; (2) 0.06999; (3) 0.20997; (4) 0.34995; (5) 0.48993; (6) 0.62991.

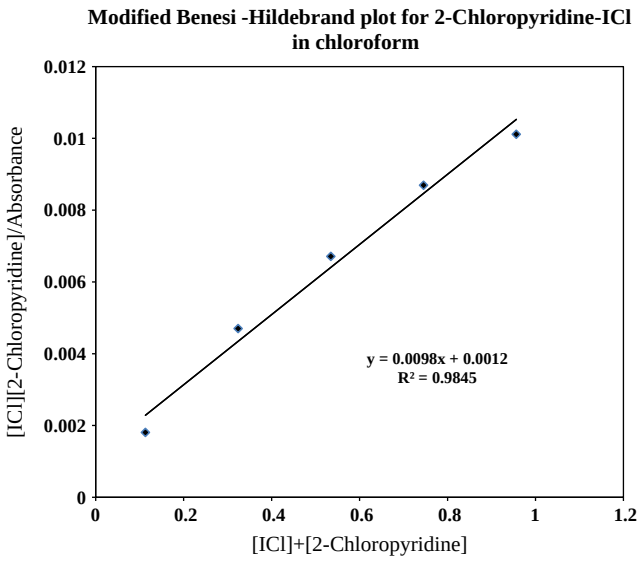

Figure 3 Modified Benesi-Hildebrand plot for 2-Chloropyridine-ICl complex in $CHCl_3$.

(R_N), and the Gibbs free energy change (ΔG) at the experimental temperature. These values are calculated with the help of established equations (Razzaq et al., 2008). The Ionisation potential values of the donor match nicely with the previously calculated values by electron impact method (Basila and Clancy, 1963).

Table 1 clearly shows the dependence of the λ_{max} value on the dielectric constant value of the experimental solvents. Similarly all the parameters linked with λ_{max} vary accordingly. It is already reported that increasing solvent polarity affects the Charge Transfer Energy by solvating the energy levels up to different extents. Lowering of the LUMO in the energy axis or stabilizing it more as compared to the HOMO, may lead to an increase in the charge transfer transition energy (ΔE_{CT}). It may occur as a result of more polar nature of the LUMO which leads to more solvation of the LUMO and as a result it gets stabilized to a greater extent. Moreover a blue shift of λ_{max} indicates n-σ^* transition. It establishes the formation of the 2-Chloropyridine-ICl complex through the lone pair on N atom as is found in case of Iodine forming compounds with lone pair donors (Kamlet et al., 1979; Salman et al., 2004).

4.1.2. Quantitative estimation of effect of solvent parameters upon CT band by MLRT

The solvent parameters for the solvents under study are in Table 2. Solvatochromic study of CT band is done in a large scale in varieties of compounds such as drugs, dyes, flavones (Catalan, 2009; Aggarwal and Khurana, 2014; Alimmari et al., 2015; Jovie et al., 2014; Dawoud et al., 2014). MLRT is a recent approach to analyse the dependence of any spectroscopic property (λ_{max}, $\Delta\bar{\nu}$ etc.) of a compound on various solvent parameters (Hmuda et al., 2013; Alimmari et al., 2015; Zakerhamidi et al., 2012). In this study, MLRT is applied using Excel 2007 at the 95% confidence level. We have examined the dependence of λ_{max} on the solvent parameters under study. Among the solvent parameters we have selected ε, n, π^*-value, Hansen parameters and Catalan parameters. ε and n determine solute-solvent interaction considering bulk environment whereas the rest three indicates solute-solvent interaction at the molecular level. The regression plot of λ_{max} (exp.) against λ_{max} (calc.) (Fig. 4) shows that Hansen parameters have excellent correlation with the λ_{max} value with R^2 value of 1. The result of regression analysis is shown in Table 3.

Table 3 shows that Solvatochromic shift is largely dependent on solute–solvent interaction at the molecular level. Similar Regression analysis with the Formation Constant value is also done. Although formation constant value of a CT complex is reported to show variation with the changing polarity no specific change is reported till now (Refat et al., 2010). Table 1 shows irregular variation in the values of K_c with polarity. Thus we tried to check whether K_c is a multi parameter dependent characteristic rather than being dependent solely upon the solvent polarity or dielectric constant value.

Table 1 Spectroscopic and physical parameters of 2-Chloropyridine-ICl.

Solvent	ε	n	λ_{max}(CT) (in nm)	ε_{max} (in L mol^{-1} cm^{-1})	K_c (in L mol^{-1})	ΔE_{CT} (in eV)	Ip (in eV)	W (in eV)	$R_N \times 10^{12}$ (in eV)	ΔG^0 (KJ/mol)
COMPOUND: 2-Chloropyridine-ICl										
n-C_6H_{14}	1.890	1.3749	340.2	269.54	6.51	3.646053	10.23	5.15	12.78	37.14
CycloC_6H_{14}	2.023	1.4262	334.0	1000.00	100.00	3.713734	10.31	5.17	48.29	570.58
CCl_4	2.238	1.4630	330.4	200.00	125.00	3.754171	10.36	5.18	9.77	713.23
$CHCl_3$	4.806	1.4457	324.0	111.11	9.00	3.828365	10.45	5.19	5.53	51.35
CH_2Cl_2	9.080	1.4235	322.8	333.33	37.50	3.842592	10.47	5.20	1.67	213.97

Table 2 Different solvent parameters.

Solvent	λ_{max} (nm)	ε	n	π^*	Hansen solubility parameter (MPa$^{1/2}$)			Catalan solvent parameters		
					δD	δP	δH	SPP	SB	SA
n-C_6H_{14}	340.2	1.890	1.3749	−0.04	14.9	0.0	0.0	0.519	0.056	0.000
CycloC_6H_{14}	334.0	2.023	1.4262	0.00	16.8	0.0	0.2	0.557	0.073	0.000
CCl_4	330.4	2.238	1.4630	0.28	17.8	0.0	0.6	0.632	0.044	0.000
$CHCl_3$	324.0	4.806	1.4457	0.58	17.8	3.1	5.7	0.786	0.071	0.047
CH_2Cl_2	322.8	9.080	1.4235	0.82	18.2	6.3	6.1	0.876	0.178	0.040

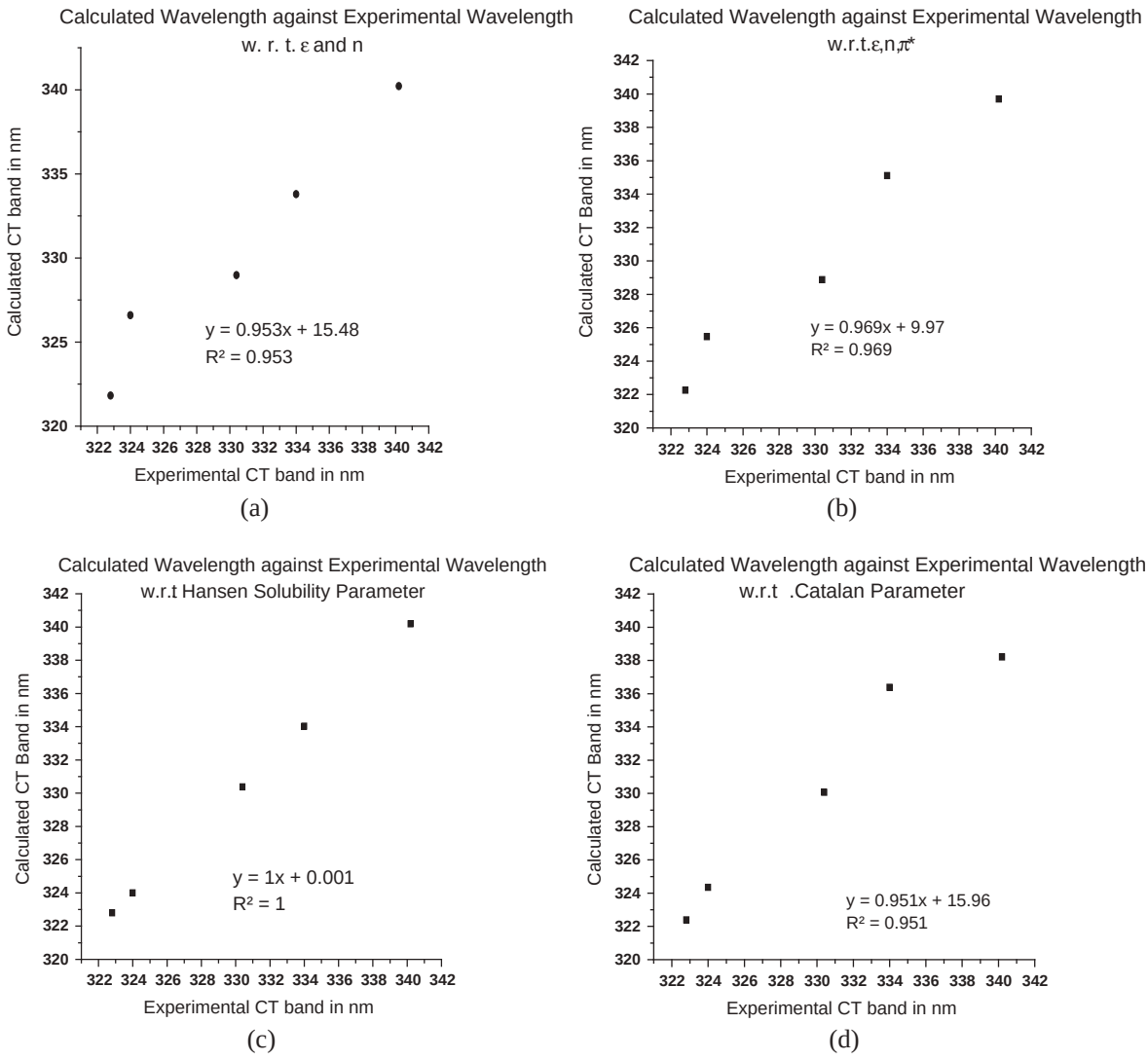

Figure 4 Calculated λ_{max} Vs experimental λ_{max} plots w. r. t. (a) ε and n, (b) ε, n, π^*, (c) Hansen solubility parameters, (d) Catalan parameters.

Table 3 Result of regression analysis for λ_{max} and K_C of CT band.

Parameter	Independent parameters	Linear equation	R^2	Comment
λ_{max}	ε, n	$\lambda_{max} = 509.43 - 1.74\varepsilon - 120.68n$	0.953	Regression valid
	ε, n, π^*	$\lambda_{max} = 448.88 - 0.52\varepsilon - 79.04n - 11.48\pi^*$	0.969	Regression valid
	Hansen solubility parameter	$\lambda_{max} = 386.39 - 3.10\delta D + 0.18\delta P - 1.36\delta H$	1.000	Excellent regression
	Catalan parameters	$\lambda_{max} = 370.80 - 67.47SPP + 43.35SB + 74.46SA$	0.951	Regression valid
K_C	ε, n	$K_C = -1399.52 - 7.469\varepsilon + 1040.93n$	0.525	Regression invalid
	ε, n, π^*	$K_C = -3519.03 + 35.43\varepsilon + 2498.47n - 40.99\pi^*$	0.888	Regression poor
	Hansen solubility parameter	$K_C = -697.374 + 47.397\delta D + 6.71\delta P - 27.83\delta H$	0.993	Good regression
	Catalan parameters	$K_C = -312.509 + 739.62\ SPP - 550.73\ SB - 4822\ SA$	0.749	Regression invalid

In case of Formation constant too Fig. 5 shows that it is dependent on Hansen parameters with a high R^2 value of 0.993 and it is completely independent of bulk parameters. Although we have performed MLRT considering a linear relation to exist between the Formation Constant of the CT complex and the solvent parameters and we are obtaining quite satisfactory result for the Hansen parameters, still we cannot put forward a conclusive remark on that until and

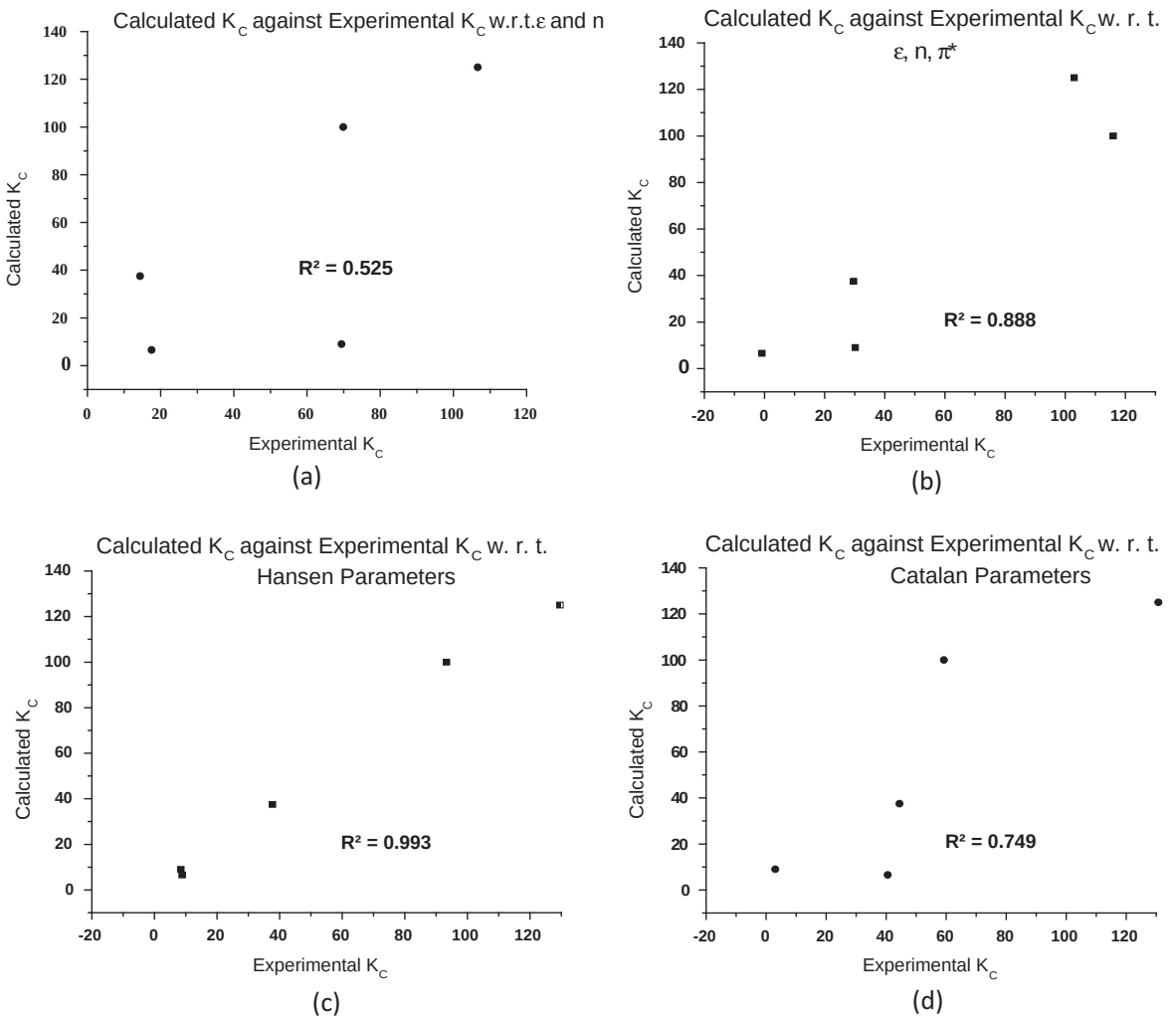

Figure 5 Calculated K_C Vs experimental K_C plots w. r. t. (a) ε and n, (b) ε, n, π^*, Hansen solubility parameters, (d) Catalan parameters.

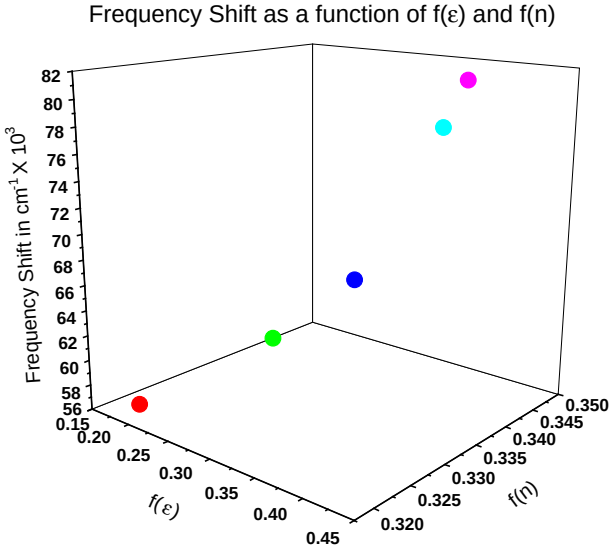

Figure 6 3D plot for Buckingham equation.

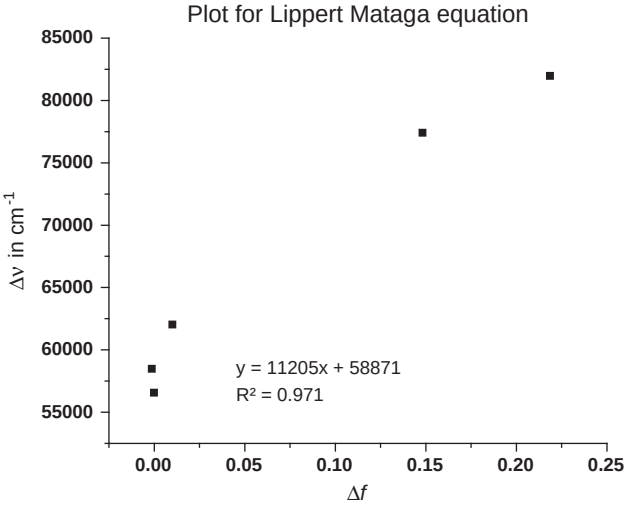

Figure 7 Graphical plot for Lippert Mataga equation.

unless we perform similar tests with other CT complexes in different media. Since it is beyond the scope of this paper to include a large number of such complexes, we propose to examine our approach in our future works.

4.1.3. Validity of Buckingham and Lippert Mataga equation

Buckingham equation relates Spectroscopic Property ($\Delta\bar{\nu}$ in our case) with the function of dielectric constant f(ε) and the function of refractive index, f(n) as given in Eq. (2).

$$XYZ = XYZ_0 + c_1\frac{(\varepsilon-1)}{(2\varepsilon+1)} + c_2\frac{(n^2-1)}{(2n^2+1)} \tag{2}$$

A 3D plot of $\Delta\bar{\nu}$, f(ε) and f(n) show the dependence of $\Delta\bar{\nu}$ on f(ε) and f(n) in Fig. 6.

Combination of f(ε) and f(n) together is called as Orientation Polarizability. Lippert Mataga equation (Reichardt and Welton, 2011) shows a linear correlation between Frequency Shift (Change in position of CT band from the respective acceptor) and the Orientation Polarizability of corresponding solvents. Fig. 7 shows good linear correlation between frequency shift and Orientation Polarizability with R^2 value of 0.971.

4.2. Computational analysis

4.2.1. Molecular geometries

The optimised geometries of 2-Chloropyridine-ICl in all the media are shown in Fig. 8 whereas selected geometrical parameters are tabulated in Table 4. It is seen from Fig. 8 that the Cl atom of acceptor ICl molecule stays a bit away from the substituent Cl atom in the donor 2-Chloropyridine molecule with an angle greater than 120^0. The reason may be the steric

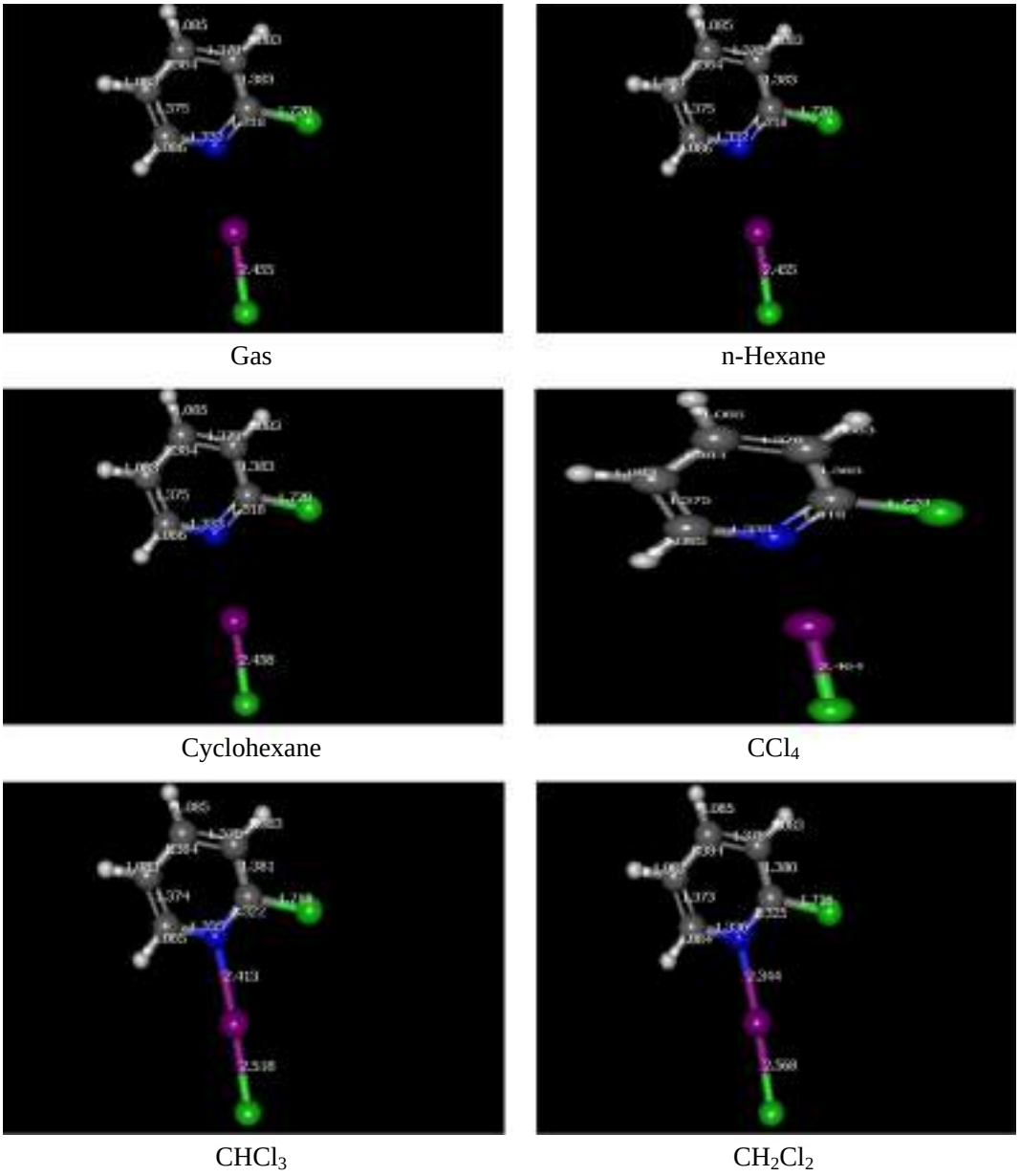

Figure 8 Optimized geometries of 2-Chloropyridine-ICl.

Table 4 Geometric parameters of 2-Chloropyridine-ICl in different media (Bond lengths are in A° and bond angles are in degrees).

	Gas phase	n-C_6H_{14} (1.890)	CycloC_6H_{14} (2.023)	CCl_4 (2.238)	$CHCl_3$ (4.806)	CH_2Cl_2 (9.080)
$r_{N–I}$	2.620	2.540	2.530	2.520	2.410	2.340
$r_{I–Cl}$ in the complex	2.430	2.450	2.460	2.460	2.520	2.570
r_{ICl} in free state	2.366	2.371	2.372	2.372	2.379	2.384
Δr_{ICl}	0.064	0.079	0.088	0.088	0.141	0.230
< C(6)N(1)I(11)	127.890	127.290	127.220	127.130	126.380	125.850

repulsion between the two Cl atoms. Moreover, it is seen from Table 4 that the < C(6)N(1)I(11) angle decreases with increase in dielectric constant of the solvent. However, this decrease in the angle is not very large. For instance, < C(6)N(1)I(11) angle in gas phase and CH_2Cl_2 solvent with dielectric constant 9.08 are 127.89° and 125.85° respectively. This observation may be attributed to slight decrease in steric repulsion between the two Cl atoms with solvent polarity. Moreover, inspection of N–I and I–Cl bond length from Table 4 indicates that N–I bond length decreases with the increasing dielectric constant of the solvent and the I–Cl bond distance increases with the increasing solvent dielectric constant. The N–I bond length in the gas phase and the increase in the I–Cl bond length due to complexation in the gas phase are close to those of previously reported values for Pyridine-I_2 CT complex (Reichardt and Welton, 2011).

Decrease in the bond length between the bridging atoms of donor and acceptor molecules with complexation and the increasing polarity of the mediums is already reported for similar compounds (Tiwary and Mukherjee, 2009; Reiling et al., 1997; Tiwary et al., 2008). From Table 4 and previous reports we thus can conclude a stronger donor acceptor interaction in polar medium.

We have tried to examine the probability of a quantitative relation between the N–I and I–Cl bond length with that of dielectric constant. Thus we made a plot of bond length against dielectric constant values for both the selected bonds under study. Satisfactorily we obtain a logarithmic relation between the bond length values with the corresponding dielectric constant values of the medium as seen in Fig. 9 with an R^2 value of 0.997 for both the plots.

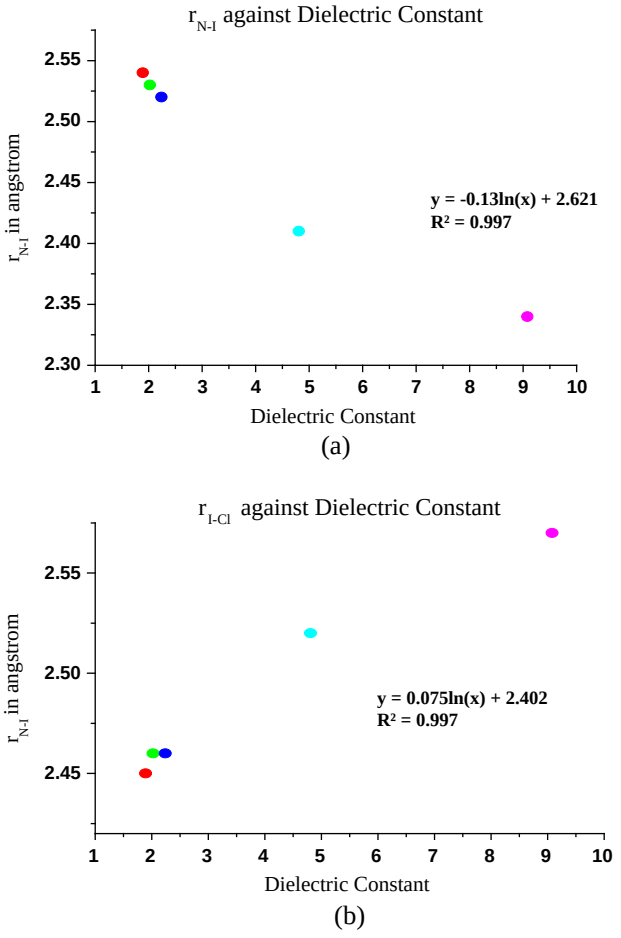

Figure 9 Dielectric constant of medium against bond length, (a) dielectric constant against $r_{N–I}$, (b) dielectric constant against $r_{I–Cl}$.

4.2.2. Natural bond orbital analysis

A single best Lewis type description of the total electron density is obtained from Natural Bond Orbital (NBO) calculations. Therefore, to understand the bonding between 2-Chloropyridine and ICl, we have performed NBO calculation on the complex between 2-Chloropyridine and ICl. In Table 5, we have tabulated the electron occupancy of the lone pair (LP) of the nitrogen and electron occupancy of valence antibond (BD*) of N–I. Moreover, the interaction energy ($E^{(2)}$) between LP of N and BD* of N–I from second order perturbation analysis is also tabulated in Table 5. It is observed that electron occupancy of LP of N decreases with increase in solvent polarity. For instance, electron occupancy of LP of N in gas phase and in CH_2Cl_2 solvent is 1.83e and 1.73e respectively. On the other hand, electron occupancy of BD* of N–I increases with increase in the solvent polarity. This behaviour indicates that electron transfer from LP of N takes place and BD* of N–I increases with the increase in solvent polarity. On inspection of $E^{(2)}$ values from Table 5, it is clear that stabilization interaction between LP of N and BD* of N–I increases with the increase in the solvent polarity.

4.2.3. Natural resonance theory analysis

Natural resonance Theory is performed to analyse the total electron density in terms of a series of idealised resonance forms. Moreover, NRT theory provides the percentage of ionic (%ionic) and covalent (%covalent) character in a bond. The %ionic and %covalent characters are tabulated in Table 6. It is observed that in gas phase, the N–I bond is almost ionic (~94%). With increase in solvent polarity, %ionic character decreases whereas %covalent character increases. For

Table 5 NBO analysis.

Medium	Dielectric constant	Occupancy of LP of nitrogen	Occupancy of BD* N–I	$E^{(2)}$ (kJ/mol)
Gas		1.83	0.11	158.172
n-C_6H_{14}	1.890	1.81	0.14	209.244
$CycloC_6H_{14}$	2.023	1.80	0.14	215.964
CCl_4	2.238	1.80	0.15	226.632
$CHCl_3$	4.806	1.76	0.20	324.744
CH_2Cl_2	9.080	1.73	0.24	411.768

Table 6 NRT analysis.

Medium	Dielectric constant	%ionic	%covalent
Gas		93.90	6.10
n-C_6H_{14}	1.890	92.41	7.59
$CycloC_6H_{14}$	2.023	92.14	7.86
CCl_4	2.238	91.89	8.11
$CHCl_3$	4.806	89.49	10.51
CH_2Cl_2	9.080	74.63	25.37

instance, in hexane, %ionic and %covalent characters are 92.41 and 7.59 respectively, whereas in CH_2Cl_2, %ionic and %covalent are 74.63 and 25.37 respectively. The decrease in %ionic and increase in %covalent indicates increase in stability of N–I bond with solvent polarity.

4.2.4. Natural energy decomposition analysis

To decompose the interaction energy (IE) to a sum of physically meaningful term, we have performed Natural Energy Decomposition Analysis (NEDA) by Glendenning and coworkers (Glendening et al., 2013). In Table 7, we have tabulated IE, Energy of charge transfer (E_{CT}) and Polarisation Energy (E_{POL}). It is seen from Table 7 that IE in gas phase is −47.99 kJ/mol. However, in hexane solvent with dielectric constant 1.89, IE drastically increases to −261.75 kJ/mol and in CH_2Cl_2 solvent with dielectric constant 9.08 IE increases to −1099.09 kJ/mol. This indicates that interaction energy increases with the increase in the solvent polarity. Inspecting the E_{CT} terms from Table 7, it is inferred that charge-transfer increases with the increase in the solvent polarity. Similar to E_{CT}, E_{POL} term also increases with the increase in the solvent polarity. However, the variation of E_{POL} with solvent polarity is small, as compared to E_{CT}. For instance, E_{CT} and E_{POL} in hexane solvent with dielectric constant 1.89 are −283.05 and −120.33 kJ/mol respectively, whereas E_{CT} and E_{POL} in CH_2Cl_2 solvent with dielectric constant 9.08 are −754.67 and −217.69 kJ/mol respectively.

4.2.5. QTAIM analysis

QTAIM analysis has been performed to analyse halogen bonded interaction between 2-Chloropyridine and ICl. The properties of the (3,−1) Bond Critical Point (BCP) between two atoms indicate the types of interaction between the two atoms. The various properties of BCP between N atom of 2-Chloropyridine and ICl are tabulated in Table 8. According to QTAIM, electron density ($\rho(r)$), Laplacian of electron density ($\nabla^2\rho(r)$) and electronic energy density ($H(r)$) at BCP are valuable parameters for probing the nature of the bond (Bader, 1990, 1991). Generally, for covalent interactions, $\rho(r)$ is large, while $\nabla^2\rho(r)$ is large and negative. On the other hand, for ionic interaction, $\rho(r)$ is small, while $\nabla^2\rho(r)$ is positive. Moreover, the magnitude of $H(r)$ reflects the covalence of interaction. A negative value of $H(r)$ indicates a significant covalent contribution while a positive value of $H(r)$ indicates a significant ionic contribution. It is observed from Table 8 that in gas phase, $\rho(r)$ is small, and $\nabla^2\rho(r)$ is positive, which indicates that the interaction between 2-Chloropyridine and ICl is ionic. However, $H(r)$ is negative, which indicates that there is also covalent contribution to the interaction. As expected, $\rho(r)$ increases with increase in dielectric constant, whereas $H(r)$ becomes more negative with increase in dielectric constant. This infers that, covalent contribution to the interaction increases with increase in dielectric constant.

Table 7 NEDA results.

Medium	Dielectric constant	λ_{max}(CT) nm	I_E (kJ/mol)	E_{CT} (kJ/mol)	E_{POL} (kJ/mol)	ES (kJ/mol)
Gas			−47.99	−136.44	−93.62	−90.89
n-C_6H_{14}	1.890	340.2	−261.75	−283.05	−120.33	−619.96
$CycloC_6H_{14}$	2.023	334.0	−290.33	−301.08	−123.73	−678.26
CCl_4	2.238	330.4	−335.05	−329.07	−129.11	−765.58
$CHCl_3$	4.806	324.0	−737.89	−566.05	−176.86	−1385.12
CH_2Cl_2	9.080	322.8	−1099.09	−754.67	−217.69	−1782.61

Table 8 QTAIM analysis.

Medium	Gas	n-C_6H_{14}	$CycloC_6H_{14}$	CCl_4	$CHCl_3$	CH_2Cl_2
Dielectric constant		1.890	2.023	2.238	4.806	9.080
Density of all electrons [$\rho(r)$]	0.035300	0.040906	0.0415850	0.0426249	0.0513022	0.0574913
Energy density $E(r)$ or $H(r)$:	−0.002024	−0.004557	−0.0049174	−0.0054242	−0.0115829	−0.0177615
Laplacian of electron density: ($\nabla^2\rho(r)$)	0.099036	0.103057	0.1031923	0.1037647	0.0961936	0.0804155

5. Conclusion

Analysis of the experimental and theoretical results confirms the dependence of the λ_{max} (CT) upon polarity of the solvents. The blue shift observed in the presence of polar medium explains the formation of $n \rightarrow \sigma^*$ CT complex between 2-Chloropyridine and ICl. Multiple Linear Regression Analysis shows that the spectroscopic parameter, λ_{max} (CT), depends on the solvent parameters under study and Hansen parameter stands as the best to determine the value of λ_{max} (CT) with an R^2 value of 1 for the plot of experimental value of λ_{max} (CT) against calculated value of λ_{max} (CT). Lippert Mataga equation shows good linear correlation between frequency shift and Polarizability term. Theoretical analysis reveals that the bond distance between the bridging atoms of the donor and acceptor decreases with complexation and the ICl bond length increases. Simultaneously theoretical result also shows that complexation increases with solvent polarity since NBO, NRT, QTAIM, analyses show increase in IE as well as covalent character with solvent polarity. Thus more polar nature of the medium indicates stronger donor acceptor interaction in case of 2-Chloropyridine-ICl CT complex which explains the blue shift of λ_{max} (CT) in polar medium. The result that has been proposed for the first time through this paper is the dependence of Formation constant value upon the solvent parameters and the logarithmic relation between the bond length and dielectric constant of the medium. Similar CT complexes are under study and the authors have already proposed the logarithmic relation between bond length and dielectric constant of the solvent medium in their ongoing communications.

Acknowledgements

PG and UM acknowledge the University Grants Commission (UGC) for granting leave on Faculty Development Program to conduct this research work. MPB acknowledges the Council of Scientific and Industrial Research (CSIR), New Delhi, for his research fellowship.

References

Aggarwal, K., Khurana, J.M., 2014. Effect of hydroxyl group on the photopysical properties of benzo(a)xanthenes-solvatochromic studies and estimation of dipole moment. J. Photochem. Photobiol., A 276, 71–82.

Alimmari, A., Bozic, B., Mizin, D., Marinkovic, A., Valentic, N., Uscumlic, G., 2015. Synthesis, structure and solvatochromic properties of some novel 5-arylazo-6-hydroxy-4-(4-methoxyphenyl)-3-cyano-2-pyridone dyes: hydrazone-azo tautomeric analysis, Arabian. J. Chem. 8, 269–278.

Augdahl, E., Klaeboe, P., 1965. Spectroscopic studies of charge transfer complexes. Acta Chem. Scand. 19, 807–816.

Bader, R.W.F., 1990. Atoms in Molecules: a Quantum Theory. Oxford University Press, Oxford.

Bader, R.W.F., 1991. A quantum theory of molecular structure and its applications. Chem. Rev. 91, 893–928.

Basavaraja, J., Inamdar, S.R., Kumar, H.M.S., 2015. Solvents effect on the absorption and fluorescence spectra of 7-diethylamino-3-thenoylcoumarin: evaluation and correlation between solvatochromism and solvent polarity parameters. Spectrochim. Acta Mol. Biomol. Spectrosc. 137, 527–534.

Basila, M., Clancy, D., 1963. The ionisation potentials of monosubstituted pyridines by electron impact. J. Phys. Chem. 67, 1551–1554.

Benesi, H.A., Hildebrand, J.H., 1949. A spectrophotometric investigation of the interaction of iodine with aromatic hydrocarbons. J. Am. Chem. Soc. 71, 2703–2707.

Botteghi, C., Chelucci, G., Ponte, G.D., Marchetti, M., Paganellit, S., 1994. New synthetic route to pheniramines via hydroformylation of functionalized olefins. Org. Chem. 59, 7125–7127.

Catalan, J., 2009. Toward a generalized treatment of the solvent effect based on four empirical scales: dipolarity (SdP, a new scale), polarizability (SP), acidity (SA), and basicity (SB) of the medium. J. Phys Chem. B 113, 5951–5960.

Dawoud, A., Yaseen, B., Al-Balawi, M., 2014. The solvatochromic, spectral, and geometrical properties of nifenezone: a DFT/TD-DFT and experimental study Phys. Chem. Chem. Phys. 16, 15519–15527.

Dreuw, A.J., Weisman, L., Head-Gordon, M., 2003. Long range charge-transfer excited states in time-dependent density functional theory require non-local exchange. J. Chem. Phys. 119, 2943–2946.

Glendening, E.D., Badenhoop, J.K., Reed, A.E., Carpenter, J.E., Bohmann, J.A., Morales, C.M., Landis, C.R., Weinhold, F., 2013. NBO 6.0, Theoretical chemistry Institute, University of Wisconsin, Madison.

Gunes, S., Neugebauer, H., Sariciftci, N.S., 2007. Conjugated polymer-based organic solar cells. Chem. Rev. 107, 1324–1338.

Guryanova, E.N., Goldstein, I.P., Romm, I.P., 1975. Donor-Acceptor Bond. Keter publishing house Jerusalem ltd.

Hansen, C.M., 1967. The Three Dimensional Solubility Parameter and Solvent Diffusion Coefficient-their Importance in Surface Coating Formulation. Danish Technical Press, Copenhagen.

Hmuda, S.F., Banjac, N.R., Trisovic, N.P., Bojic, B.D., Valentic, N. V., Uscumlic, G.S., 2013. Solvent effect on the absorption spectra of potentially pharmacologically active 5-alkyl-5arylhydantoins: a structure-property relationship study. J. Serb. Chem. Soc. 78, 627–637.

Iikura, H., Tsuneda, T., Yanai, T., Hirao, K., 2001. A long-range correction scheme for generalized-gradient-approximation exchange functional. J. Chem. Phys. 115, 3540–3544.

Jadaun, P., Movva, H.C.P., Register, L.F., Benerjee, S.K., 2013. Theory and synthesis of bilayer grapheme intercalated with ICl and IBr for low power device application. J. Appl. Phys. 114, 063702–063707.

Janas, D., Herman, A.P., Boncel, S., Kozoil, K.K.K., 2014. Iodine monochloride as a powerful enhancer of electrical conductivity of carbon nanotube wires. Carbon 73, 225–233.

Jovie, B., Nikolic, A., Petrovic, S., Kordic, B., Dakovic-Sekulie, T., Stojanoic, N., 2014. FTIR investigation of solvent effects of N-methyl and N-tert-butyl benzamide. J. Struct. Chem. 55, 1616–1622.

Kamlet, M.J., Jones, M.E., Taft, R.W., Jose-Luis, Abboud., 1979. Linear solvation energyrelationships. Part 1. Solvent polarity olarizability effects on infrared spectra. JCS Perkins 2, 342–348.

Kamlet, M.J., Taft, R.W., 1979. Linear solvation energy relationships. Part 1. Solvent polarity-polarizability effects on infrared spectra. JCS Perkins 2, 349–356.

Kohn, W., Sham, L.J., 1965. Seif-consistent equations including exchange and correlation effects. Phys. Rev. A, A1133–A1138.

Lahyani, A., Trabelsi, M., 2016. Ultrasonic assisted synthesis of flavones by oxidative cyclization of 2′-hydroxychalcones using iodine monochloride. Ultrasonic Sonochem. 31, 626–630.

Leininger, T., Stoll, H., Werner, H.J., Savin, A., 1997. Combining long-range configuration interaction with short-range density functional. Chem. Phys. Lett. 275, 151–160.

Lu, Y., Shi, T., Wang, Y., Yang, H., Yan, X., Luo, X., Jiang, H., Zhu, W., 2009. Halogen bonding – a novel interaction for rational drug design? J. Med. Chem. 52, 2854–2862.

Lyatajka, Z., Ratajozaka, H., Orville-Thomas, W.J., 1977. A study of the properties of charge transfer complexes in systems composed of pyridine derivatives and chloride by the CNDO/2 method Brief Communications. Theor. Exp. Chem. 13, 389–391.

Matter, H., Nazare, M., Gussregen, S., Will, D.W., Schreuder, H., Bauer, A., Urmann, M., Ritter, K., Wagner, M., Wehner, V., 2009. Evidence for C–Cl/C–Br$\cdots\pi$ interactions as important contributions to protein-ligand binding affinity. Angew. Chem. Int. Ed. Engl. 48, 2911–2916.

Mckinney, W.J., Popov, A.I., 1969. Studies on the chemistry of halogens and of polyhalides, XXX. The influence of solvent properties on the formation of pyridine-iodine charge transfer complexes. J. Am. Chem. Soc. 91, 5215–5218.

Mulliken, R.S., 1952. Molecular compounds and their spectra. III. The interaction of electron donors and acceptors. J. Phys. Chem. 56, 801–822.

Mulliken, R.S., 1956. Molecular complexes and their spectra. VI. Some problems and new developments. Recl. Trav. Chim. Pays-Bas. Belg. 75, 845–852.

Mulliken, R.S., Pearson, W.B., 1969. Molecular Complexes. Wiley Interscience, New York.

Peverati, R., Truhlar, D.G., 2012. Performance of the M11 and M11-L density functionals for calculations of electronic excitation energies by adiabatic time-dependent density functional theory. Phys. Chem. Chem. Phys. 14, 11363–11370.

Politzer, P., Lane, P., Concha, M.C., Ma, Y., Murray, J.S., 2007. An overview of halogen bonding. J. Mol. Model. 13, 305–311.

Politzer, P., Murray, J.S., Clark, T., 2010. Halogen bonding: an electrostatically-driven highly directional noncovalent interaction. Phys. Chem. Chem. Phys. 12, 7748–7757.

Razzaq, H., Qureshi, R., Janjua, N.K., Saira, F., Saleemi, S., 2008. Charge transfer complexes of picolines with σ-and π-acceptors. Spectrochim. Acta Part A 70, 1034–1040.

Refat, M.S., El-Sayed, M., Adam, A.M.A., Saad, H.A., Eldaroti, H. H., 2013. Charge transfer complexes as a semiconductor models: outline of spectroscopic studies on electron donor-acceptor complexes of hexane-1,6-diol with different π-acceptors. Int. J. Electrochem. Sci. 8, 4234–4259.

Refat, M.S., Ibrahim, O.B., Al-Didamony, H., Abou El-Nour, Kh.M., El-Zayat, L., 2010. Synthesis and spectroscopic characterization of piperidine/I_2 charge-transfer complex in different chlorinated organic solvents. Bul. Chem. Commun. 43, 439–448.

Reichardt, C., Welton, T., 2011. Solvents and Solvent Effects in Organic Chemistry, fourth ed. WILEY-VCH Verlag GmbH & Co. KGaA, Weinheim.

Reiling, S., Besnard, M., Bopp, P.A., 1997. Theoretical studies on the pyridine$-I_2$ charge-transfer complex. 1. Ab-initio calculations on I_2 and pyridine$-I_2$. J. Phys. Chem. A 101, 4409–4415.

Salman, H.M., Rabie, U.M., Abd-Allab, E.M., 2004. Charge transfer complexes of some pyrimidines with π- and σ-acceptors. Can. J. Anal. Sci. Spectrosc. 49, 1–7.

Savin, A., 1996. On degeneracy, near degeneracy and density functional theory. In: Seminario, J.M. (Ed.), Recent Developments and Applications of Modern Density Functional Theory. Elsevier, Amsterdam, pp. 327–357.

Schmidt, M.W., Baldridge, K.K., Boatz, J.A., Elbert, S.T., Gordon, M.S., Jensen, J.H., Koseki, S., Matsunga, N., Nguyen, K.A., Su, S. J., Windus, T.L., Dupuis, M., Montgomery, J.A., 1993. General atomic and molecular electronic structure system. J. Comput. Chem. 14, 1347–1363.

Sekino, H., Maeda, Y., Kamiya, M., Hirao, K., 2007. Polarizability and second hyperpolarizability evaluation of long molecules by the density functional theory with long-range correction. J. Chem. Phys. 126, 014107–014113.

Shimizu, S., Watanabe, N., Kataoke, T., Shoje, T., Abe, N., Morishita, S., Ichimura, H., 2012. In: Pyridine and alkylpyridines in Ullmann's encyclopedia of industrial chemistry, vol. 30. Wiley-VCH. Verlag GmbH & Co, KGaA, Weinheim, pp. 557–589.

Subhani, M.S., Aslam, S., Qureshi, R., Rahman, A., 2008. UV spectroscopic studies of charge transfer complexes of 2-hydroxy-1,4-naphthoquinone. J. Chem. Soc. Pak. 30, 232–236.

Taft, R.W., Kamlet, M.J., 1976. The solvatochromic comparison method. 2. The α-scale of solvent hydrogen-bond donor (HBD) acidities. J. Am. Chem. Soc. 98, 2886–2894.

Tawada, Y., Tsuneda, T., Yanagisawa, S., Yanai, T., Hirao, K., 2004. A long-range-corrected time-dependent density functional theory. J. Chem. Phys. 120, 8425–8433.

Tiwary, A.S., Mukherjee, A.K., 2009. Calculation of the charge transfer transition energy of the mesitylene-ICl complex by ab initio and TDDFT methods: comparison with other methylbenzene-ICl complexes. Mol. Phys. 107, 2063–2070.

Tiwary, A.S., Sengupta, P.S., Mukherjee, A.K., 2008. Modelling the ground state geometry and estimating the charge transfer transition energy of the Toluene-ICl molecular complex by ab initio and DFT methods. J. Chem. Theory 7, 331–346.

Tozer, D.J., Amos, R.D., Handy, N.C., Roos, B.O., Serrano-Andres, L., 1999. Does density functional theory contribute to the understanding of excited states of unsaturated organic compounds? Mol. Phys. 97, 859–868.

Tozer, D.J., Handy, N.C., 1998. Improving virtual Kohn–Sham orbitals and eigenvalues: application to excitation energies and static polarizabilities. J. Chem. Phys. 109, 10180–10189.

Tsai, C.W., Su, Y.C., Lia, G.D., Chai, J.D., 2013. Assessment of density functional methods with correct asymptotic behaviour. Phys. Chem. Chem. Phys. 15, 8352–8361.

Vasilyev, A.V., Lindeman, S.V., Kochi, J.K., 2001. Molecular structures of the metastable charge-transfer complexes of benzene (and toluene) with bromine as the pre-reactive intermediates in electrophilic aromatic bromination. New J. Chem. 26, 582–592.

Vydrov, O.A., Scuseria, G.E., 2006. Assessment of a long-range corrected hybrid functional. J. Chem. Phys. 125, 234109–234117.

Walzer, K., Maennig, B., Pfeiffer, M., Leo, K., 2007. Highly efficient organic devices based on electrically doped transport layers. Chem. Rev. 107, 1233–1271.

Xiong, G.Z., Yu, Z.L., Chu, W., 1999. A method of preparing the Wij's reagent with molar ratio Iodine/Chlorine = 1.0 and its application for the determination of iodine value. Chin. J. Anal. Chem. 27, 949–952.

Zakerhamidi, M.S., Ghanadzadeh, A., Moghadan, M., 2012. Solvent effects on the UV/Visible absorption spectra of some aminobenzene dyes. Chem. Sci. Trans. 1, 1–8.